Università di Genova

PhD Program in Health Sciences
Biostatistics and Methods for Big Data Analysis
XXXVIII Cycle

Disease Progression in Multiple Sclerosis:
From Pathophysiological Mechanisms to Therapeutic Targets

PhD candidate: Alessandro Cagol

Supervisor: Prof. Maria Pia Sormani

Table of Contents

1. List of Abbreviations

AD: axial diffusivity

APC: annualized percent change

ARR: annualized relapse rate

AUC: area under the curve

BMI: body mass index

BPF: brain parenchymal fraction

BTK: Bruton's tyrosine kinase

BVL: brain volume loss

CAL: chronic active lesion

CC: corpus callosum

CI: confidence interval

CIS: clinically isolated syndrome

CL: cortical lesion

CNS: central nervous system

CSA: cross-sectional area

CSF: cerebrospinal fluid

CST: corticospinal tract

CTh: cortical thickness

DMTs: disease-modifying therapies

DTI: diffusion tensor imaging

DW-MRI: diffusion-weighted magnetic resonance imaging

EDSS: Expanded Disability Status Scale

EPI: echo-planar imaging

FA: fractional anisotropy

FAST-T2: fast acquisition with spiral trajectory and adiabatic T2-prep

FDA: Food and Drug Administration

FLAIR: fluid-attenuated inversion recovery

GM: gray matter

HC: healthy control

HR: hazard ratio

ICC: intraclass correlation coefficient

ICVF: intracellular volume fraction

IQR: interquartile range

ISOVF: isotropic volume fraction

LASSO: least absolute shrinkage and selection operator

MD: mean diffusivity

MD-ApC: mean difference in annualized percentage change

MEDI: morphology enabled dipole inversion

MP2RAGE: magnetization-prepared 2 rapid acquisition gradient echoes

MPRAGE: magnetization-prepared rapid acquisition gradient echo

MRI: magnetic resonance imaging

MTI: magnetization transfer imaging

MTR: magnetization transfer ratio

MTsat: magnetization transfer saturation

MS: multiple sclerosis

MuSIC: Multiple Sclerosis Inventory of Cognition

MVF: myelin volume fraction

MWF: myelin water fraction

NAWM: normal-appearing white matter

NDI: neurite density index

NMA: network meta-analysis

NODDI: neurite orientation dispersion and density imaging

ODI: orientation dispersion index

PET: positron emission tomography

PIRA: progression independent of relapse activity

PIRMA: progression independent of relapse and MRI activity

PMS: progressive multiple sclerosis

PPMS: primary progressive multiple sclerosis

PRL: paramagnetic rim lesion

pwMS: people with multiple sclerosis

pwRRMS: people with relapsing-remitting multiple sclerosis

qMRI: quantitative MRI

QSM: quantitative susceptibility mapping

qT1: quantitative T1

RAW: relapse-associated worsening

RCT: randomized controlled trial

RD: radial diffusivity

RIS: radiologically isolated syndrome

ROI: region of interest

ROM: ratio of means

RRMS: relapsing-remitting multiple sclerosis

S1P: sphingosine-1-phosphate receptor

SC: spinal cord

SCR: superior corona radiata

SD: standard deviation

SDMT: Symbol Digit Modalities Test

SEL: slowly expanding lesion

sGFAP: serum glial fibrillary acidic protein

SIENA: Structural Image Evaluation, using Normalization, of Atrophy

SMSC: Swiss Multiple Sclerosis Cohort

SMT: spherical mean technique

sNfL: serum neurofilament light chain

SPMS: secondary progressive multiple sclerosis

SUCRA: surface under the cumulative ranking curve

T2LV: T2 lesion volume

TE: echo time

TIV: total intracranial volume

TR: repetition time

TSPO: translocator protein

VLMT: Verbal Learning and Memory Test

WM: white matter

WML: white matter lesion

2. Abstract

Multiple sclerosis (MS) is a chronic inflammatory and neurodegenerative disease of the central nervous system in which disability accumulation increasingly occurs independently of acute inflammatory activity. Progression independent of relapse activity (PIRA) has emerged as a major contributor to long-term disability, yet its biological substrates, imaging correlates, and responsiveness to disease-modifying therapies (DMTs) remain incompletely understood.

This thesis aimed to characterize the structural and microstructural correlates of disease progression in MS, identify biomarkers associated with disability severity and future progression, and evaluate the impact of current therapies on neurodegenerative outcomes. To address these objectives, the thesis integrates and discusses findings from five complementary studies employing advanced MRI techniques, multimodal biomarker analyses and machine learning, real-world observational data, and meta-analytical approaches.

Using diffusion tensor imaging (DTI), the first study showed that people with MS (pwMS) experiencing PIRA exhibit diffuse microstructural damage in major white matter tracts compared with matched pwMS without PIRA, even in the absence of subclinical focal inflammatory activity. These findings support the concept that silent progression is associated with diffuse tissue injury extending beyond focal lesions, consistent with mechanisms such as secondary axonal injury and Wallerian degeneration. The second study applied a multiparametric quantitative MRI (qMRI) protocol to the thalamus, revealing extensive macrostructural and microstructural alterations in pwMS, with accelerated degeneration over time and more pronounced changes in progressive phenotypes. Thalamic qMRI abnormalities were more severe close to the cerebrospinal fluid (CSF), associated with disability progression, and diffusely affected normal-appearing tissue, suggesting concurrent mechanisms of lesion-related disconnection and surface-in neurodegeneration.

In the third study, a multimodal machine-learning framework integrating a wide array of conventional MRI, advanced qMRI, and serum biomarkers was applied to identify the most informative predictors of neurological disability, cognitive impairment, and future PIRA. Across two independent cohorts, measures of upper cervical spinal cord atrophy and cortical degeneration emerged as key contributors to physical disability and progression risk, while qMRI metrics and serum biomarkers provided complementary information. These findings

underscore the central role of cortical and spinal cord biomarkers for progression risk stratification.

The fourth study compared teriflunomide and ocrelizumab in a real-world cohort of relapsing-remitting MS, focusing on the incidence of PIRA and MRI biomarkers associated with smoldering disease activity, using propensity score matching. No differences were observed in PIRA incidence, paramagnetic rim lesion burden, or DTI-based microstructural measures, suggesting comparable effects on smoldering disease activity. These findings highlight the need for further studies specifically designed to investigate the effects of current therapies on progression-related and neurodegenerative outcomes.

Finally, a network meta-analysis of randomized clinical trials showed that multiple DMTs significantly reduce brain volume loss and disability accumulation compared with placebo, and that a relationship exists between treatment effects on brain atrophy and reduced disability progression, independent of effects on MRI inflammatory activity. These findings support brain volume loss as a clinically relevant therapeutic outcome, indicating that atrophy metrics retain value as therapeutic endpoints even as inflammatory activity becomes increasingly controlled. At the same time, the incomplete overlap between treatment effects on brain volume loss and disability progression suggests that additional mechanisms contribute to disease progression beyond global atrophy.

Collectively, this thesis indicates that MS progression is associated with diffuse and regionally heterogeneous patterns of neurodegeneration involving major white matter tracts, deep gray matter, cerebral cortex, and cervical spinal cord, and that these processes can be captured using both advanced and more widely available biomarkers. While current therapies partially mitigate neurodegenerative outcomes, disease progression remains only partially addressed, highlighting the need for improved biomarkers and targeted strategies to better characterize and ultimately address silent disease progression in MS.

3. Introduction

3.1 Disease progression in multiple sclerosis

Multiple sclerosis (MS) is a chronic disease of the central nervous system (CNS) characterized by inflammation, demyelination, and neurodegeneration.[1] It is the most common non-traumatic cause of disability in young adults and is associated with substantial impairment in quality of life and significant socioeconomic and healthcare burdens.[2]

Disability accumulation in MS occurs through two principal mechanisms. The first is incomplete recovery from relapses – acute inflammatory episodes causing neurological dysfunction – commonly referred to as relapse-associated worsening (RAW). The second mechanism is a gradual accumulation of disability that occurs independently of relapse activity, termed progression independent of relapse activity (PIRA).[3]

While the acute inflammatory component of MS has been extensively investigated and effectively targeted by disease-modifying therapies (DMTs), a substantial proportion of people with MS (pwMS) continue to experience disability accumulation despite marked suppression of relapses and magnetic resonance imaging (MRI)-visible lesions. This residual disability accrual is largely driven by PIRA. As a result, disease progression has emerged as the dominant determinant of long-term disability and reduced quality of life, prompting a major shift in MS research toward understanding progressive disease mechanisms.[4–6]

In the contemporary treatment era, the contribution of PIRA to overall disability accumulation has become particularly evident. Longitudinal studies have shown that PIRA accounts for a substantial proportion of disability accumulation even in patients with relapsing-remitting MS (RRMS) and relatively short disease duration, and is associated with worse long-term outcomes.[3,6–10] These observations underscore disease progression as a critical target for mechanistic investigation and therapeutic intervention.

Despite its clinical relevance, the biological basis of disease progression – and PIRA in particular – remains incompletely understood. Neuropathological evidence indicates that progression in MS is associated with widespread neurodegenerative changes, including axonal loss, synaptic degeneration, and neuronal death, accompanied by chronic glial activation.[4] These processes are thought to arise from a complex interplay between residual

compartmentalized inflammation, mitochondrial dysfunction, oxidative stress, and impaired repair mechanisms. Notably, many of these changes evolve slowly and diffusely, and are poorly captured by conventional measures or standard imaging markers of disease activity.[4]

A comprehensive understanding of MS progression therefore requires biomarkers that extend beyond focal inflammatory lesions. In this context, MRI plays a central role, enabling in vivo, longitudinal, and non-invasive assessment of both inflammatory and neurodegenerative pathology across the brain and spinal cord. Fully exploiting this potential, however, requires moving beyond conventional lesion-based approaches toward imaging strategies sensitive to diffuse tissue damage, subtle microstructural alterations, and region-specific vulnerability.

3.2 Neurodegeneration and disease progression

Neurodegeneration is now widely recognized as the core pathological substrate underlying disease progression in MS.[4,11] Although inflammatory demyelination predominates in the early stages of the disease, neurodegenerative processes begin early and accumulate over time, ultimately driving irreversible disability. Post-mortem studies have consistently demonstrated that axonal loss and neuronal degeneration occur not only within focal lesions but also extensively within normal-appearing white and gray matter, highlighting the diffuse nature of MS-related tissue damage.[12–14]

A unifying framework for characterizing disease progression has emerged in recent years, emphasizing the role of chronic, compartmentalized inflammation within the CNS.[4,5] In this model, immune activity becomes partially sequestered behind an intact blood–brain barrier, sustaining low-grade inflammation within the meninges, perivascular spaces, and chronically active lesions. This smoldering inflammatory environment is thought to promote neurodegeneration through the persistent activation of microglia, release of soluble neurotoxic mediators, and metabolic stress affecting neurons and oligodendrocytes.[4]

Neurodegeneration in MS is not spatially uniform. Certain structures and pathways appear particularly vulnerable, including long white matter tracts, the spinal cord, deep gray matter nuclei, and highly connected network hubs. Damage in these regions is likely to have a disproportionate impact on clinical function and disability accumulation. Understanding the basis of this selective vulnerability, and its relationship with clinical progression, is essential for the development of targeted biomarkers and therapeutic strategies.

MRI provides a powerful means to investigate these neurodegenerative processes. Measures of tissue atrophy and microstructural integrity allow assessment of both the cumulative burden of damage and its regional distribution. When integrated with longitudinal clinical data, MRI offers critical insights into the temporal evolution of neurodegeneration and its contribution to disability progression in MS.

3.3 Brain atrophy

Brain atrophy represents one of the most robust markers of neurodegeneration in MS. Although MRI-derived volume loss does not correspond directly to histopathologically proven neuronal or axonal loss, changes in brain volume correlate closely with post-mortem measures of tissue atrophy and are therefore widely accepted as a reliable in vivo biomarker of neurodegeneration.[15,16] Brain volume loss (BVL) is a physiological phenomenon of normal aging; however, in MS this process is pathologically accelerated, occurring at a substantially higher rate than in healthy individuals.[17,18] Importantly, accelerated brain atrophy is evident from the earliest disease stages and has been described not only in established MS but also in patients with clinically isolated syndrome (CIS) and even radiologically isolated syndrome (RIS), indicating that neurodegeneration begins early in the disease course.[19,20]

Brain atrophy has been consistently associated with physical disability accumulation and cognitive impairment, underscoring its close link to clinical outcomes.[16,21] Beyond reflecting disease severity, BVL also carries prognostic value: it predicts conversion from CIS to clinically definite MS, future disability progression, transition to secondary progressive MS (SPMS), and the risk of PIRA.[22–26]

Importantly, brain atrophy in MS affects both white matter (WM) and gray matter (GM), although these compartments differ in their temporal dynamics and clinical relevance.[27,28] While global measures of brain volume provide valuable markers of neurodegeneration, they inevitably obscure important spatial information. Extensive evidence indicates that atrophy in specific brain compartments – particularly deep GM structures and the cerebral cortex – occurs early, progresses rapidly, and shows a stronger relationship with clinical outcomes than whole-brain measures alone.[16] As a result, regional analyses of brain atrophy have gained prominence, offering greater pathophysiological specificity and improved clinical relevance.

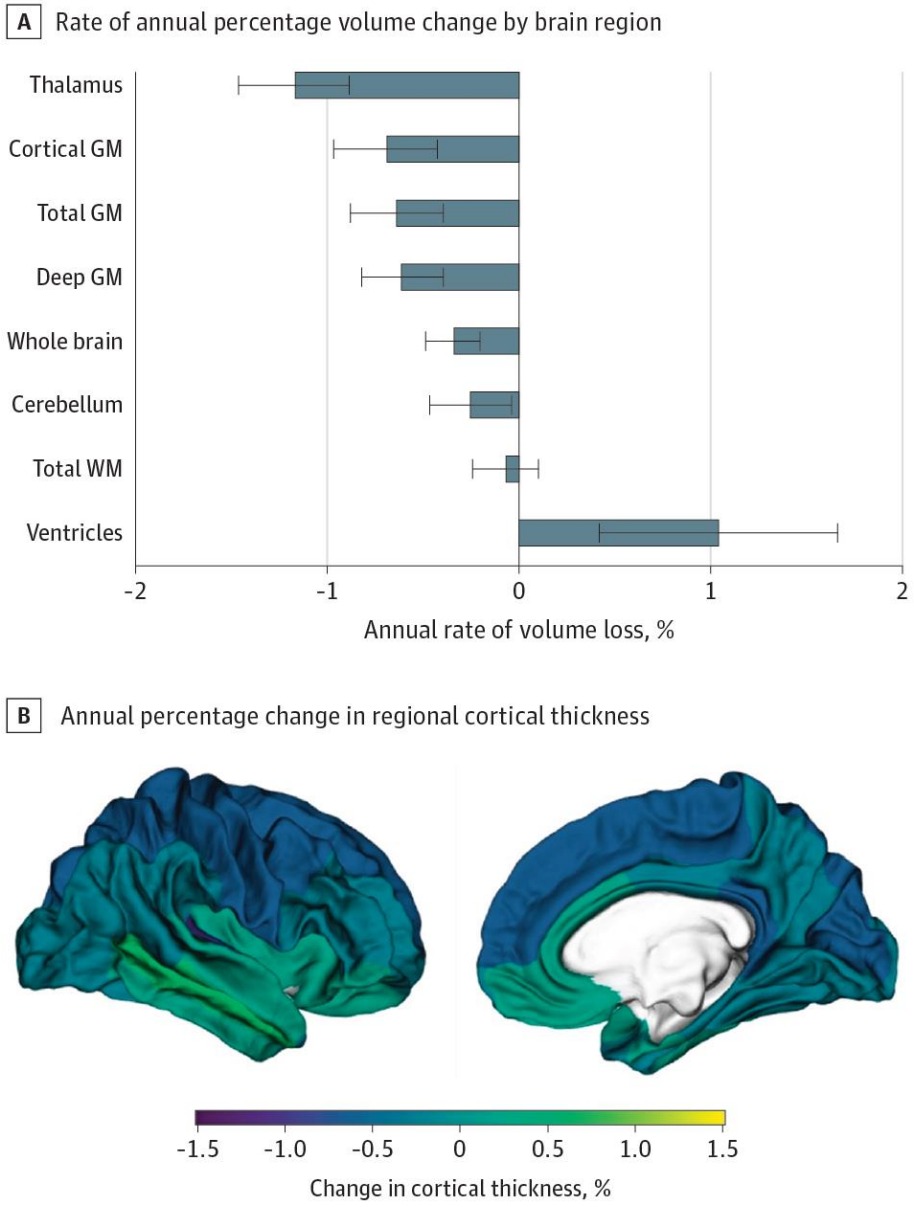

***Figure 3.1**: Annualized rates of percentage volume change by brain region, and cortical thinning by cortical area, in a cohort of 516 people with relapsing multiple sclerosis. From Cagol et al., JAMA Neurology, 2022*

3.4 Spinal cord atrophy

MS is a disease of the entire CNS, and pathological involvement of the spinal cord (SC) represents a fundamental component of its clinical expression. SC damage is particularly critical from a clinical perspective, given the high functional relevance of this anatomically compact and clinically eloquent structure. Nevertheless, most imaging studies in MS have historically focused on brain atrophy, largely because the assessment of SC atrophy poses substantial technical challenges. These include the small cross-sectional size of the SC, its complex anatomy, susceptibility to magnetic field inhomogeneities, partial volume effects, and

physiological motion related to respiration and cardiac pulsation.[29] Despite these challenges, SC atrophy has emerged as a key imaging marker of neurodegeneration in MS.[16] Pathologically, SC atrophy reflects a combination of demyelination, neuroaxonal loss, and gliosis,[30] with evidence indicating that it can occur at least partially independently of focal SC lesions and brain pathology.[31,32]

Similar to brain atrophy, SC volume loss is detectable from the earliest disease stages, including early relapsing forms,[33] suggesting that SC neurodegeneration begins early in the disease course. In vivo, SC atrophy is most commonly assessed in the upper cervical cord, particularly at the C2-C3 level.[32] Longitudinal studies have shown that SC atrophy progresses at a faster rate than brain atrophy and is more pronounced in progressive MS phenotypes compared with RRMS.[34] Importantly, SC atrophy is strongly associated with physical disability, predicts long-term clinical outcomes, and has emerged as a promising predictor of PIRA.[35,36] Together, these findings highlight SC atrophy as a reliable biomarker of disease severity and progression in MS.

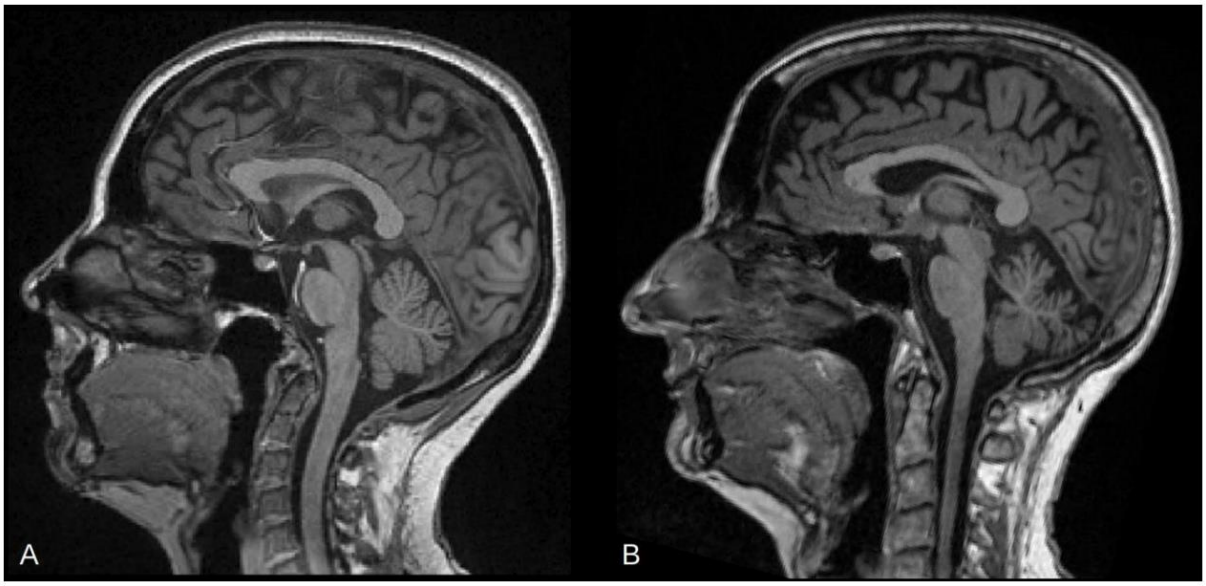

Figure 3.2. *Example of a preserved cervical spinal cord in a 48-year-old woman with relapsing–remitting multiple sclerosis and clinical stability (A) and pronounced cervical spinal cord atrophy in a 46-year-old woman who experienced progression independent of relapse activity (PIRA) (B). From Cagol et al., Neurology, 2023*

3.5 Compartmentalized inflammation in chronic active lesions

An increasingly recognized driver of non-relapsing disease progression in MS is compartmentalized inflammation within the CNS, with chronic active lesions (CALs) representing one of its most relevant manifestations.[37] Unlike acute inflammatory lesions

associated with a blood-brain barrier breakdown, CALs sustain inflammatory activity behind a relatively intact barrier, thereby promoting ongoing tissue injury over prolonged periods and contributing to disability accumulation independent of relapse activity.

MS lesions exhibit marked biological heterogeneity. Following their acute phase, lesions may undergo substantial remyelination – resulting in shadow plaques – or evolve into chronic inactive lesions characterized by low cellularity and no ongoing damage. In contrast, CALs are defined by persistent inflammatory activity at the lesion edge, with gradual expansion into surrounding normal-appearing white matter.[37] This smoldering lesion behavior is thought to reflect sustained activation of innate immune cells and has emerged as a key substrate of progressive pathology in MS.[38]

Several imaging approaches have been developed to identify CALs in vivo. These include the detection of slowly expanding lesions (SELs) on longitudinal conventional MRI, visualization of microglial activation using TSPO-PET, and identification of paramagnetic rim lesions (PRLs) using susceptibility-based MRI.[38–40] Among these, PRLs currently represent the most mature and clinically feasible biomarker.[38] On susceptibility-weighted imaging or quantitative susceptibility mapping (QSM), PRLs appear as lesions surrounded by a paramagnetic rim, reflecting iron-laden microglia and macrophages at the lesion border.[38,41] Converging neuropathological evidence has demonstrated that PRLs correspond to CALs, establishing a direct link between this imaging phenotype and chronic active pathology.[42]

PRLs have also gained relevance beyond pathophysiological characterization. They are observed across all MS clinical phenotypes, with a pooled prevalence greater than 50% while remaining exceedingly rare in non-MS conditions.[43] In patients with CIS, their presence predicts conversion to clinically definite MS, supporting their utility as a disease-specific imaging marker.[44] Accordingly, PRLs have recently been incorporated as a supportive feature in updated diagnostic criteria for MS.[45]

Importantly, CALs – and PRLs in particular – appear to play an active role in disease progression rather than merely reflecting prior inflammatory damage.[38] PRLs are associated with more severe pathological changes, including pronounced axonal loss, impaired remyelination, and sustained microglial activation.[40] At the patient level, PRL burden correlates with biomarkers of ongoing neuroaxonal injury, such as elevated serum neurofilament light chain (sNfL), and with accelerated brain atrophy.[38,46,47] Clinically, the presence and number of

PRLs are associated with greater physical and cognitive disability, predict disability worsening and conversion to SPMS, and have been specifically linked to PIRA.[35,38,47]

Together, these observations identify CALs as a key biological site of compartmentalized inflammation in MS, providing a mechanistic link between persistent innate immune activation, neurodegeneration, and non-relapsing disease progression.

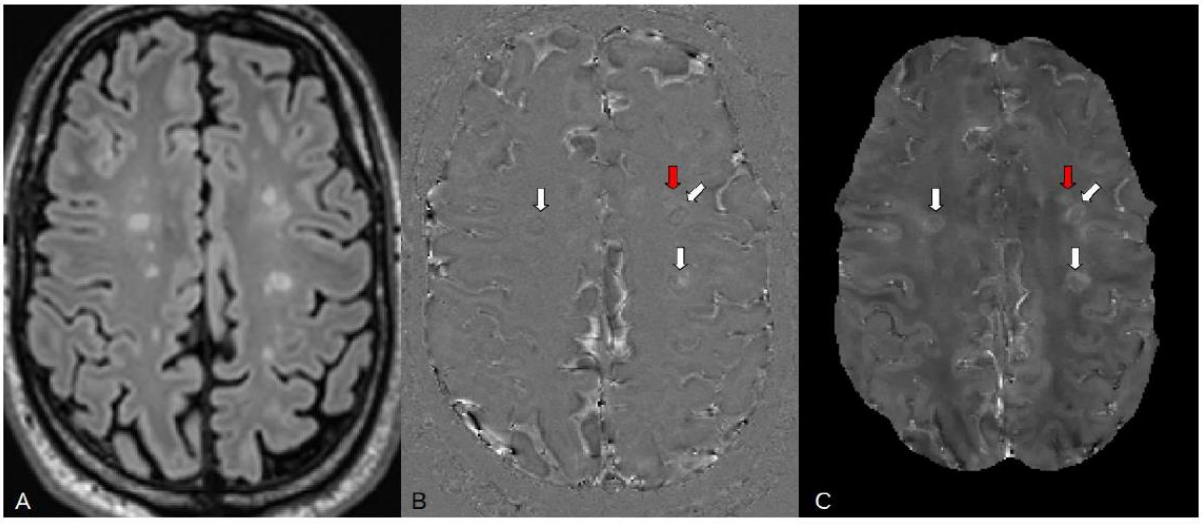

Figure 3.3. *Example of hyperintense lesions on FLAIR (A) presenting as paramagnetic rim lesions on unwrapped filtered phase (B) and quantitative susceptibility mapping (C). White arrows indicate paramagnetic rim lesions; the lesion indicated by the red arrow shows a paramagnetic rim that is only partially visible in this slice. From Cagol et al., Neurology, 2023*

3.6 Characterization of tissue microstructural changes using quantitative MRI

While conventional MRI remains indispensable for the management of MS, it provides limited insight into the microstructural substrates of tissue damage and repair that drive long-term disability. Conventional contrasts are inherently qualitative, influenced by scanner- and sequence-specific factors, and lack biological specificity, resulting in a well-recognized dissociation between radiological findings and clinical outcomes.[48] These limitations are particularly relevant for diffuse pathology affecting normal-appearing tissue and slowly evolving neurodegenerative processes, which are poorly captured by standard imaging markers. Quantitative MRI (qMRI) has emerged as an approach to address these shortcomings by providing voxel-wise, biologically informed metrics derived from biophysical modeling of MR signal properties.[49,50] By generating quantitative maps expressed in physical units, qMRI

improves reproducibility, enables longitudinal assessment, and facilitates comparison across individuals, thereby offering a more robust framework for studying disease progression.

qMRI encompasses a broad set of techniques sensitive to complementary aspects of CNS pathology, including demyelination, neuroaxonal loss, gliosis, iron dysregulation, inflammation, and metabolic dysfunction.[50] Among these, T1 relaxometry (qT1) provides a sensitive marker of tissue integrity, with prolonged relaxation times reflecting a combination of demyelination, axonal loss, increased water content, and iron depletion.[51,52] Magnetization transfer imaging (MTI) probes the exchange of magnetization between protons bound to macromolecules – including myelin-associated lipids and proteins – and free water protons, making it sensitive to variations in tissue macromolecular content and microstructural integrity.[53–56] Compared with the conventional magnetization transfer ratio (MTR), magnetization transfer saturation (MTsat) offers improved specificity by correcting for confounding effects related to T1 relaxation and B1 field inhomogeneities.[57] Both qT1 and MTI have demonstrated sensitivity to microstructural damage within lesions and normal-appearing tissue, as well as to gradients of pathology across the cortex and periventricular regions, making them well suited to study diffuse neurodegeneration and repair processes.[58] Myelin water imaging provides a more direct and sensitive measure of myelin content by exploiting the distinct relaxation properties of water trapped between the lipid bilayers of the myelin sheath. By separating this short component from other water pools, myelin water fraction (MWF) maps offer a quantitative estimate of myelin density with strong histopathological validation, albeit at the cost of increased acquisition and processing complexity.[59–62] QSM further complements these approaches by estimating tissue magnetic susceptibility, primarily driven by iron and myelin content, and has proven particularly informative for characterizing CALs and alterations in iron homeostasis within deep GM structures.[63–70] Notably, QSM has also been shown to potentially enable the identification of remyelinated lesions, supported by converging evidence from pathological and multimodal imaging modalities.[71]

Diffusion MRI plays a key role within the qMRI framework by enabling in vivo characterization of WM microstructure and large-scale network organization. Diffusion tensor imaging (DTI), despite its limited biological specificity, remains one of the most widely used approaches for assessing tissue integrity across large white matter tracts.[72,73] Metrics such as fractional anisotropy (FA), mean diffusivity (MD), axial diffusivity (AD), and radial diffusivity (RD) are sensitive to alterations in axonal organization, myelin integrity, and extracellular water content.[74,75] DTI has been instrumental in revealing that MS-related damage extends far beyond

visible lesions, affecting long WM tracts involved in motor, sensory, and cognitive functions.[76] More advanced diffusion models build upon these foundations by increasing biological interpretability through multi-compartment approaches, enabling estimation of neurite density, orientation dispersion, and extracellular diffusion.[77] While these techniques offer improved specificity, they come at the cost of longer acquisition times and increased methodological complexity, which may limit their applicability in large clinical cohorts. In this context, conventional DTI retains value as a sensitive and widely available tool for characterizing WM degeneration.

Taken together, qMRI provides a multidimensional framework for investigating MS pathology beyond focal inflammation, capturing complementary aspects of microstructural damage, chronic inflammation, and neurodegeneration. The integration of qT1, MTsat, MWF, QSM, and diffusion MRI enables a comprehensive characterization of tissue integrity across GM and WM, offering critical insights into the mechanisms underlying disability accumulation and disease progression.

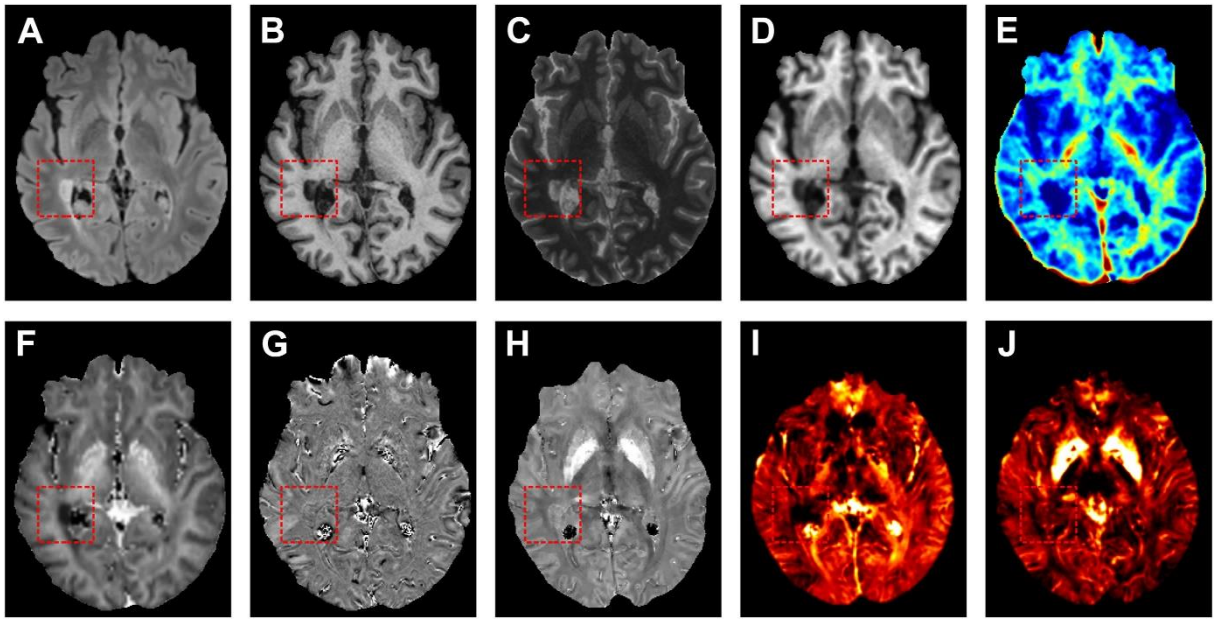

Figure 3.4. *Examples of advanced MR images from a patient with MS, with a right periventricular lesion highlighted by a red-dotted square. (A) Conventional FLAIR, (B) MP2RAGE, (C) qT1, (D) MTsat, (E) MWF, (F) neurite density index from multi-shell diffusion, (G) unwrapped phase, (H) QSM, (I) χ-separation diamagnetic component, (J) χ-separation paramagnetic component. From Cagol et al., Neuroimaging Clin N Am, 2024*

3.7 Regional brain alterations in multiple sclerosis

Pathological changes in MS are not uniformly distributed across the brain but preferentially affect specific regions and networks whose damage is particularly relevant for disease progression. While global measures of brain atrophy provide a general overview of neurodegenerative burden, regionally selective damage has greater pathophysiological specificity and stronger clinical relevance. Among these regions, deep GM structures and the cerebral cortex have emerged as key substrates of progressive pathology, reflecting both their intrinsic vulnerability and their central role in the disease evolution.[16]

Within deep GM, the thalamus stands out as one of the earliest and most consistently affected structures in MS. As a central relay hub with extensive cortico-subcortical connectivity, the thalamus is highly susceptible to widespread inflammatory and neurodegenerative processes, including trans-synaptic degeneration arising from WM tract injury.[78] MRI studies have consistently demonstrated that thalamic atrophy occurs from the earliest disease stages, progresses steadily over time, and shows robust associations with both physical disability and cognitive dysfunction.[78–80] Beyond volumetric loss, qMRI characteristically reveals microstructural changes within the thalamus that precede and accompany atrophy, further underscoring the thalamus as a sensitive and biologically informative marker of MS-related neurodegeneration.[78]

Cortical damage represents another major contributor to MS pathology and reflects both focal and diffuse pathological processes. Cortical demyelination, particularly in subpial lesions, is recognized as a hallmark linked to compartmentalized inflammation in the meninges and cerebrospinal fluid.[4] In parallel, diffuse cortical thinning occurs early, progresses over time, and is strongly associated with cognitive impairment and disability accumulation.[81] Remarkably, a higher burden of cortical lesions has been associated with an increased risk of conversion to SPMS, and patients exhibiting PIRA show accelerated cortical thinning compared with clinically stable patients.[26,82] qMRI techniques have shown diffuse cortical alterations within the normal-appearing cortex, revealing gradients of damage that are more pronounced in superficial cortical layers.[42,83] Collectively, these findings indicate that cortical pathology is not merely a late-stage phenomenon but a process closely reflecting disease progression, complementing deep GM degeneration and reinforcing the concept of MS as a disease driven by regionally selective neurodegeneration.

3.8 Efficacy of disease-modifying therapies on disease progression

Over the past three decades, the therapeutic landscape of MS has expanded dramatically, with a substantial increase in both the number and efficacy of DMTs.[84] These advances have progressively shifted treatment goals toward initiating therapy as early as possible to alter long-term disease trajectories and prevent irreversible disability. Historically, MS management largely relied on an escalation approach, whereby patients started with moderately effective therapies and transitioned to higher-efficacy agents in response to ongoing disease activity. More recently, an induction strategy has gained increasing acceptance, particularly in patients with highly active disease, aiming to rapidly suppress inflammatory activity through early use of high-efficacy therapies and thereby modify the subsequent course of the disease.[85] Compared with more moderate or stepwise escalation approaches, induction therapy has been associated with superior control of disease activity and more favorable long-term disability outcomes.[86–88]

Contemporary DMTs are highly effective in controlling the acute inflammatory component of MS, as evidenced by marked reductions in relapse rates and MRI lesion accumulation. In randomized clinical trials, treatment efficacy on disability accumulation is typically assessed with endpoints such as confirmed disability progression. However, these outcomes intrinsically reflect a combination of effects on RAW and PIRA, limiting their ability to isolate treatment effects on the progressive component of the disease. As a consequence, despite the growing recognition of PIRA as a major driver of long-term disability, its specific modulation by DMTs remains incompletely understood.[7]

Evidence addressing this question has mainly derived from observational studies and post-hoc analyses of phase III trials, with heterogeneous results. While some real-world studies suggest a beneficial association between DMT exposure and long-term disability progression, others have failed to demonstrate a clear reduction in the risk of PIRA, potentially reflecting limited sample sizes and residual confounding.[7,89,90] More recent analyses incorporating strategies to mitigate indication bias have provided more consistent signals, suggesting that higher-efficacy therapies can reduce the risk of PIRA.[7,91] In addition, post-hoc analyses of clinical trials have indicated that some high-efficacy therapies are superior to comparator treatments, supporting the concept that some DMTs may exert effects beyond suppression of acute focal inflammation.[3,7,92]

Nonetheless, specifically evaluating the impact of DMTs on non-relapsing disease progression remains particularly challenging. There is currently no universally accepted definition of PIRA, and established criteria may fail to exclude subclinical focal inflammatory activity detectable on MRI. To address this limitation, more stringent concepts such as progression independent of relapse and MRI activity (PIRMA) have been proposed, although their application remains inconsistent.[7,10] In observational studies, residual confounding – particularly indication bias – remains a significant limitation, even when advanced statistical adjustments are applied. In randomized clinical trials, PIRA represents a complex outcome over the typically short duration of follow-up, reducing statistical power. Moreover, it has been demonstrated that commonly used definitions of PIRA may produce biased estimates of treatment effects in the presence of treatment-induced relapse reduction, further complicating interpretation of trial results.[93]

Taken together, these methodological and conceptual challenges highlight the limitations of relying exclusively on clinical endpoints to assess therapeutic effects on non-relapsing disease progression. Accordingly, MRI-based biomarkers reflecting disease progression – capturing neurodegeneration, chronic active inflammation, and microstructural tissue damage – have become an integral and complementary component in the evaluation of treatment effects in MS.

In this context, BVL has become one of the most widely used MRI outcomes in randomized clinical trials, reflecting its established role as an integrative marker of neurodegeneration.[16] Measures of brain atrophy are currently recommended as secondary endpoints in relapsing MS trials and have been proposed as primary endpoints in progressive MS, where demonstrating an effect of the neurodegenerative component of the disease is of particular relevance.[16] However, the interpretation of treatment effects on brain atrophy is subject to several important confounders, which can be broadly categorized as methodological, physiological, and disease-related.[16,94] Among the latter, pseudoatrophy represents a well-recognized phenomenon, characterized by an apparent acceleration of BVL following treatment initiation, driven by the resolution of inflammation-related edema rather than true tissue loss. This paradoxical effect, typically observed during the first months of therapy, complicates the interpretation of short-term atrophy measures and necessitates careful consideration of timing and analytical strategies in clinical trials.

Beyond global and regional atrophy, increasing attention has been directed toward MRI markers of focal smoldering inflammation as complementary treatment outcomes. Several recent trials have begun to integrate measures related to chronic active lesions, including PRLs and SELs.[43] For PRLs, longitudinal observational studies have shown that favorable lesion evolution – such

as rim resolution or the absence of new PRLs – is associated with a lower risk of disability progression.[95] Nevertheless, to date, observational studies have not demonstrated an effect of available DMTs on PRL resolution.[43,96] In contrast, post-hoc analyses of randomized controlled trials have provided preliminary evidence that certain treatments may reduce SELs, suggesting a potential impact on smoldering inflammatory activity within CALs.[97,98]

qMRI further represents a particularly promising approach for capturing treatment effects on neurodegeneration and tissue repair. Multiple trials have employed MTR as a surrogate marker of tissue integrity and myelin content.[99] More recently, MWF has been introduced into clinical trial settings, with emerging evidence indicating that some therapies may be associated with more favorable longitudinal trajectories of myelin content, consistent with neuroprotective or reparative effects.[100,101] Collectively, these MRI-based measures complement clinical outcomes by providing biologically informed endpoints that may be more sensitive to treatment effects on the progressive and smoldering components of MS.

4. Knowledge Gaps and Aims of the Thesis

Despite major advances in the understanding and treatment of MS, several critical gaps remain in our knowledge of disease progression and its biological substrates. PIRA is now recognized as a critical contributor to long-term disability across all MS phenotypes, including RRMS. However, the mechanisms underlying PIRA remain incompletely characterized, and robust biomarkers capable of capturing relapse-independent neurodegenerative processes in vivo are still limited. While PIRA has been associated with accelerated brain and spinal cord atrophy and with compartmentalized chronic inflammation,[25,26,35,36] the contribution of diffuse WM tract degeneration – beyond focal lesions – has been insufficiently explored. In parallel, although GM pathology is increasingly acknowledged as central to disease progression, current evidence is largely based on volumetric measures, leaving important gaps in our understanding of microstructural alterations within key regions such as the thalamus, how these changes accumulate over time, and how they relate to disability and cognitive impairment across disease phases.

At the same time, the growing availability of advanced MRI and serum biomarkers has profoundly expanded our ability to probe focal inflammation, chronic inflammatory activity, and neurodegeneration. However, most studies have focused on a limited subset of biomarkers, often examined in isolation. As a result, the relative contribution, redundancy, and complementary value of different biomarkers in explaining clinical severity, disease phenotype, and risk of future progression remain unclear, limiting their translation into clinical decision-making. In particular, markers of smoldering disease activity and relapse-independent disability accumulation have not been systematically integrated within a unified analytical framework.

Further gaps concern the evaluation of treatment effects on disease progression and MRI-based markers of smoldering pathology. While DMTs are highly effective in suppressing acute inflammatory activity, their impact on non-relapsing progression and on imaging markers of neurodegeneration and chronic inflammation remains poorly characterized. Evidence in this area is limited and fragmented, and comparative data across therapies are scarce due to the lack of head-to-head comparisons. BVL exemplifies this limitation: although several DMTs have demonstrated efficacy in reducing BVL, their relative effects are difficult to compare across studies. Moreover, while an earlier meta-analysis established an association between treatment effects on BVL and disability progression, many therapies approved in recent years were not

included.[102] Whether this relationship holds across the modern therapeutic landscape remains an open question, with important implications for supporting brain atrophy as a clinically meaningful biomarker of neurodegeneration and treatment response.

Against this background, the studies included in this thesis were designed to address these questions through complementary and integrative approaches. Specifically, the first study (presented in **chapter 5**) aimed to investigate the relationship between PIRA and microstructural integrity of major WM tracts using DTI, including the more stringent concept of PIRMA. The second study (presented in **chapter 6**) focused on characterizing thalamic damage beyond volumetric loss by combining multiparametric qMRI measures to capture microstructural alterations across disease stages and their clinical relevance. The third study (presented in **chapter 7**) sought to disentangle the relative contribution of a broad range of MRI and serum biomarkers to clinical disability, cognitive impairment, and risk of future progression, using a data-driven machine learning framework validated in an independent cohort. The fourth study (presented in **chapter 8**) examined the association of two widely used DMTs with PIRA and MRI markers of smoldering disease activity in a real-world multicenter cohort, addressing the limited evidence on treatment effects beyond relapse suppression. Finally, the fifth study (presented in **chapter 9**) aimed to provide a comprehensive and up-to-date synthesis of the comparative effects of all approved DMTs on BVL and to evaluate whether treatment-induced reductions in BVL are consistently associated with reduced disability progression, thereby strengthening the role of BVL as a clinically relevant marker of neurodegeneration.

Together, these studies aim to advance the understanding of disease progression in MS by integrating clinical outcomes with advanced imaging biomarkers, elucidating mechanisms of relapse-independent disability accumulation, and refining the assessment of treatment effects on the progressive and smoldering components of the disease.

5. White Matter Tract Degeneration in Multiple Sclerosis Patients With Progression Independent of Relapse Activity

Authors: Mario Ocampo-Pineda,[1,2,3,] Alessandro Cagol,[1,2,3,4,*] Pascal Benkert,[2,3,5] Muhamed Barakovic,[1,2,3] Po-Jui Lu,[1,2,3] Jannis Müller,[1,2,3] Sabine Anna Schaedelin,[1,2,3,5] Lester Melie-Garcia,[1,2,3] Matthias Weigel,[1,2,3,6] Maria Pia Sormani,[4,7] Ludwig Kappos,[1,2,3] Jens Kuhle,[2,3] and Cristina Granziera[1,2,3]*

**These authors contributed equally to this work.*

Affiliations: 1 Translational Imaging in Neurology (ThINk) Basel, Department of Biomedical Engineering, Faculty of Medicine, University Hospital Basel and University of Basel, Switzerland; 2 Multiple Sclerosis Centre, Department of Neurology, University Hospital Basel, Switzerland; 3 Research Center for Clinical Neuroimmunology and Neuroscience Basel (RC2NB), University Hospital Basel and University of Basel, Switzerland; 4 Dipartimento di Scienze della Salute, Universita' degli Studi di Genova, Italy; 5 Department of Clinical Research, University Hospital Basel, University of Basel, Switzerland; 6 Division of Radiological Physics, Department of Radiology, University Hospital Basel, Switzerland; and 7 Istituto di Ricovero e Cura a Carattere Scientifico, Ospedale Policlinico San Martino, Genova, Italy.

Published in: Neurol Neuroimmunol Neuroinflamm 2025;12:e200388. doi:10.1212/NXI.0000000000200388

Abstract

Background and Objectives: Progression independent of relapse activity (PIRA) is associated with worse outcomes in people with multiple sclerosis (pwMS). Although previous research has linked PIRA to accelerated brain and spinal cord atrophy and compartmentalized chronic inflammation, the role of white matter (WM) tract degeneration remains unclear. This study aimed to explore the relationship between PIRA and the integrity of major WM tracts using diffusion tensor imaging (DTI).

Methods: A cohort of 258 pwMS was stratified based on the presence or absence of PIRA over a 4-year follow-up period. At the end of follow-up, DTI metrics were compared between groups using propensity score–weighted linear regression models to account for potential confounders.

Results: PwMS with ≥1 PIRA event (n = 39) exhibited significant reductions in fractional anisotropy and increases in radial, axial, and mean diffusivity within the corpus callosum and motor tracts (false discovery rate–adjusted $p \leq 0.04$) compared with those without PIRA, indicating more pronounced WM damage.

Discussion: Our findings highlight an association between PIRA and microstructural damage in key WM tracts. The observed DTI changes likely reflect processes such as Wallerian degeneration and contribute to the growing evidence linking PIRA to neurodegeneration.

Introduction

In people with multiple sclerosis (pwMS), disability can accumulate because of incomplete recovery from relapses or through progression independent of relapse activity (PIRA).[103] A growing body of evidence highlights PIRA as a frequent phenomenon across all MS phenotypes,[7] including the typical relapsing-remitting multiple sclerosis (RRMS) form.[7]

PIRA is associated with unfavorable clinical outcomes,[6] emphasizing the critical need to effectively address it for improving long-term prognosis in pwMS. Achieving this goal necessitates a comprehensive understanding of the pathophysiologic mechanisms underlying PIRA. In addition, identifying biomarkers sensitive to the degenerative changes linked to PIRA is crucial for guiding personalized therapeutic strategies.

Previous investigations have linked PIRA to accelerated brain and spinal cord atrophy,[7,25,26,35,36] and compartmentalized chronic inflammation indicated by brain paramagnetic rim lesions (PRLs).[35] Although it is plausible that degeneration in white matter (WM) tracts may also be implicated in the pathogenesis of PIRA, data on this aspect are currently lacking. To address this gap, we aimed to investigate the relationship between PIRA and the integrity of major WM tracts by conducting a diffusion tensor imaging (DTI) study, using a magnetic resonance imaging (MRI) protocol compatible with clinical practice. DTI is a quantitative technique based on diffusion-weighted MRI (DW-MRI) that allows for exploring the magnitude and direction of water diffusion in biological tissues, providing insights into their microstructural architecture.[72] In addition, we explored DTI changes in progression independent of relapse and

MRI activity (PIRMA), a recent concept introduced to specifically reflect disability accumulation in the absence of both relapses and focal MRI activity.[7]

Methods

Participants

From the Swiss Multiple Sclerosis Cohort study,[104] we selected individuals with (1) a diagnosis of RRMS according to the 2017 revised McDonald criteria, (2) availability of a brain MRI scan including a standardized protocol suitable for DTI reconstruction, and (3) availability of regular clinical follow-up over a predefined 4-year period preceding the DTI scan.

The study follows the Strengthening the Reporting of Observational Studies guideline.

Standard Protocol Approvals, Registrations, and Patient Consents

The local ethics committee approved the study, and all patients provided written informed consent.

Clinical Data

All patients underwent standardized neurologic assessments, using the Expanded Disability Status Scale (EDSS) score (*neurostatus.net/*). The occurrence of PIRA during follow-up was defined as an event of EDSS increase (≥1.5/≥1.0/≥0.5 points if baseline EDSS was 0/1.0–5.5/>5.5, respectively) using a roving reference, confirmed at least after 6 months, in the absence of relapses (1) between the EDSS increase and the precedent reference visit (performed ≥90 days before the EDSS increase) and (2) between the EDSS increase and its confirmation.[7,35]

MRI Acquisition and Analysis

MRI scans were obtained with a 3T magnetic resonance system (Siemens Skyra); the protocol included (1) 3D, 1 mm isotropic fluid-attenuated inversion recovery; (2) 3D, 1 mm isotropic magnetization prepared rapid gradient echo; and (3) single-shell DW-MRI (resolution: 1.8 × 1.8 × 1.8 mm^3; 20 b-value = 1,000 seconds/mm^2 and 10 b-value = 0 seconds/mm^2).

WM lesions were identified automatically[105] and manually corrected. DW-MRI images were denoised and corrected for ringing artifacts, eddy current distortions, misaligning artifacts, and the bias field. Maps of fractional anisotropy (FA), radial diffusivity (RD), mean diffusivity (MD), and axial diffusivity (AD) were reconstructed with *MRtrix* (version: 3.0.3;

mrtrix.org/). Mean FA, RD, MD, and AD values were quantified in 7 regions of interest (ROIs), which were identified using the Johns Hopkins University DTI-based WM atlas[106]: the genu, body, and splenium of the corpus callosum (CC); the superior corona radiata, the posterior limb of internal capsule, cerebral peduncle, and the corticospinal tract (CST). DTI metrics were extracted after registering the DTI maps to the *MNI152* space. WM lesions were also registered to the *MNI152* space and used to exclude lesional tissue from the ROIs, limiting the analysis to the normal-appearing WM (NAWM).

A subgroup of patients with PIRMA was identified by assessing the absence of new/enlarging lesions during the 4-year follow-up.[107] Concomitant absence of contrast-enhancing lesions was also confirmed in cases where gadolinium was administered (86.7% of total scans).

Statistical Analysis

The statistical analysis was conducted in *R*.

DTI metrics were compared between patients with and without episodes of PIRA during clinical follow-up, after propensity score matching of the groups. Specifically, a full propensity score weighting was obtained using age, sex, disease duration, annualized relapse rate in the prior 2 years, use of disease-modifying therapies, and total WM lesion volume as criteria. Between-group differences were then assessed with linear regression models, including the weights obtained from propensity score matching. Results were corrected for multiple comparisons using the Benjamini-Hochberg false discovery rate.

In addition, we conducted 3 separate sensitivity analyses: (1) including EDSS as an additional criterion for propensity score matching; (2) including the lesion load in each ROI as an additional covariate in the regression models; and (3) restricting the PIRA group to the subset of patients with PIRMA.

Data Availability

The data supporting this study's findings are available on reasonable request.

Results

In total, 258 pwMS followed up between 2016 and 2022 were included in the study. Patients who had experienced PIRA during the preceding 4-year follow-up (n = 39) exhibited higher disability ($p < 0.001$) and T2-lesion load ($p = 0.01$) at MRI compared with those without, while

showing no significant differences in age, sex distribution, disease duration, relapse rate, and treatment regimen (Table 1).

Table 1 Demographic and Clinical Characteristics of Patients With and Without PIRA Before and After Matching

	Before matching			After matching		
	Patients with PIRA	Patients without PIRA	SMD	Patients with PIRA	Patients without PIRA	SMD
Main analysis						
Participants, n	39	219				
Age, mean (SD), y	50.3 (12.1)	48.0 (11.3)	0.19	50.3	49.9	0.03
Female, n (%)	29 (74.4)	140 (63.9)	0.24	(74.4)	(73.1)	0.03
Disease duration, mean (SD), y	18.8 (9.7)	16.5 (8.6)	0.24	18.8	18.4	0.04
ARR previous 2 y, median (IQR)	0 (0; 0)	0 (0; 0)	0.18	0 (0; 0)	0 (0; 0)	0.06
DMT class						
Platform, n (%)	2 (5.1)	20 (9.1)				
Oral, n (%)	17 (43.6)	115 (52.5)				
mAb, n (%)	14 (35.9)	62 (28.3)				
Untreated, n (%)	6 (15.4)	22 (10.0)				
T2-lesion volume, median (IQR), ml	9.3 (4.0; 24.5)	4.8 (1.4; 15.8)	0.31	9.3 (4.0; 24.2)	9.4 (2.1; 23.6)	−0.08
Sensitivity analysis including EDSS						
EDSS, median (IQR)	3.5 (2.75; 4.25)	2.0 (1.5; 3.0)	0.83	3.5 (2.5; 4.0)	3.5 (2.5; 4.5)	−0.08

Abbreviations: ARR = annualized relapse rate; DMT = disease-modifying therapy; EDSS = Expanded Disability Status Scale; IQR = interquartile range; mAb = monoclonal antibodies; PIRA = progression independent of relapse activity; SMD = standardized mean difference.
Platform treatments included glatiramer acetate and interferon preparations; oral treatments included cladribine, dimethyl fumarate, fingolimod, ozanimod, and teriflunomide; monoclonal antibody treatments included natalizumab, ocrelizumab, and rituximab.

Patients with PIRA displayed alterations in DTI metrics indicative of more severe WM damage than those without PIRA. Significant between-group differences were observed for FA in the genu of CC; RD in the genu and splenium of CC; MD in the genu of CC, splenium of CC, CST, and SCR; AD in the splenium of CC and CST (Figure).

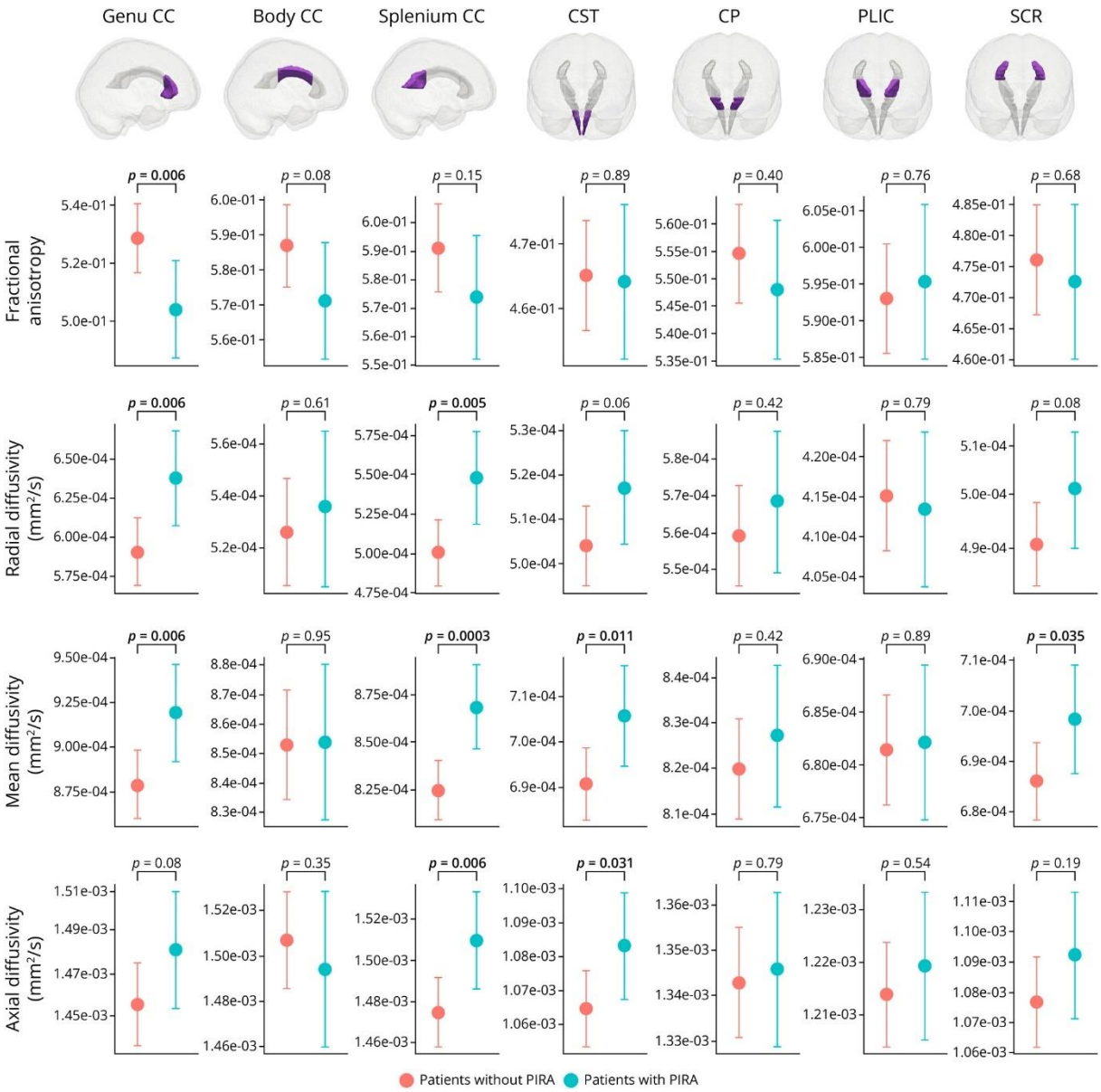

DTI metrics in each group are displayed as the estimated marginal mean (and associated 95% CI) derived from the regression models. Significant differences are presented in bold. CC = corpus callosum; CST = corticospinal tract; CP = cerebral peduncle; DTI = diffusion tensor imaging; PIRA = progression independent of relapse activity; PLIC = posterior limb of internal capsule; SCR = superior corona radiata.

Consistent results were observed in the sensitivity analyses (Table 2, eTables 1 and 2).

Table 2 Sensitivity Analysis: Comparisons of DTI Metrics Between Patients With and Without PIRMA

DTI metric	ROI	Patients with PIRMA (n = 19)	Patients without PIRMA (n = 219)	*p* Value
Fractional anisotropy	Genu CC	0.502 (0.480–0.524)	0.535 (0.521–0.548)	**0.0090**
	Body CC	0.568 (0.547–0.589)	0.586 (0.573–0.599)	0.2455
	Splenium CC	0.562 (0.537–0.587)	0.592 (0.577–0.608)	**0.0382**
	CST	0.457 (0.441–0.473)	0.457 (0.447–0.467)	0.9910
	CP	0.543 (0.528–0.558)	0.552 (0.543–0.561)	0.4788
	PLIC	0.594 (0.581–0.606)	0.589 (0.581–0.597)	0.6540
	SCR	0.469 (0.453–0.486)	0.471 (0.461–0.481)	0.8676
Radial diffusivity (mm^2/second)	Genu CC	$6.55*10^{-4}$ ($6.18*10^{-4}$–$6.91*10^{-4}$)	$5.91*10^{-4}$ ($5.69*10^{-4}$–$6.14*10^{-4}$)	**0.0024**
	Body CC	$5.54*10^{-4}$ ($5.16*10^{-4}$–$5.92*10^{-4}$)	$5.31*10^{-4}$ ($5.08*10^{-4}$–$5.54*10^{-4}$)	0.4650
	Splenium CC	$5.67*10^{-4}$ ($5.33*10^{-4}$–$6.01*10^{-4}$)	$4.98*10^{-4}$ ($4.78*10^{-4}$–$5.19*10^{-4}$)	**0.0003**
	CST	$5.18*10^{-4}$ ($5.02*10^{-4}$–$5.35*10^{-4}$)	$5.13*10^{-4}$ ($5.03*10^{-4}$–$5.23*10^{-4}$)	0.6540
	CP	$5.72*10^{-4}$ ($5.48*10^{-4}$–$5.96*10^{-4}$)	$5.62*10^{-4}$ ($5.47*10^{-4}$–$5.76*10^{-4}$)	0.6540
	PLIC	$4.13*10^{-4}$ ($4.02*10^{-4}$–$4.25*10^{-4}$)	$4.21*10^{-4}$ ($4.14*10^{-4}$–$4.28*10^{-4}$)	0.3826
	SCR	$5.01*10^{-4}$ ($4.86*10^{-4}$–$5.17*10^{-4}$)	$4.97*10^{-4}$ ($4.88*10^{-4}$–$5.06*10^{-4}$)	0.6540
Mean diffusivity (mm^2/second)	Genu CC	$9.37*10^{-4}$ ($9.04*10^{-4}$–$9.70*10^{-4}$)	$8.86*10^{-4}$ ($8.66*10^{-4}$–$9.06*10^{-4}$)	**0.0070**
	Body CC	$8.72*10^{-4}$ ($8.37*10^{-4}$–$9.07*10^{-4}$)	$8.60*10^{-4}$ ($8.38*10^{-4}$–$8.81*10^{-4}$)	0.6540
	Splenium CC	$8.83*10^{-4}$ ($8.57*10^{-4}$–$9.09*10^{-4}$)	$8.24*10^{-4}$ ($8.09*10^{-4}$–$8.40*10^{-4}$)	**<0.0001**
	CST	$7.02*10^{-4}$ ($6.88*10^{-4}$–$7.16*10^{-4}$)	$6.96*10^{-4}$ ($6.88*10^{-4}$–$7.05*10^{-4}$)	0.6540
	CP	$8.26*10^{-4}$ ($8.06*10^{-4}$–$8.46*10^{-4}$)	$8.22*10^{-4}$ ($8.10*10^{-4}$–$8.35*10^{-4}$)	0.7524
	PLIC	$6.80*10^{-4}$ ($6.71*10^{-4}$–$6.89*10^{-4}$)	$6.86*10^{-4}$ ($6.81*10^{-4}$–$6.92*10^{-4}$)	0.3634
	SCR	$6.95*10^{-4}$ ($6.81*10^{-4}$–$7.10*10^{-4}$)	$6.90*10^{-4}$ ($6.82*10^{-4}$–$6.99*10^{-4}$)	0.6540
Axial diffusivity (mm^2/second)	Genu CC	$1.50*10^{-3}$ ($1.46*10^{-3}$–$1.54*10^{-3}$)	$1.47*10^{-3}$ ($1.45*10^{-3}$–$1.50*10^{-3}$)	0.3634
	Body CC	$1.51*10^{-3}$ ($1.47*10^{-3}$–$1.55*10^{-3}$)	$1.52*10^{-3}$ ($1.49*10^{-3}$–$1.54*10^{-3}$)	0.7524
	Splenium CC	$1.52*10^{-3}$ ($1.49*10^{-3}$–$1.55*10^{-3}$)	$1.48*10^{-3}$ ($1.46*10^{-3}$–$1.49*10^{-3}$)	**0.0260**
	CST	$1.07*10^{-3}$ ($1.05*10^{-3}$–$1.09*10^{-3}$)	$1.06*10^{-3}$ ($1.05*10^{-3}$–$1.08*10^{-3}$)	0.6540
	CP	$1.34*10^{-3}$ ($1.31*10^{-3}$–$1.36*10^{-3}$)	$1.35*10^{-3}$ ($1.33*10^{-3}$–$1.36*10^{-3}$)	0.6540
	PLIC	$1.21*10^{-3}$ ($1.19*10^{-3}$–$1.23*10^{-3}$)	$1.22*10^{-3}$ ($1.21*10^{-3}$–$1.23*10^{-3}$)	0.7524
	SCR	$1.08*10^{-3}$ ($1.06*10^{-3}$–$1.11*10^{-3}$)	$1.08*10^{-3}$ ($1.06*10^{-3}$–$1.09*10^{-3}$)	0.7524

Abbreviations: CC = corpus callosum; CP = cerebral peduncle; CST = corticospinal tract; DTI = diffusion tensor imaging; PLIC = posterior limb of internal capsule; PIRMA= progression independent of relapse and MRI activity; ROI = regions of interest; SCR = superior corona radiata.
The estimates within each group are the marginal means (95% CIs) derived from the regression models. Reported *p* values are false discovery rate adjusted. Significant differences are presented in bold.

Discussion

Our study showed that pwMS experiencing PIRA exhibit increased damage in major WM tracts compared with counterparts without PIRA, matched for relevant demographic, clinical, and conventional MRI characteristics. Between-group differences were evident across all the examined DTI-derived quantitative maps, encompassing WM structures spanning both the CC and motor tracts.

DTI enables straightforward mathematical representation of diffusion signals, providing measures sensitive to tissue integrity at both macrostructural and microstructural levels. Although pathologic studies have reported associations between myelin content and FA, AD, and RD, as well as between MD and FA and axonal content,[74,75] inherent limitations of DTI—such as its inability to accurately represent complex tissue architecture—pose challenges in interpreting DTI metrics at the microstructural level. Nonetheless, DTI demonstrates good sensitivity to tissue injury associated with MS, with reported correlations between the severity of changes and both neurologic and cognitive disability.[108] Previous research has also indicated associations between DTI metrics and disability progression;[109] our study extends these findings by demonstrating that DTI is sensitive to the specific component of disability progression attributable to PIRA.

Our results collectively indicate microstructural damage in major WM tracts as a pathologic correlate of PIRA, adding to previously described findings of enhanced brain and spinal cord atrophy and nonresolving compartmentalized inflammation in PRLs.[25,26,35,36] The observed DTI changes suggest the potential involvement of neurodegenerative processes including Wallerian degeneration, in the NAWM of pwMS experiencing PIRA. The simultaneous increases in AD and RD point to co-occurring axonal and myelin damage, reflecting more extensive WM disruption in line with progressive neurodegeneration in MS. Remarkably, the pattern of NAWM damage was confirmed in the subgroup of patients with PIRMA, where any detectable focal inflammatory activity was excluded.

Our study has some limitations. First, although our focus was on a clinically compatible MRI approach, the use of DTI may introduce challenges in interpreting findings at the microstructural level, particularly in areas with crossing tracts. To mitigate this bias, we restricted our analyses to major WM tracts with a single predominant orientation. Second, DTI metrics were available for a single time-point after the 4-year follow-up, which was defined a priori as a plausible time interval to assess the relationship between PIRA occurrence and DTI

alterations.[35] Third, although our cohort consisted of patients with a typical RRMS course, their relatively long disease duration precluded the investigation of WM degeneration in early stages of the disease.

In conclusion, our findings demonstrated that patients with PIRA are characterized by significant degeneration of major WM tracts, which can be identified using a clinically compatible DTI protocol.

6. Advanced Quantitative MRI Unveils Microstructural Thalamic Changes Reflecting Disease Progression in Multiple Sclerosis

Authors: Alessandro Cagol, MD, Mario Ocampo-Pineda, PhD, Po-Jui Lu, PhD, Matthias Weigel, PhD, Muhamed Barakovic, PhD, Lester Melie-Garcia, PhD, Xinjie Chen, MD, Antoine Lutti, PhD, Pasquale Calabrese, PhD, Jens Kuhle, MD, PhD, Ludwig Kappos, MD, Maria Pia Sormani, PhD, and Cristina Granziera, MD, PhD

Affiliations: From the Translational Imaging in Neurology (ThINk) Basel (A.C., M.O.-P., P.-J.L., M.W., M.B., L.M.-G., X.C., L.K., C.G.), Department of Biomedical Engineering, Faculty of Medicine, University Hospital Basel and University of Basel; Department of Neurology (A.C., M.O.-P., P.-J.L., M.W., M.B., L.M.-G., X.C., J.K., L.K., C.G.), University Hospital Basel; Research Center for Clinical Neuroimmunology and Neuroscience Basel (RC2NB) (A.C., M.O.-P., P.-J.L., M.W., M.B., L.M.-G., X.C., J.K., L.K., C.G.), University Hospital Basel and University of Basel, Switzerland; Dipartimento di Scienze della Salute, (A.C., M.P.S.), Universit`a degli Studi di Genova, Italy; Division of Radiological Physics (M.W.), Department of Radiology, University Hospital Basel; Laboratory for Research in Neuroimaging (A.L.), Department of Clinical Neuroscience, Lausanne University Hospital and University of Lausanne; Neuropsychology and Behavioral Neurology Unit (P.C.), Division of Cognitive and Molecular Neuroscience, University of Basel, Switzerland; and IRCCS Ospedale Policlinico San Martino (M.P.S.), Genova, Italy.

Published in: Neurol Neuroimmunol Neuroinflamm 2024;11:e200299. doi:10.1212/NXI.0000000000200299

Abstract

Background and Objectives: In patients with multiple sclerosis (PwMS), thalamic atrophy occurs during the disease course. However, there is little understanding of the mechanisms

leading to volume loss and of the relationship between microstructural thalamic pathology and disease progression. This cross-sectional and longitudinal study aimed to comprehensively characterize in vivo pathologic changes within thalamic microstructure in PwMS using advanced multiparametric quantitative MRI (qMRI).

Methods: Thalamic microstructural integrity was evaluated using quantitative T1, magnetization transfer saturation, multishell diffusion, and quantitative susceptibility mapping (QSM) in 183 PwMS and 105 healthy controls (HCs). The same qMRI protocol was available for 127 PwMS and 73 HCs after a 2-year follow-up period. Inclusion criteria for PwMS encompassed either an active relapsing-remitting MS (RRMS) or inactive progressive MS (PMS) disease course. Thalamic alterations were compared between PwMS and HCs and among disease phenotypes. In addition, the study investigated the relationship between thalamic damage and clinical and conventional MRI measures of disease severity.

Results: Compared with HCs, PwMS exhibited substantial thalamic alterations, indicative of microstructural and macrostructural damage, demyelination, and disruption in iron homeostasis. These alterations extended beyond focal thalamic lesions, affecting normal-appearing thalamic tissue diffusely. Over the follow-up period, PwMS displayed an accelerated decrease in myelin volume fraction [mean difference in annualized percentage change (MD-ApC) = −1.50; $p = 0.041$] and increase in quantitative T1 (MD-ApC = 0.92; $p < 0.0001$) values, indicating heightened demyelinating and neurodegenerative processes. The observed differences between PwMS and HCs were substantially driven by the subgroup with PMS, wherein thalamic degeneration was significantly accelerated, even in comparison with patients with RRMS. Thalamic qMRI alterations showed extensive correlations with conventional MRI, clinical, and cognitive disease burden measures. Disability progression over follow-up was associated with accelerated thalamic degeneration, as reflected by enhanced diffusion ($\beta = -0.067$; $p = 0.039$) and QSM ($\beta = -0.077$; $p = 0.027$) changes. Thalamic qMRI metrics emerged as significant predictors of neurologic and cognitive disability even when accounting for other established markers including white matter lesion load and brain and thalamic atrophy.

Discussion: These findings offer deeper insights into thalamic pathology in PwMS, emphasizing the clinical relevance of thalamic damage and its link to disease progression. Advanced qMRI biomarkers show promising potential in guiding interventions aimed at mitigating thalamic neurodegenerative processes.

Introduction

Gray matter pathology is prominent in patients with multiple sclerosis (PwMS), with degenerative processes initiating early in the disease course and correlating with clinical disability and cognitive performance.[16,110] Among gray matter structures, the thalamus plays a pivotal role, serving as a relay and integration center within the CNS. In PwMS, the thalamus is distinctively affected, because of the complex interplay between heterogeneous pathophysiologic mechanisms.[78] Inflammatory processes can directly cause thalamic damage, leading to the development of focal demyelinating lesions.[78,111] Thalamic damage can also occur indirectly due to pathologic processes involving the white matter, where axonal transection in white matter lesions can trigger retrograde, anterograde, and trans-synaptic degeneration, ultimately resulting in thalamic neuronal loss.[11,78] Besides, an increasingly recognized mechanism contributing to thalamic pathology is the damage following a distinctive "surface-in" pattern, hypothesized to be triggered by soluble inflammatory factors contained in the CSF.[112–115] Finally, oxidative stress, mitochondrial dysfunction, and disturbances in iron homeostasis contribute to thalamic degeneration.[78,116,117]

Quantification of thalamic damage in multiple sclerosis has been the focus of extensive research, primarily through the measurement of thalamic volume, which exhibits consistent loss across disease phases and closely correlates with neurologic disability and cognitive impairment.[78–80,118] While other neuroimaging techniques such as MR spectroscopy and quantitative MRI (qMRI) approaches have also been used,[78,119–121] our understanding of the microstructural alterations accumulating in the thalamus of PwMS, particularly in relation to disease progression, remains limited. To comprehensively characterize thalamic tissue damage in PwMS and its accumulation across different disease phases, we conducted a multiparametric qMRI study. Our investigation leveraged quantitative T1-relaxometry (qT1) for a comprehensive assessment of tissue microstructural and macrostructural integrity,[50,51] myelin volume fraction (MVF) as a proxy measure of tissue myelin and macromolecular content,[50,122] neurite density index (NDI) as a surrogate measure of axon and dendrite density,[123] and quantitative susceptibility mapping (QSM) to characterize changes in iron homeostasis and myelin damage.[50] Thalamic atrophy, serving as a marker of the overall accumulation of thalamic neurodegenerative processes, was also measured.

We investigated thalamic microstructural damage and its accumulation over time, by performing a prospective, cross-sectional, and longitudinal study. Pathologic changes were investigated in both focal lesions and the "normal-appearing" tissue, by comparing PwMS with

a reference group of healthy controls (HCs). Thalamic alterations associated with different disease phases were examined by comparing 2 subgroups of patients, one with active relapsing-remitting MS (RRMS) and another with inactive progressive MS (PMS), specifically selected to represent the opposing ends of the clinical spectrum. In addition, we investigated the relationship between qMRI measures of thalamic integrity and their rate of change over time with (1) conventional MRI markers of disease burden and (2) clinical measures of neurologic disability and cognitive impairment.

Methods

Participants

Participants were prospectively recruited at the University Hospital of Basel between 2018 and 2022, as part of the INsIDER study (NCT05177523). Inclusion criteria for patients were as follows: (1) age between 18 and 80 years; (2) diagnosis of MS fulfilling the 2017 revised McDonald criteria[124]; (3) disease course either active relapsing-remitting (with ≥1 relapse and/or ≥1 gadolinium-enhancing lesion during the year before enrollment) or nonactive primary/secondary progressive (without relapses and MRI activity during the year before enrollment); (4) absence of neurologic or psychiatric comorbidities. HCs were volunteers aged between 18 and 80 years, with a medical history negative for neurologic or psychiatric disorders. Exclusion criteria for patients and controls encompassed pregnancy, contraindication to MRI, and inability to provide consent. This study follows the STROBE guideline for reporting observational studies.[125]

A total of 183 PwMS and 105 HCs met the inclusion criteria. At baseline, all underwent a brain MRI scan, with additional neurologic examination for PwMS and cognitive assessment for a subset of 99 PwMS and 100 HCs. 127 PwMS and 73 HCs volunteered to undergo a second brain MRI scan after a period of 2 years (±3 months), with the same acquisition protocol. Concurrent neurologic follow-up was obtained for PwMS. The study design is presented in Figure 1.

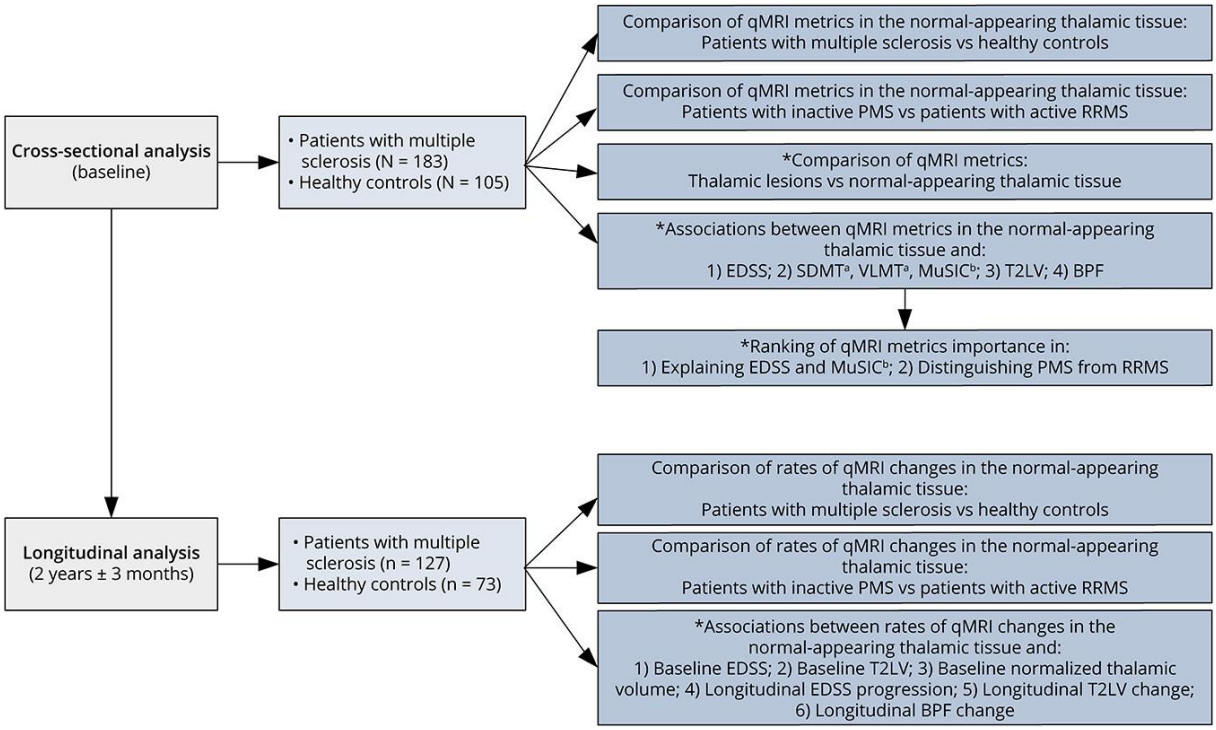

Figure 1 *Study Design*

**Analyses performed in the group of patients with multiple sclerosis only. [a]Available in 99 patients with multiple sclerosis and 100 healthy controls. [b]Available in 98 patients with multiple sclerosis and 100 healthy controls. BPF = brain parenchymal fraction; EDSS = Expanded Disability Status Scale; MuSIC = Multiple Sclerosis Inventory Cognition; PMS = progressive multiple sclerosis; qMRI = quantitative MRI; RRMS = relapsing-remitting multiple sclerosis; SDMT = Symbol Digit Modalities Test; T2LV = T2-hyperintense lesion volume; VLMT = Verbal Learning and Memory Test.*

Clinical Assessment

The neurologic examination for PwMS included the calculation of the Expanded Disability Status Scale (EDSS) score, by certified raters (*neurostatus.net/*).[126]

Cognitive performance was assessed using (1) the oral version of the Symbol Digit Modalities Test (SDMT),[127] (2) the Verbal Learning and Memory Test (VLMT),[128] and (3) the Multiple Sclerosis Inventory Cognition (MuSIC)[129] test. SDMT and VLMT scores were converted to z-scores,[127,128] and the MuSIC score was corrected for age and sex.[129]

MRI Acquisition

All brain MRI scans were obtained with the same acquisition protocol on a 3T whole-body MR system (*Magnetom Prisma, Siemens Healthineers*), using a 64-channel phased-array head and neck coil for radio-frequency reception. The MRI protocol included the following: (1) 3D fluid-attenuated inversion recovery (FLAIR) [TR/TE/TI = 5,000/386/1,800 ms; resolution = 1 × 1 ×

1 mm^3]; (2) 3D magnetization-prepared 2 rapid gradient-echo (MP2RAGE) [TR/TI1/TI2 = 5,000/700/2,500 ms; resolution = 1 × 1 × 1 mm^3]; (3) multishell diffusion (TR/TE/δ/Δ = 4,500/75/19/36 ms; resolution = 1.8 × 1.8 × 1.8 mm^3; b-values 0/700/1,000/2,000/3,000 s/mm^2 with 12/6/20/45/66 measurements, respectively, per shell; diffusion acquisition with 12 measurements of b-value 0 s/mm^2 with reversed phase encoding); (4) 3D segmented echo planar imaging (EPI) [TR/TE = 64/35 ms; resolution = 0.67 × 0.67 × 0.67 mm^3]; (5) three 3D radio-frequency spoiled gradient-echo acquisitions with predominantly magnetization transfer–weighted (TR/α = 25 ms/5°), proton density–weighted (TR/α = 25 ms/5°), and T1-weighted (TR/α = 11 ms/15°) contrasts, used to obtain magnetization transfer saturation (MTsat) maps (resolution = 1.33 × 1.33 × 1.33 mm^3).[130]

MRI Processing

qT1 maps were obtained from MP2RAGE images as previously described.[130,131] MTsat maps were computed as previously proposed,[132,133] and MVF was then estimated by multiplying the MTsat signal by a calibration constant (α).[134,135] Diffusion images were denoised and corrected for motion, eddy currents, and susceptibility-induced distortions; microscopic diffusion processes were then modeled using the spherical mean technique (SMT) to obtain NDI, a proxy measure of the signal originating from axons and dendrites.[123] SMT was preferred over alternative approaches such as neurite orientation dispersion and density imaging (NODDI), given its effectiveness in addressing challenges posed by fiber crossing populations and orientation dispersion, which are particularly prominent within gray matter regions.[123] QSM was reconstructed from 3D EPI images using the morphology enabled dipole inversion algorithm to compute the susceptibility from the local field, with ventricular CSF used as the zero reference.[136]

MRI Analysis

In PwMS, T2-hyperintense lesions were detected with a deep learning–based tool[36]; the resulting masks were manually corrected and used to estimate total T2-hyperintense lesion volume (T2LV).

FIRST[137] was applied on MP2RAGE images to obtain an initial reference for thalamic segmentation, and the automatic output was manually refined following the previously proposed protocol for the manual segmentation of the thalamus.[138] In PwMS, a mask of T2-hyperintense lesions contained within the thalamus was obtained by intersecting the lesion mask (registered to the MP2RAGE space) with the thalamic mask. Thalamic lesions were then

subtracted from thalamic masks to obtain a segmentation of normal-appearing thalamic tissue. For each thalamic lesion, we investigated the morphology and the presence of a central vein or a paramagnetic rim (eMethods).

Thalamus optimized multi atlas segmentation (THOMAS) was used to segment the thalamus into 12 nuclei.[139] In addition, the thalamus was partitioned into 3 bands having increasing distance from the CSF, to explore the "ependymal-in" gradient of damage. The 3 bands were identified by performing progressive expansions of a CSF mask (after a 1-mm erosion at the thalamus-CSF and thalamus-internal capsule boundaries, to reduce partial volume effect).

MVF, NDI, and QSM maps were linearly registered to the MP2RAGE space using *FLIRT*, and the results were visually inspected. The transformation matrices obtained in the process were then used to move the regions of interest (i.e., thalamic lesions and normal-appearing tissue, segmented on the MP2RAGE space) back to the original MVF, NDI, and QSM spaces. For all regions and contrasts of interest, the mean intensity values were extracted in the original space using *fslstats*. For thalamic lesions, qMRI metrics were extracted exclusively in lesions with volume ≥10 mm^3.

Total brain volume and total intracranial volume (TIV) were measured with *SAMSEG.*[140] Brain parenchymal fraction (BPF) was calculated as the ratio between total brain volume and TIV; similarly, normalized thalamic volume was estimated as the ratio between thalamic volume and TIV.

Statistical Analysis

All statistical analyses were performed with R (version 4.2.1; R Core Team, 2022). The threshold of statistical significance was set at $p < 0.05$.

Demographic, clinical, and MRI variables were compared between groups using the Welch *t*-test, Mann-Whitney *U* test, Pearson χ^2 test, and linear regression models, as appropriate.

qMRI measures in the normal-appearing thalamic tissue were compared cross-sectionally, at baseline, between (1) PwMS and HCs and (2) patients with inactive PMS and patients with active RRMS. Comparisons were performed with general linear models, adjusting for age and sex. Differences in qMRI measures were also explored regionally, both in thalamic nuclei and in the 3 bands having increasing distance from the CSF; the results were corrected for multiple comparisons with the false discovery rate approach, using the Benjamini-Hochberg method.

To characterize the microstructural damage within T2-hyperintense thalamic lesions, we compared the qMRI metrics measured within the lesions with those obtained in a 2-voxel area of perilesional normal-appearing tissue. The comparison was performed using the Wilcoxon signed-rank test.

In PwMS, general linear models were used to explore the association of qMRI measures in the normal-appearing thalamic tissue with clinical and conventional MRI features, including (1) neurologic disability, as assessed with the EDSS; (2) cognitive impairment, as assessed with the SDMT, VLMT, and MuSIC test; (3) burden of T2-hyperintense lesion volume (T2LV); and (4) BPF. The relative importance of the different qMRI thalamic measures—together with T2LV and BPF—in (1) explaining neurologic disability (as measured with the EDSS), (2) explaining multidomain cognitive performance (as measured with the MuSIC score), and (3) distinguishing between progressive and relapsing-remitting phenotypes was ranked using multivariable least absolute shrinkage and selection operator (LASSO) regression models. We performed 10-fold cross-validation to select the optimal regularization parameter (lambda). For each patient, we calculated the deviation of the thalamic qMRI metrics (and the BPF) from the HC population, accounting for age and sex. Specifically, we fitted a linear regression in HCs with the MRI measure as the dependent variable and age and sex as independent variables. The deviation from the regression line (residual of the fit) of each MRI measure in PwMS was the variable entered in the LASSO models.[141]

Longitudinal changes in thalamic qMRI metrics were quantified with mixed-effect models, using the qMRI measurements at each given time point as dependent variables. Models included time (to estimate the rate of change), age at baseline, and sex as covariates and a random intercept for participants. To estimate annual percentage change from the slope over time, the qMRI metrics were log-transformed. Comparisons in the rates of change between (1) PwMS and HCs and (2) patients with inactive PMS and patients with active RRMS were performed by introducing in the mixed-effect models the interaction term between the group and time. Similarly, the association between the rates of qMRI change and (1) baseline EDSS, (2) baseline T2LV, (3) baseline normalized thalamic volume, (4) disease activity over follow-up, (5) EDSS progression over follow-up, (6) change in T2LV over follow-up, and (7) change in BPF over follow-up was explored by introducing in the mixed-effect models the interaction term between the variables of interest and time. EDSS progression was defined as an increase in the EDSS score of ≥1.5 points if the baseline EDSS score was 0, ≥1.0 points if the baseline EDSS score was 1.0–5.5, or ≥0.5 points if the baseline EDSS score was greater than 5.5.[43] Mixed-effect

models were also used to investigate baseline demographic, clinical, and MRI predictors of subsequent thalamic atrophy.

Sensitivity analyses were conducted to (1) exclude a significant impact of partial volume effect on the estimations of thalamic qMRI measures (by comparing the qMRI values derived with the original thalamic masks with those obtained with thalamic masks that underwent a 1-voxel erosion process); (2) compare the estimations of NDI obtained with SMT with those derived from NODDI; (3) explore between-group differences in thalamic microstructure accounting for treatment effect and presence of disease activity over the follow-up; (4) explore between-group differences in subgroups matched for age and sex; and (5) investigate regional microstructural changes in thalamic nuclei defined with a different probabilistic atlas (as implemented in FreeSurfer; eFigures 1–5).

Additional analyses were conducted to explore (1) between-group differences in thalamic measures of orientation dispersion index (ODI) and isotropic volume fraction (ISOVF) derived with NODDI (eTables 1–4); (2) the extent of microstructural changes as a function of the distance from the CSF (eFigure 6); (3) the correlation between different thalamic qMRI metrics (eFigure 7); (4) the impact of T2-hyperintense lesion burden specifically within thalamocortical bundles as a proxy for thalamic disconnectivity (eTables 5–9); and (5) the relative importance of demographic, clinical, and conventional MRI measures and the global and regional thalamic qMRI metrics explored in the study, in explaining clinical outcomes using random forests (eFigures 8–10). Further methodological details are available in eMethods.

Standard Protocol Approvals, Registrations, and Patient Consents

Study approval was obtained from the local ethics committee (IRM of Northwest Switzerland); informed consent was obtained from all participants before study entry.

Data Availability

The data that support the findings of this study are available on reasonable request.

Results

The main cohort's demographic, clinical, and MRI characteristics are summarized in Table 1. Baseline characteristics of patients undergoing clinical and MRI follow-up are reported in eTable 10. The qMRI contrasts included in the study are illustrated in Figure 2.

Table 1 Baseline Demographic, Clinical, and Conventional MRI Characteristics of the Cohort

	Healthy controls	Patients with active RRMS	Patients with inactive PMS	*p* Values
n	105	101	82	—
Female/male	58/47	66/35	44/38	RRMS vs HCs: 0.18[a]
				PMS vs HCs: 0.95[a]
				PMS vs RRMS: 0.15[a]
Mean (SD) [range] age, y	37.8 (13.0) [18.1–69.0]	37.6 (10.9) [18.3–62.8]	58.1 (9.5) [36.9–77.2]	RRMS vs HCs: 0.92[b]
				PMS vs HCs: <0.001[b]
				PMS vs RRMS: <0.001[b]
Median [IQR] disease duration, y	—	2.5 [0.6–9.3]	15.4 [8.0–25.0]	RRMS vs HCs:/
				PMS vs HCs:/
				PMS vs RRMS: <0.001[c]
Disease-modifying therapy	—			
Platform, n (%)		3 (3)	4 (5)	RRMS vs HCs:/
Oral, n (%)		36 (36)	15 (18)	PMS vs HCs:/
Monoclonal antibodies, n (%)		50 (50)	48 (59)	PMS vs RRMS: <0.001[a]
Untreated, n (%)		12 (12)	15 (18)	
Median [IQR] EDSS score	—	2.0 [1.5–2.5]	5.0 [4.0–6.0]	RRMS vs HCs:/
				PMS vs HCs:/
				PMS vs RRMS: < 0.001[c]
Mean (SD) SDMT z-score*	0.55 (1.16)	0.29 (1.15)	−0.49 (1.50)	RRMS vs HCs: 0.19[b]
				PMS vs HCs: <0.001[b]
				PMS vs RRMS: 0.004[b]
Mean (SD) VLMT z-score*	1.00 (1.17)	0.89 (1.06)	0.08 (1.08)	RRMS vs HCs: 0.57[b]
				PMS vs HCs: <0.001[b]
				PMS vs RRMS: <0.001[b]
Mean (SD) MuSIC score**	27.0 (3.5)	25.9 (4.6)	19.5 (6.4)	RRMS vs HCs: 0.10[b]
				PMS vs HCs: <0.001[b]
				PMS vs RRMS: <0.001[b]
Mean (SD) BPF	0.74 (0.02)	0.73 (0.02)	0.69 (0.03)	RRMS vs HCs: 0.005[d]
				PMS vs HCs: <0.001[d]
				PMS vs RRMS: <0.001[d]
Median [IQR] T2LV, ml	0.0 [0.0–0.2]	4.0 [1.2–10.3]	12.6 [5.8–26.8]	RRMS vs HCs: <0.001[c]
				PMS vs HCs: <0.001[c]
				PMS vs RRMS: <0.001[c]

Abbreviations: BPF = brain parenchymal fraction; EDSS = Expanded Disability Status Scale; IQR = interquartile range; MuSIC = Multiple Sclerosis Inventory and Cognition; PMS = progressive multiple sclerosis; PPMS = primary progressive multiple sclerosis; RRMS = relapsing-remitting multiple sclerosis; SDMT = Symbol Digit Modalities Test; SPMS = secondary progressive multiple sclerosis; VLMT = Verbal Learning and Memory Test.
[a] Chi-square test.
[b] Welch *t*-test.
[c] Mann-Whitney *U* test.
[d] General linear model, age and sex-adjusted. *Available in 100 healthy controls and 99 patients with multiple sclerosis. **Available in 100 healthy controls and 98 patients with multiple sclerosis. Platform disease-modifying therapies included glatiramer acetate and interferon-beta preparations; oral disease-modifying therapies included dimethyl fumarate, fingolimod, siponimod, and teriflunomide; monoclonal antibody disease-modifying therapies included natalizumab, ocrelizumab, and rituximab.

Owing to insufficient image quality, data from 5 PwMS for MVF analysis and 3 PwMS for NDI analysis were excluded.

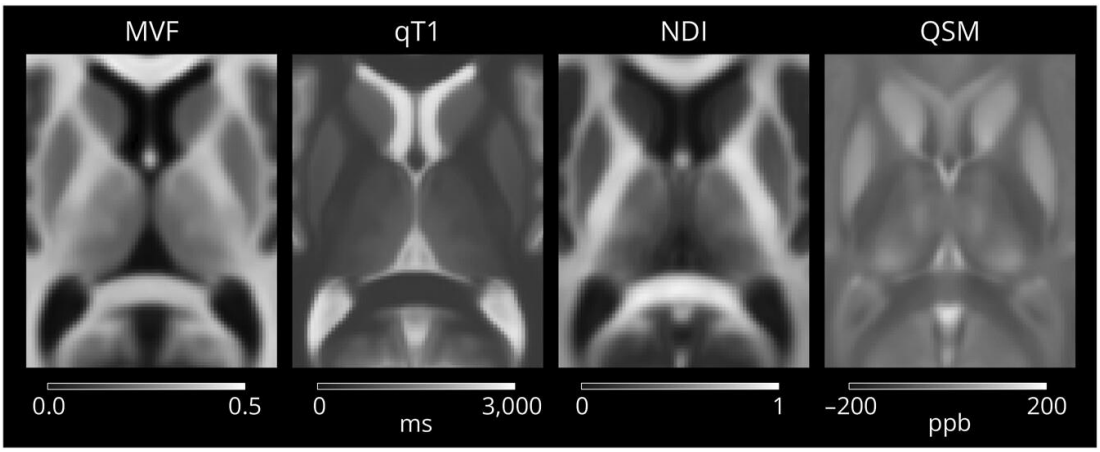

Figure 2 *qMRI Contrasts Included in the Study*

The images displayed were obtained by averaging data from all healthy controls included in the study, after nonlinear registration to the MNI152 template. MP2RAGE = magnetization-prepared 2 rapid gradient-echo; MVF = myelin volume fraction; NDI = neurite density index; QSM = quantitative susceptibility mapping; qT1 = quantitative T1-relaxometry.

Thalamic qMRI Metrics at Baseline

PwMS vs HCs

At baseline, PwMS had reduced thalamic volume ($\beta = -0.232$; $p < 0.0001$) compared with HCs. In addition, in the normal-appearing thalamic tissue, PwMS displayed decreased MVF ($\beta = -0.120$; $p = 0.032$) and QSM ($\beta = -0.138$; $p = 0.013$) values, along with increased qT1 values ($\beta = 0.145$; $p = 0.016$); no difference in NDI values was observed between groups (Figure 3).

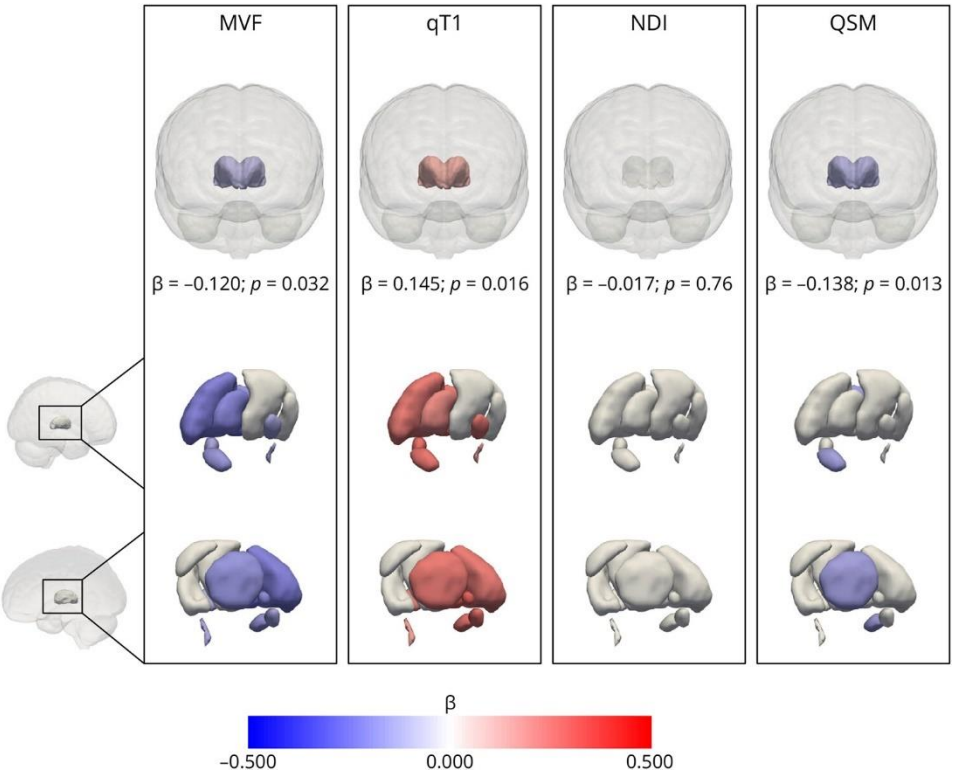

Figure 3 *Comparisons in Thalamic qMRI Metrics Between Patients With Multiple Sclerosis and Healthy Controls at Baseline (in the Entire Thalamus and Thalamic Nuclei). The difference between groups is graphically displayed on a segmentation of the thalamus, with colors reflecting the effect size (expressed in terms of standardized regression coefficient, β). Only differences reaching statistical significance are displayed. MVF = myelin volume fraction; NDI = neurite density index; QSM = quantitative susceptibility mapping; qT1 = quantitative T1-relaxometry.*

The greatest between-group difference in MVF, QSM, and qT1 values was evident in the thalamic area closest to the CSF (Figure 4). Graphical representations of between-group comparisons at the thalamic nuclei level are displayed in Figure 3 and eFigure 11 while a comprehensive description of the results is reported in eTables 11–12.

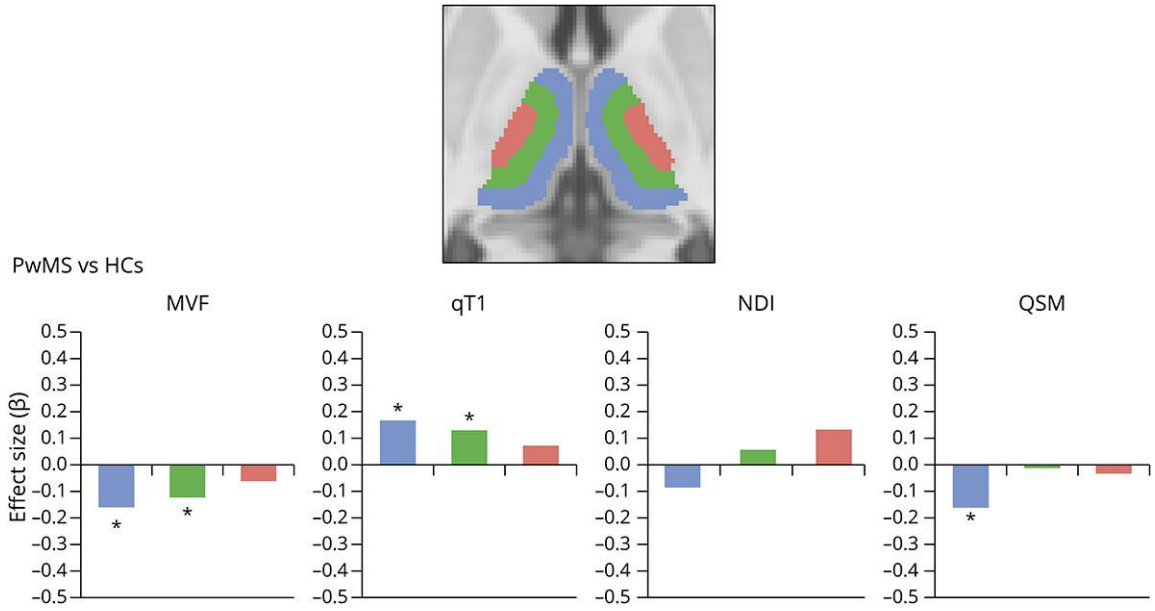

Figure 4 *Between-Group Comparisons in Thalamic qMRI Metrics in the 3 Bands Presenting Increasing Distance From the CSF. The 3 bands are associated with different colors, graphically displayed in the panel on top. The height of the bars reflects the magnitude of the effect size (β) of the between-group comparisons. *p < 0.05; **p < 0.01; ***p < 0.001. HCs = healthy controls; MS = multiple sclerosis; MVF = myelin volume fraction; NDI = neurite density index; QSM = quantitative susceptibility mapping; qT1 = quantitative T1-relaxometry.*

The differences in thalamic qMRI measures between PwMS and HCs were mainly driven by the subset of patients with inactive PMS (Figure 5). While patients with active RRMS differed from HCs only in thalamic volume ($\beta = -0.145$; $p = 0.015$), patients with inactive PMS differed from HCs in thalamic volume ($\beta = -0.490$; $p < 0.0001$), MVF ($\beta = -0.328$; $p < 0.0001$), qT1 ($\beta = 0.324$; $p < 0.0001$), and QSM ($\beta = -0.258$; $p = 0.0005$) values. Patients with inactive PMS also showed significant differences in thalamic volume ($\beta = -0.356$; $p < 0.0001$), MVF ($\beta = -0.310$; $p < 0.0001$), qT1 ($\beta = 0.270$; $p = 0.0007$), and QSM ($\beta = -0.183$; $p = 0.013$) values compared with patients with active RRMS. The most substantial differences between patients with inactive PMS and patients with active RRMS were observed in the thalamic region close to the CSF for MVF and qT1 and in the central thalamic area for QSM (eFigure 12).

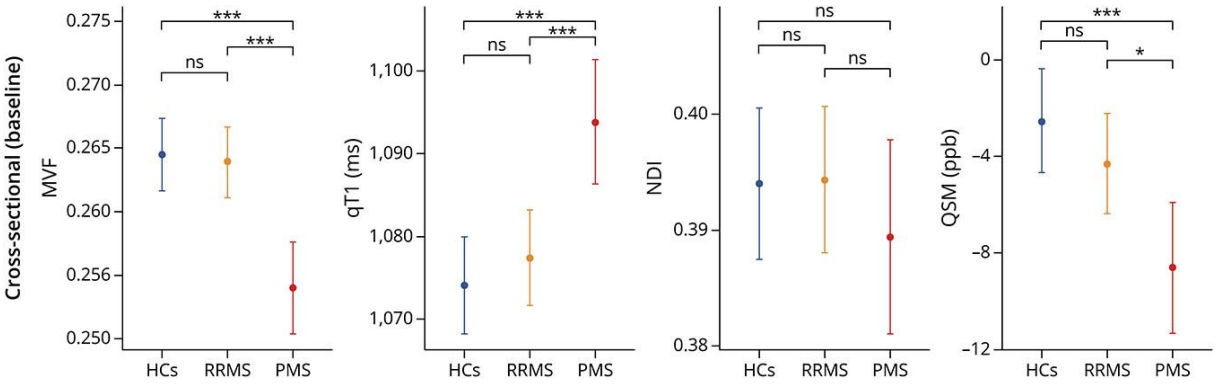

Figure 5 *Between-Group Comparisons of Baseline Thalamic qMRI Metrics. *p < 0.05; **p < 0.01; ***p < 0.001. HCs = healthy controls; MVF = myelin volume fraction; NDI = neurite density index; PMS = progressive multiple sclerosis; QSM = quantitative susceptibility mapping; qT1 = quantitative T1-relaxometry; RRMS = relapsing-remitting multiple sclerosis.*

Thalamic Lesions vs Normal-Appearing Thalamic Tissue

T2-hyperintense thalamic lesions were identified in 66 PwMS. The proportion of patients presenting with thalamic lesions was not statistically different between PMS and RRMS groups (43% vs 31%; $p = 0.09$). Of 112 observed thalamic lesions, 92 were discrete ovoid lesions and 20 were more diffuse periventricular lesional areas. 51.1% of thalamic lesions exhibited the central vein sign, with a higher prevalence in ovoid lesions compared with periventricular lesions (57.4% vs 30.0%; $p = 0.031$). No lesions displayed a paramagnetic rim (eTable 13). The distribution of lesions across different thalamic nuclei is detailed in eTable 14. Compared with the normal-appearing perilesional tissue, thalamic lesions exhibited reduced MVF and NDI and increased qT1 values (all $p < 0.0001$). No differences were measured in QSM values between thalamic lesions and the perilesional normal-appearing tissue (eTable 15).

Association Between Thalamic qMRI Measures and Clinical/MRI Features in PwMS

Thalamic volume was associated with the EDSS score ($\beta = -0.471$; $p < 0.0001$), cognitive performance in all tests considered in the study (SDMT: $\beta = 0.345$; $p = 0.0002$; VLMT: $\beta = 0.300$; $p = 0.0009$; MuSIC: $\beta = 0.461$; $p < 0.0001$), T2LV ($\beta = -0.650$; $p < 0.0001$), and BPF ($\beta = 0.824$; $p < 0.0001$).

Various associations with clinical and conventional MRI measures were evident also for qMRI measures of microstructural integrity within the normal-appearing thalamic tissue. Specifically, MVF was associated with the EDSS score ($\beta = -0.246$; $p = 0.0009$), MuSIC score ($\beta = 0.307$; $p = 0.004$), T2LV ($\beta = -0.249$; $p = 0.0007$), and BPF ($\beta = 0.361$; $p < 0.0001$); qT1 was associated with the EDSS score ($\beta = 0.198$; $p = 0.007$), SDMT ($\beta = -0.193$; $p = 0.036$), MuSIC score ($\beta =$

−0.197; p = 0.034), T2LV (β = 0.229; p = 0.002), and BPF (β = −0.317; p < 0.0001); NDI was associated with the EDSS score (β = −0.198; p = 0.008) and BPF (β = 0.188; p = 0.012); QSM was associated with the EDSS score (β = −0.224; p = 0.002), T2LV (β = −0.248; p = 0.0007), and BPF (β = 0.312; p < 0.0001) (eTable 16).

In the LASSO regression models, the variables selected as predictors of the EDSS score, in order of importance, were BPF (β = −0.382), T2LV (β = 0.155), thalamic MVF (β = −0.051), thalamic QSM (β = −0.022), and thalamic NDI (β = −0.012) [R^2 of the model: 0.296]; the variables selected as predictors of the MuSIC score, in order of importance, were BPF (β = 0.262), normalized thalamic volume (β = 0.100), and thalamic MVF (β = 0.031) [R^2 of the model: 0.248]; in the model for discrimination between PMS and RRMS, the selected features, in order of importance, were BPF (odds ratio [OR] = 0.356), thalamic MVF (OR = 0.712), T2LV (OR = 1.231), normalized thalamic volume (OR = 0.783), and thalamic NDI (OR = 0.876) [area under the curve of the model: 0.836].

Longitudinal Thalamic qMRI Changes

PwMS vs HCs

During the 2-year follow-up, PwMS had accelerated thalamic atrophy compared with HCs [mean difference in annualized percentage change (*MD-ApC*): −0.88 (95% CI −1.56 to −0.20); p = 0.013]. PwMS also exhibited an accelerated rate of i) decrease in thalamic MVF values [*MD-ApC*: −1.50 (95% CI −2.91 to −0.07); p = 0.041] and ii) increase in qT1 values [*MD-ApC*: 0.92 (95% CI 0.54–1.30); p < 0.0001].

Compared with HCs, patients with active RRMS had an accelerated rate of increase in qT1 values [*MD-ApC*: 0.74 (95% CI 0.33–1.15); p = 0.0005]; the difference in thalamic atrophy rates approached but did not reach statistical significance [*MD-ApC*: −0.71 (95% CI −1.46 to 0.04); p = 0.066]. Compared with HCs, patients with inactive PMS had accelerated thalamic atrophy [*MD-ApC*: −1.20 (95% CI −2.07 to −0.32); p = 0.008], as well as accelerated rates of decrease in thalamic MVF values [*MD-ApC*: −2.52 (95% CI −4.28 to −0.72); p = 0.007] and increase in thalamic qT1 values [*MD-ApC*: 1.24 (95% CI 0.76–1.73); p < 0.0001]. Patients with inactive PMS had accelerated rates of qT1 increase also when compared with patients with active RRMS [*MD-ApC*: 0.50 (95% CI 0.03–0.97); p = 0.039]. No differences in the rates of change between groups were measured in the other thalamic qMRI metrics (Figure 6).

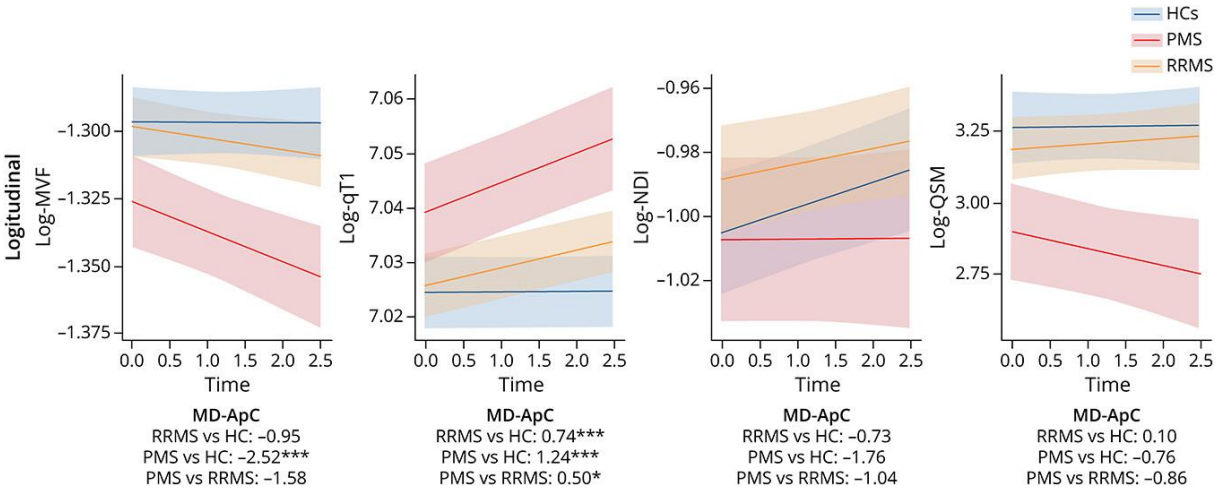

Figure 6 *Between-Group Comparisons of Longitudinal Thalamic qMRI Metric Changes. *p < 0.05; **p < 0.01; ***p < 0.001. HCs = healthy controls; MD-APC: mean difference in annual percentage change; MS = multiple sclerosis; MVF = myelin volume fraction; NDI = neurite density index; PMS = progressive multiple sclerosis; RRMS = relapsing-remitting multiple sclerosis; QSM = quantitative susceptibility mapping; qT1 = quantitative T1-relaxometry.*

Association Between Quantitative Thalamic Changes and Clinical/MRI Features in PwMS

Higher baseline T2LV was associated with accelerated thalamic MVF reduction (β = −0.118; p = 0.039) and qT1 increase (β = 0.088; p = 0.007). Similarly, the increase in T2LV over follow-up was associated with an acceleration in thalamic MVF reduction (β = −0.100; p = 0.038) and qT1 increase (β = 0.075; p = 0.008). Patients with disease activity over follow-up had accelerated qT1 increase compared with those without (β = 0.106; p = 0.034). While the baseline EDSS score was not associated with the rates of thalamic qMRI changes, the EDSS progression over follow-up correlated with accelerated rates of decrease in NDI (β = −0.067; p = 0.039) and QSM (β = −0.077; p = 0.027) values. Baseline normalized thalamic volume was linked to the rates of change in MVF (β = 0.462; p = 0.035), qT1 (β = −0.577; p < 0.0001), and NDI (β = 0.343; p = 0.036) values. The rate of brain volume loss over follow-up was associated with the rate of qT1 change (β = −0.059; p = 0.018) (eTable 17).

Baseline variables associated with the subsequent rate of thalamic volume loss in PwMS included age (β = −0.045; p = 0.034), T2LV (β = −0.084; p = 0.004), and MVF and qT1 in the thalamic region close to the CSF (β = 0.111; p = 0.028 and β = −0.425; p = 0.0001, respectively). In HCs, baseline age was the only significant predictor of the rate of thalamic volume loss (β = −0.103; p = 0.0002) (eTable 18).

Sensitivity Analyses

Excellent agreement was observed between qMRI values obtained with the original thalamic masks and with 1-voxel eroded thalamic masks [qT1: ICC = 0.91 (95% CI 0.90–0.93); MVF: ICC = 0.93 (95% CI 0.91–0.94); NDI: ICC = 0.95 (95% CI 0.94–0.96); QSM: ICC = 0.98 (95% CI 0.98–0.98)].

Good agreement was also measured between the estimations of NDI obtained with SMT and NODDI [ICC = 0.85 (95% CI 0.83–0.88)].

Significant between-group differences in thalamic microstructural changes were confirmed also when accounting for treatment effect (eTables 19–22) and disease activity over the follow-up (eTable 23) and in subgroups matched for age, sex, and disease duration (eTables 24–35).

Discussion

We conducted an in vivo multiparametric qMRI study to investigate the pathophysiologic processes occurring in the thalamus of PwMS. Our selection of qMRI contrasts, which leverage different biophysical tissue properties,[50] aimed to provide a comprehensive characterization of microstructural changes linked to demyelination, neuroaxonal loss, and disturbances in iron homeostasis.

The study revealed substantial thalamic alterations in PwMS compared with HCs at baseline and accelerated rates of thalamic degeneration over a 2-year follow-up. Remarkably, the observed thalamic qMRI changes were more severe in patients with PMS and exhibited extensive correlations with both MRI-derived measures of disease burden and clinical measures of neurologic disability and cognitive impairment.

Thalamic pathology in PwMS manifested at a macroscopic level by significant thalamic atrophy. At a microstructural level, thalamic damage was demonstrated by extensive qMRI alterations, not limited to focal lesions but diffusely extending to the tissue without visible changes on conventional FLAIR images. The reduction in thalamic volume that we observed in PwMS, especially in those with PMS, is a well-recognized hallmark of the disease, reflecting heterogeneous neurodegenerative processes.[78,80] Owing to its dependence on widespread pathophysiologic mechanisms involving the entire CNS, thalamic atrophy has been proposed as a marker of the overall extent of MS-related damage[80] and used as an end point in clinical trials.[78] Nevertheless, thalamic volume loss is a relatively unspecific marker, representing the final result of a complex interplay between various pathologic mechanisms occurring at the

microstructural level. These microstructural changes in our study were demonstrated by alterations in qT1, MVF, and NDI values within thalamic lesions and qT1, MVF, and QSM values within the normal-appearing thalamic tissue.

qT1, which measures the time of recovery of longitudinal magnetization, was prolonged in both thalamic lesions and normal-appearing tissue, indicating microstructural and macrostructural tissue damage.[50,51] Alterations in qT1 have been previously reported in the thalamus of PwMS.[67,142] Notably, while qT1 exhibits overall low specificity to MS pathology, it is highly sensitive to a large spectrum of pathologic changes, encompassing demyelination, axonal loss, iron loss, and accumulation of free water.[50]

As a more specific indicator of macromolecular damage (including demyelination and cellular loss), we observed a diffuse reduction in thalamic MVF values. MVF maps were derived from MTsat images, which quantify the exchange of magnetization between free protons and macromolecular protons.[55] Previous studies have investigated magnetization transfer changes in the thalamus of PwMS, providing mixed results; in a recent meta-analysis, no difference in thalamic magnetization transfer values was measured between patients with RRMS and controls.[99] In line with these findings, in our cohort, patients with active RRMS did not differ from HCs in MVF levels within the normal-appearing tissue; conversely, a substantial reduction in MVF values was observed in patients with inactive PMS, reflecting a remarkable degree of demyelination and macromolecular damage in the thalamus of this subgroup of patients compared with both HCs and patients with active RRMS. In addition, MVF also showed high sensitivity to the focal damage in thalamic lesions.

We also observed significant alterations in NDI values in thalamic lesions compared with the surrounding tissue, suggesting increased neuroaxonal loss. By contrast, no differences were found in the normal-appearing thalamic tissue between PwMS and HCs. It is noteworthy that in our study, we chose to model microstructural diffusion processes using SMT because of its effectiveness in addressing challenges posed by fiber crossing populations and orientation dispersion, particularly prominent within gray matter regions.[123] Nonetheless, it is important to note that, like NODDI, SMT is primarily designed for assessing white matter and limitations may arise when exploring structures such as the thalamus.

Previous research on magnetic susceptibility in the thalamus of PwMS has yielded conflicting results.[70,143] In our cohort, we observed a significant decrease in thalamic QSM values among PwMS, consistent with findings in other QSM studies.[67,70,144] An intriguing interpretation

involves the depletion of iron from oligodendrocytes, potentially triggered by chronic microglia activation.[70] On the contrary, focal thalamic lesions within our cohort exhibited no discernible changes in QSM values when compared with perilesional tissue. Notably, QSM is influenced by not only paramagnetic iron concentration but also diamagnetic myelin content.[50] Therefore, we can speculate that a substantial reduction in myelin content within focal lesions might have mitigated the effect of a potential concomitant decline in iron levels, given the opposing impacts of iron and myelin on the QSM signal.[50]

Regionally, the observed qMRI changes in PwMS were predominant in the tissue in proximity to the CSF. Accordingly, a distinctive "ependymal-in" gradient of thalamic damage, characterized by neuroaxonal loss and microglia activation, has been described in MS.[113] This phenomenon is consistently observed across diverse stages of the disease, being evident from the earliest phases of pediatric MS to the progressive stages in patients with advanced disease.[112–114] In our cohort, qMRI changes were also evident regionally in multiple distinct thalamic nuclei. Of interest, a prevalent involvement of the posterior and medial thalamic compartments was evident. Notably, these compartments, which are closest to the CSF, have previously been shown to be more frequently atrophic in MS.[145] Recent research has also indicated that these compartments are more affected by the disconnection of thalamocortical projections due to MS lesions.[146]

The clinical relevance of the observed qMRI thalamic changes was demonstrated by their extensive correlations with both conventional MRI and clinical measures of disease burden. All qMRI metrics showed robust associations with both the EDSS score and BPF—a proxy measure of cumulative neurodegenerative processes within the CNS. Furthermore, select qMRI measures exhibited correlations with the T2-hyperintense lesion load and clinical measures of cognitive impairment, including SDMT and MuSIC scores. Notably, qMRI metrics of microstructural integrity also proved to substantially contribute to explaining neurologic and cognitive disability and supporting the differentiation between active RRMS and inactive PMS phenotypes, in multivariable LASSO regression models including normalized thalamic volume, BPF, and T2LV as additional predictors.

In our study cohort, significant differences between PwMS and HCs emerged also in the longitudinal rates of thalamic qMRI changes over a 2-year follow-up period. In comparison with HCs, PwMS exhibited accelerated thalamic atrophy and enhanced rates of MVF decrease and qT1 increase, reflecting accentuated neurodegenerative and demyelinating processes. As for cross-sectional findings, between-group differences in longitudinal rates of change were

substantially driven by the subgroup of patients with an inactive PMS phenotype, in whom the neurodegenerative processes were notably accentuated. Nevertheless, a significant difference was measurable between the subgroup of patients with active RRMS and HCs in the pace of thalamic qT1 increase. This observation indicates the accumulation of subtle microstructural changes within the normal-appearing thalamic tissue even in patients with a typical RRMS phenotype. In longitudinal studies, thalamic volume has been shown to decline faster in PwMS compared with HCs, but not differently across disease phenotypes[79,80]; such a pattern is in line with our results. In our study, this lack of difference in thalamic atrophy rates between disease phases was confirmed even between phenotypes specifically selected to represent the extremes of the clinical spectrum: active RRMS, dominated by neuroinflammatory processes, and inactive PMS, governed by neurodegenerative mechanisms. Conversely, qT1 emerged as a valuable metric for differentiating between patients with active RRMS and inactive PMS. Specifically, patients with inactive PMS exhibited a notable acceleration in qT1 prolongation, suggesting enhanced accumulation of microstructural alterations.

Similar to the cross-sectional analyses, the longitudinal changes of thalamic qMRI metrics showed substantial clinical relevance. Specifically, longitudinal qMRI changes proved to be associated with MRI markers of disease burden, including the accumulation of T2LV and the rate of brain volume loss over time. Moreover, significant differences in longitudinal qMRI changes were observed between patients with clinical stability and those exhibiting disability progression over the clinical follow-up period. Specifically, patients manifesting disease progression over the 2-year interval exhibited an accelerated reduction in thalamic NDI and QSM values, suggestive of hastened neuroaxonal and iron loss.

Overall, our findings suggest 2 concurrent mechanisms as crucial drivers of thalamic degeneration in PwMS: an indirect damage due to the transection of thalamic projections by white matter lesions and a direct surface-in gradient of damage possibly resulting from toxic factors in the CSF. The impact of focal white matter lesions was evidenced by the association between T2LV and more severe microstructural alterations, as well as accelerated pathologic degeneration over time. Furthermore, the burden of T2LV within thalamocortical projections was significantly more impactful in explaining thalamic microstructural and macrostructural degeneration compared with the general T2LV. The role of surface-in degeneration was suggested by the pronounced pathologic changes in the thalamic regions near the CSF. Notably, the extent of microstructural degeneration in these thalamic areas, but not in other regions, was a significant predictor of the subsequent rate of thalamic volume loss.

Strengths of our study include the large sample size and the inclusion of multiple advanced qMRI contrasts obtained with a standardized acquisition protocol allowing for an extensive concomitant investigation of different pathophysiologic processes. In addition, the availability of clinical and advanced MRI follow-up enabled the investigation of the trajectories of thalamic damage over time, along with their predictors and clinical implications. Furthermore, the study design allowed us to reliably demonstrate the added value of microstructural thalamic changes in explaining disease severity beyond other well-established MRI markers. This study also has some limitations. First, follow-up data were not available for the entire cohort; although the loss to follow-up did not seem to disproportionately affect any specific subgroup of patients, the potential for biases cannot be entirely excluded. Second, given the exploratory nature of this study, we limited the application of multiple comparisons correction to instances where multiple regions of interest were simultaneously investigated. Considering the distinct primary focus of the various qMRI contrasts, each probing different pathophysiologic processes with minimal overlap, we chose not to apply multiple comparisons correction for the remaining hypotheses. This decision was intended to mitigate the risk of type II errors while aligning with the overarching objectives of the investigation. Third, disease progression over the follow-up period was determined solely based on 2 EDSS assessments, conducted at baseline and after 2 years. The absence of an additional follow-up assessment to establish a "confirmed disability progression" criterion potentially limits the accuracy in estimating the actual incidence of disease progression. Fourth, although we ensured the absence of neurologic or psychiatric comorbidities in all participants, we did not systematically collect information on cardiovascular risk factors, which might potentially have had an influence on the extent of the observed neurodegenerative changes.

In conclusion, our extensive qMRI protocol revealed substantial pathologic alterations in the thalamus of PwMS. These changes, extending beyond focal lesions to involve normal-appearing tissue, indicated significant micro/macrostructural alterations, including demyelination and perturbations in iron homeostasis. Thalamic damage accumulated faster in PwMS, particularly in those with inactive PMS, and exhibited extensive clinical correlations. Collectively, these findings contribute to a deeper understanding of the pathologic changes in the thalamus of PwMS, underscoring the clinical importance of thalamic damage and its link to disease progression.

7. Assessing the Relative Importance of Imaging and Serum Biomarkers in Capturing Disability, Cognitive Impairment, and Clinical Progression in Multiple Sclerosis

Authors: Alessandro Cagol[1,2,3,4], Pascal Benkert[5], Sabine Schaedelin[1,5], Mario Ocampo-Pineda[1,2,3], Noemi Montobbio[4], Po-Jui Lu[1,2,3], Batuhan Ayci[1,6], Antonia Wenger[1,2,3,8], Alfi Aran Shukur[1], Kornelius Kaim[1], Lester Melie-Garcia[1,2,3], Matthias Weigel[1,2,3,7], Alessio Signori[4], Pasquale Calabrese[8], Ludwig Kappos[1,2,3], Maria Pia Sormani[4,9], Jens Kuhle[2,3], and Cristina Granziera[1,2,3]

Affiliations: 1. Translational Imaging in Neurology (ThINk) Basel, Department of Biomedical Engineering, Faculty of Medicine, University Hospital Basel and University of Basel, Basel, Switzerland. 2. Multiple Sclerosis Centre, Departments of Neurology, Clinical Research and Biomedicine, University Hospital and University Basel, Switzerland. 3. Research Center for Clinical Neuroimmunology and Neuroscience Basel (RC2NB), University Hospital Basel and University of Basel, Basel, Switzerland. 4. Dipartimento di Scienze della Salute, Università degli Studi di Genova, Italy. 5. Department of Clinical Research, University Hospital Basel, University of Basel, Basel, Switzerland. 6. Istanbul University-Cerrahpasa, Cerrahpasa Medical School, Istanbul, Turkey. 7. Division of Radiological Physics, Department of Radiology, University Hospital Basel, Basel, Switzerland. 8. Neuropsychology and Behavioral Neurology Unit, Division of Cognitive and Molecular Neuroscience, University of Basel, Switzerland. 9. IRCCS Ospedale Policlinico San Martino, Genova, Italy.

Abstract

Background: The heterogeneity of multiple sclerosis (MS) pathology calls for robust biomarkers to predict disability and progression, particularly progression independent of relapse activity (PIRA).

Objective: To identify the most informative MRI and serum biomarkers for predicting clinical outcomes in people with MS (pwMS), including disability severity, cognitive impairment, disease phenotype, and risk of PIRA.

Methods: We applied a machine learning–based feature selection approach to cross-sectional and longitudinal data from two independent pwMS cohorts. Cohort 1 (n=120) included 57 MRI biomarkers, incorporating advanced quantitative MRI (qMRI). Cohort 2 (n=279) included 35 MRI biomarkers derived from conventional MRI. Both cohorts obtained serum neurofilament light chain (sNfL) and glial fibrillary acidic protein (sGFAP) measurements.

Results: Spinal cord atrophy consistently emerged as the strongest predictor of disability severity and predicted PIRA, along with cortical thinning and subcortical atrophy – particularly in deep gray matter. sNfL, sGFAP, and qMRI metrics independently contributed to the prediction of PIRA and progressive disease phenotype.

Conclusion: Spinal cord atrophy and cortical degeneration are the most robust and consistent predictors of MS severity and progression. Serum biomarkers of neuroaxonal and astrocytic damage, together with qMRI-derived tissue metrics, provide independent and complementary value for outcome prediction.

1. Introduction

Multiple sclerosis (MS) is a chronic condition characterized by demyelination, inflammation, and neurodegeneration within the central nervous system (CNS). Magnetic resonance imaging (MRI) plays a pivotal role in the diagnosis and clinical management of people with MS (pwMS), primarily by enabling the detection of white matter lesions (WMLs). However, despite the recognized importance of WML assessment in clinical practice, the correlation between WML burden and clinical symptoms is often weak – a phenomenon referred to as the clinico-radiological paradox.[48] This discrepancy stems from several factors, encompassing the limited pathological specificity of conventional MRI, the frequent oversight of spinal cord involvement, and the insensitivity of standard imaging techniques to diffuse damage in normal-appearing tissue.[48] Additionally, reparative mechanisms and adaptive processes largely go undetected by conventional MRI.

These limitations have driven the search for biomarkers with greater sensitivity and specificity to quantify pathological changes in pwMS. Significant progress has been made in

characterizing focal damage, particularly through the development of techniques to identify cortical lesions (CLs), which are closely associated with physical and cognitive impairment, as well as disease progression.[82,147] Advanced imaging techniques have also emerged to capture the heterogeneity of WMLs in terms of demyelination, neuroaxonal loss, smoldering inflammation, and repair. For instance, the detection of paramagnetic rim lesions (PRLs) has enabled the identification of chronic active lesions, which are characterized by persistent inflammatory activity and are linked to worse clinical outcomes.[47,148] Furthermore, quantitative MRI (qMRI) has enriched our understanding of MS pathology by offering microstructural insights into tissue changes and providing proxy measures of demyelination, macromolecular loss, neuroaxonal degeneration, and iron dysregulation.[50] These metrics are valuable for characterizing WMLs and detecting subtle abnormalities in tissue that appears normal on conventional MRI.[58] Besides, brain volumetric measurements have also become a widely used research tool for quantifying tissue loss, serving as a surrogate marker for the overall neurodegenerative burden.[16] Improved techniques for assessing spinal cord pathology, both in terms of focal lesions and diffuse tissue damage, have similarly been developed.[16] Beyond imaging, serum biomarkers such as neurofilament light chain (sNfL) and glial fibrillary acidic protein (sGFAP) have demonstrated significant potential in capturing inflammatory and neurodegenerative processes. While sNfL primarily reflects axonal damage, sGFAP serves as a marker of astrocytic activation, and both have been shown to correlate with clinical severity and predict disease progression.[149–151]

These advancements have expanded our knowledge of MS pathology and provided a broad array of potential biomarkers for use in clinical trials and practice. However, most studies to date have focused on a limited subset of these biomarkers, leaving gaps in our understanding of their relative contributions. Moreover, implementing all these biomarkers in clinical practice is impractical and could lead to redundancy. Thus, it is essential to identify the most relevant biomarkers for disease management, monitoring, and treatment decisions to optimize care for pwMS. This is particularly critical for developing biomarkers that predict disease evolution, especially in addressing the neurodegenerative component of MS, which is considered the primary driver of progression independent of relapse activity (PIRA).[10] Tackling PIRA remains one of the most pressing unmet needs for improving long-term outcomes in pwMS.

In this context, we conducted a cross-sectional and longitudinal study to assess the relative contribution of a wide range of MRI biomarkers reflecting brain and spinal cord pathology, along with serum biomarkers, in explaining clinical outcomes in pwMS. Our analysis

incorporated both conventional and advanced MRI metrics, capturing focal and diffuse inflammatory as well as neurodegenerative changes at macroscopic and microstructural levels. To identify the most informative biomarkers, we applied a data-driven machine learning approach designed to robustly capture the relative importance of each feature in explaining clinical outcomes. Specifically, we aimed to determine the extent to which each biomarker contributes to explaining: (1) the severity of neurological disability, (2) the degree of cognitive impairment, (3) the clinical disease phenotype, and (4) the risk of future disease progression due to PIRA. Associations of a subset of the selected biomarkers with outcomes (1), (3), and (4) were further evaluated in an independent validation cohort.

2. Methods

2.1. Participants and study design

In this longitudinal, prospective observational study, we used data from two independent cohorts. Cohort 1 included both pwMS and healthy controls (HCs) who underwent advanced MRI and serum assessments at baseline, along with longitudinal clinical follow-up. Cohort 2 included pwMS who underwent conventional MRI and serum assessments at baseline, also followed by longitudinal clinical observation.

The study was approved by the local ethics committee, and all patients provided written informed consent before study entry. An overview of the study design is provided in Figure 1.

This study followed the STROBE reporting guideline.

2.1.1. Cohort 1

Cohort 1 included pwMS who participated in both the INsIDER study (NCT05177523) and the Swiss Multiple Sclerosis Cohort (SMSC) study.[104] Inclusion criteria for pwMS were as follows:

1. Availability of an advanced brain MRI scan conducted as part of the INsIDER study. The MRI scan date served as the study baseline for each participant.

2. Availability of at least two clinical follow-up examinations, each conducted at least six months apart from one another and from the study baseline, performed prospectively as part of the SMSC study protocol.

3. Diagnosis of MS according to the 2017 revised McDonald criteria.[124]

4. Age between 18 and 80 years.

5. Absence of relevant neurological or psychiatric comorbidities.

Additionally, Cohort 1 included HCs participating in the INsIDER study, with the availability of an advanced brain MRI scan obtained using the same protocol as in PwMS.

Exclusion criteria for all participants encompassed pregnancy, contraindications to MRI, inability to provide informed consent, relapses or steroid treatment within the prior 3 months, and insufficient MRI quality. All eligible participants were enrolled.

2.1.1. Cohort 2

Cohort 2 included pwMS participating in the SMSC study, followed at the University Hospital of Basel, and meeting the following inclusion criteria:

1. Availability of a 3-Tesla (3T) brain MRI scan conducted as part of the SMSC study. The date of the first available 3T MRI scan served as the study baseline for each participant.

2. Availability of at least two clinical follow-up examinations, each conducted at least six months apart from one another and from the study baseline, performed prospectively as part of the SMSC study protocol.

3. Diagnosis of MS according to the 2017 revised McDonald criteria.[124]

4. Age between 18 and 80 years.

5. Absence of relevant neurological or psychiatric comorbidities.

Exclusion criteria were identical to those applied in Cohort 1.

2.2. Clinical data

All participants in both cohorts underwent regular clinical evaluations, conducted at least annually, as part of the SMSC study.[13] Standardized assessments included the calculation of the Expanded Disability Status Scale (EDSS) score (https://www.neurostatus.net/) by certified raters.

The occurrence of PIRA during follow-up was defined as an increase in EDSS score (≥1.5, ≥1.0, or ≥0.5 points if baseline EDSS was 0, 1.0-5.5, or >5.5, respectively) using a roving baseline,[152] confirmed at least after 6 months, in the absence of relapses between the EDSS increase and the preceding reference visit (conducted ≥90 days before the EDSS increase) and between the EDSS increase and its confirmation.[7] PIRA events were identified using the msprog package.[153]

In Cohort 1, cognitive performance was assessed using the oral version of the Symbol Digit Modalities Test (SDMT) in a subset of 97 pwMS and 100 HCs, with raw SDMT scores converted to z-scores based on normative data.[127]

2.3. MRI acquisition and analysis

For Cohort 1, advanced brain MRI examinations were conducted using a standardized acquisition protocol on a 3T whole-body MR system (Magnetom Prisma, Siemens Healthineers), using a 64-channel phased-array head and neck coil for radiofrequency reception. The protocol included: (1) 3D fluid-attenuated inversion recovery (FLAIR), (2) 3D magnetization-prepared 2 rapid gradient-echo (MP2RAGE), (3) multi-shell diffusion, (4) 3D echo planar imaging (EPI), (5) three 3D radiofrequency spoiled gradient echo acquisitions used to obtain magnetization transfer saturation (MTsat) maps,[130] and (6) fast acquisition with spiral trajectory and adiabatic T2-prep (FAST-T2). FLAIR and MP2RAGE images covered the spinal cord from C1 to C4.

The standardized brain MRI protocol for Cohort 2 included: (1) 3D FLAIR, and (2) 3D magnetization-prepared rapid gradient-echo (MPRAGE), both covering the spinal cord from C1 to C4. Further protocol details are provided in eTables 1-2.

Due to differences in MRI acquisition protocols, only a subset of MRI biomarkers could be quantified in Cohort 2 (Figure 1).

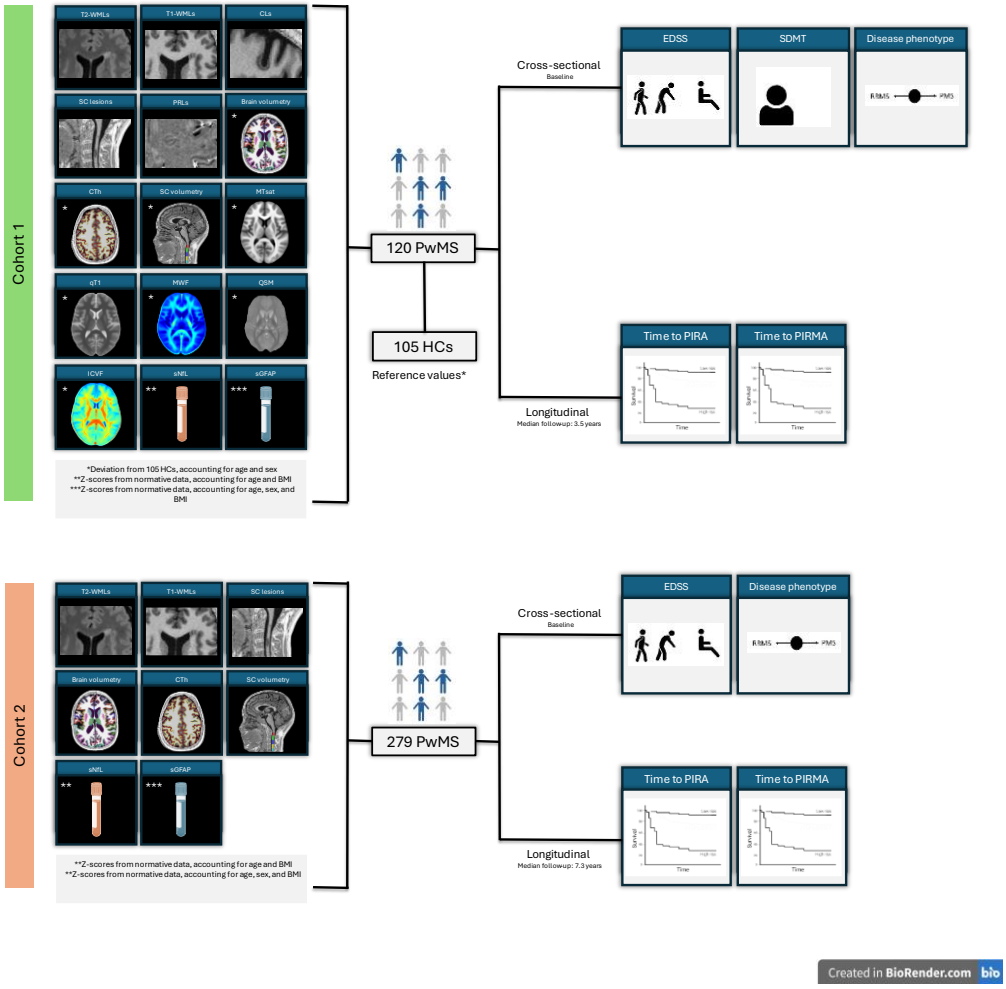

Figure 1. *Study design. Two independent cohorts of people with multiple sclerosis (PwMS) were analyzed. Cohort 1 included extensive multimodal MRI and serum biomarkers and was used for cross-sectional analyses of disability and disease phenotype, as well as longitudinal analyses of time to progression independent of relapse activity (PIRA) and progression independent of relapse and MRI activity (PIRMA). Cohort 2 included a more limited set of clinically available MRI and serum measures and was used for replication and validation analyses. Cross-sectional outcomes were assessed at baseline, while longitudinal outcomes were evaluated over follow-up.*

Abbreviations: CLs, cortical lesions; CSA, cross-sectional area; CTh, cortical thickness; EDSS, Expanded Disability Status Scale; HCs, healthy controls; ICVF, intracellular volume fraction; MTsat, magnetization transfer saturation; MWF, myelin water fraction; PIRMA, progression independent of relapse and MRI activity; PIRA, progression independent of relapse activity; PMS, progressive multiple sclerosis; PRLs, paramagnetic rim lesions; PwMS, people with multiple sclerosis; qT1, quantitative T1; QSM, quantitative susceptibility mapping; RRMS, relapsing–remitting multiple sclerosis; SC, spinal cord; SDMT, Symbol Digit Modalities Test; sGFAP, serum glial fibrillary acidic protein; sNfL, serum neurofilament light chain; T1-WMLs, T1-weighted white matter lesions; T2-WMLs, T2-weighted white matter lesions.

2.3.1. Lesion segmentation

T2-hyperintense white matter lesions (T2-WMLs) were segmented using a deep learning-based tool[105] and manually refined. Cortical lesions (CLs) were manually segmented on MP2RAGE by two expert raters.[154] T1-hypointense WMLs (T1-WMLs) were automatically segmented on

MP2RAGE/MPRAGE using SAMSEG (v7.2.0).[140] PRLs, defined as discrete FLAIR-hyperintense lesions either completely or partially encircled by a rim of paramagnetic signal, visible in at least one contrast between unwrapped phase and quantitative susceptibility mapping (QSM),[35] were manually detected by two expert raters. Spinal cord lesions in the C1-C4 tract were manually identified on FLAIR and MP2RAGE/MPRAGE images.

2.3.2. Brain morphometry

Segmentation of brain structures and calculation of global/regional brain volumes and cortical thickness (CTh) were performed with FreeSurfer (v.6.0.0; http://surfer.nmr.mgh.harvard.edu/), with lesion-filled MP2RAGE/MPRAGE images as input. Results were manually checked and edited as needed. Brain volumes were normalized by the total intracranial volume (TIV) obtained with SAMSEG.[155]

2.3.3. Spinal cord morphometry

The mean cross-sectional area (CSA) at C1, C2, C3, and C4 was measured using Spinal Cord Toolbox[156] (v.5.3.0) on MP2RAGE/MPRAGE images. Manual labelling of intervertebral discs was performed to ensure accuracy, and outputs were manually checked.

2.3.4. qMRI analysis

We analyzed 5 different qMRI contrasts providing insights into: (1) micro/macrostructural integrity (quantitative T1 [qT1]), (2) macromolecular content (MTsat), (3) myelin content (myelin water fraction [MWF]), (4) axon and dendrite density (intracellular volume fraction [ICVF]), and (5) iron and myelin content (QSM).[50] qT1 maps were derived from MP2RAGE images.[131] MTsat maps were reconstructed using magnetization transfer-weighted, proton density-weighted, and T1-weighted images.[130] MWF maps were generated from FAST-T2 data.[157] ICVF values were estimated using Neurite Orientation Dispersion and Density Imaging (NODDI) applied to diffusion images,[158] after denoising and correction for motion, geometric distortions, and eddy-currents. QSM maps were reconstructed from 3D-EPI images using the morphology-enabled dipole inversion (MEDI) algorithm.[136]

Mean qMRI values were extracted within WMLs, normal-appearing white matter (NAWM), normal-appearing cortical and deep gray matter (GM), and the normal-appearing thalamus.

2.3.5. Longitudinal WML changes

All longitudinal conventional MRI scans acquired as part of the SMSC study during the clinical follow-up were analyzed to identify new or enlarging T2-WMLs. These lesions were automatically detected[107] and manually verified to ensure accuracy. The identification of new or enlarging WMLs was instrumental in determining who among pwMS experienced progression independent of relapse and MRI activity (PIRMA), defined as PIRA occurring in the absence of MRI-detected inflammatory activity.[7,10] The protocol details for conventional MRI scans are provided in eTable 2.

2.4. Neurofilament light chain

sNfL and sGFAP levels were quantified using the ultrasensitive single molecule array (Simoa) technology (Quanterix), following the manufacturer's protocol.10 Z-scores were calculated using normative reference data, accounting for age and body mass index (BMI) for sNfL, and for age, BMI, and sex for sGFAP.[159]

2.5. Statistical analysis

All statistical analyses were conducted using R (version 4.3.1), with statistical significance set at $p<0.05$.

The Boruta algorithm (configured with 10,000 trees, 2,000 iterations),[160,161] an extension of the random forest algorithm, was employed to evaluate the contribution of each biomarker in explaining neurological disability, cognitive performance, disease phenotype, and occurrence of PIRA. The Boruta algorithm is a feature selection method that compares the importance of original variables against randomly permuted "shadow" variables. By iteratively fitting random forest models, it evaluates feature importance by comparing it to the highest importance achieved by the shadow variables.

In Cohort 1, we included as predictors in the Boruta models clinical and demographic factors, brain and spinal cord volumetric measurements, qMRI metrics, measures of lesion burden, and serum biomarkers. A comprehensive list of the 59 included predictors is available in eTable 3.

To account for the linear dependence of brain and spinal cord volumetric measurements and qMRI metrics on age and sex, these variables were adjusted by calculating their deviation from the HC population. Linear regressions were fitted within the HC population with volumetric or qMRI metrics as the dependent variables and age and sex as explanatory variables. The residuals from these regressions in pwMS, representing deviations from expected values, were used as input variables in the Boruta models.[141] Age and sex were also included as predictors in the models to minimize potential remaining confounding effects.

Separate Boruta models were applied to the following dependent variables: (1) EDSS, analyzed both as a continuous variable and dichotomized based on a cut-off of either ≥3.0 or ≥6.0; (2) SDMT z-score; (3) disease phenotype (PMS vs. RRMS); and (4) PIRA incidence. For PIRA, we used a survival model to analyze time-to-event data and additionally assessed PIRA as a binary outcome. To account for potential baseline differences in demographic and clinical variables between patients with and without PIRA, 1:1 nearest-neighbor propensity score matching was conducted. The matching criteria included age, sex, disease duration, EDSS, disease modifying treatment (DMT) class, disease phenotype, and follow-up duration.

The predictive performance of variables selected by the Boruta models was assessed using random forest models with 10-fold cross-validation. Performance metrics included mean R^2 for regression tasks, mean area under the receiver operating characteristic curve (AUC) for classification tasks, and mean concordance index (C-index) for survival analysis.

Sensitivity and complementary analyses were conducted to address methodological limitations, improve interpretability, and further characterize model performance. Because variable-importance estimates in the Boruta model may be affected by strong collinearity among predictors, we conducted sensitivity analyses using conditional Boruta models implemented with conditional random forests (cforest, party R package), which estimate conditional variable importance while accounting for correlations between predictors. To further evaluate the temporal stability of PIRA prediction, model performance was additionally quantified using time-dependent AUCs calculated at multiple follow-up time intervals. To improve interpretability of the PIRA prediction models, we explored post hoc explanation approaches based on Shapley additive explanations, including SHAP dependence plots, which describe

both the relative importance and the directionality of individual predictors in the random forest models. In parallel, we fitted linear survival models using ridge-penalized Cox regression as a complementary, more interpretable modeling framework.

Additional sensitivity analyses included: (1) recalculating SDMT z-scores based on the HC population rather than normative data, (2) including EDSS as an additional explanatory variable in the model predicting time to PIRA, (3) including DMT class as an additional explanatory variable in the model predicting time to PIRA, (4) analyzing time to PIRA specifically within the RRMS patient group, and (5) investigating time to PIRMA.

Analogous Boruta models, implemented with the same hyperparameters, were applied to the validation cohort (Cohort 2) to assess the relative importance of biomarkers. In this cohort, data were available for a subset of 37 out of the 59 biomarkers used in Cohort 1, as detailed in eTable 4. Due to the absence of a paired HC cohort, biomarkers were entered into the models using their original values; all models included age, sex, and disease duration as covariates. As in Cohort 1, outcomes of interest included cross-sectional EDSS and disease phenotype at baseline, as well as prediction of future time to PIRA and discrimination between propensity score-matched pwMS with and without PIRA during follow-up. Matching criteria were identical to those applied in Cohort 1. To assess clinical applicability, we derived a parsimonious risk score using ridge regression based on clinically accessible biomarkers identified as predictors of PIRA by the Boruta analysis in Cohort 2; this score was subsequently validated in Cohort 1.

Additional methodological details are available in eMethods.

3. Results

3.1 Cohort 1

A total of 120 pwMS and 105 HCs (55% female; mean age: 37.8 (SD: 13.0) years) were included in Cohort 1. Key characteristics of pwMS are provided in Table 1.

	Cohort 1	Cohort 2
Participants, No.	120	279
Females, No. (%)	70 (58.3)	200 (71.7)
Age, mean (SD), years	47.7 (13.6)	45.6 (11.6)
Disease duration, median [IQR], years	12.4 [4.2; 24.5]	10.2 [6.0; 17.8]
Disease phenotype: - RRMS - SPMS - PPMS	 89 (74.2) 20 (16.7) 11 (9.2)	 259 (92.8) 10 (3.6) 10 (3.6)
DMT: - Platform treatments, No. (%) - Oral treatments, No. (%) - Monoclonal antibody treatments, No. (%) - Untreated, No. (%)	 5 (4.2) 40 (33.3) 57 (47.5) 18 (15.0)	 26 (9.3) 160 (57.3) 47 (16.8) 46 (16.5)
EDSS, median [IQR]	3.0 [2.0; 5.0]	2.0 [1.5; 3.25]
sNfL Zscore, median [IQR]	0.39 [-0.36; 1.08]	0.23 [-0.63; 0.99]
sGFAP Zscore, median [IQR]	0.14 [-0.71; 1.00]	0.00 [-0.71; 0.60]
T2LV, median [IQR], mL	7.2 [2.8; 16.3]	5.6 [2.2; 14.1]
Cortical lesion count, median [IQR]	2 [0; 5.5]	/
PRL count, median [IQR]	3 [0.3; 6.0]	/
C1-C4 lesion count, median [IQR]	1 [0; 2.3]	3 [3; 5]
Normalized brain volume, median [IQR]	0.70 [0.66; 0.74]	0.69 [0.66; 0.72]
Normalized WM volume, median [IQR]	0.29 [0.27; 0.30]	0.28 [0.27; 0.30]
Normalized GM volume, median [IQR]	0.40 [0.37; 0.42]	0.38 [0.36; 0.41]
Normalized cortical volume, median [IQR]	0.30 [0.27; 0.32]	0.29 [0.20; 0.30]
Normalized DGM volume, median [IQR]	0.03 [0.03; 0.04]	0.03 [0.03; 0.04]
CTh, median [IQR], mm	2.33 [2.2; 2.41]	2.38 [2.28; 2.45]
C2-C3 CSA, median [IQR], mm^2	60.2 [53.3; 65.6]	60.8 [55.7; 65.9]
Follow-up duration, median [IQR], years	3.5 [2.6; 4.2]	7.3 [6.7; 7.9]
Patients exhibiting PIRA during follow-up, No. (%)	28 (23.3)	79 (28.3)

Table 1. Key characteristics of pwMS.

Abbreviations: CTh = cortical thickness; DMT = disease modifying treatment ; EDSS = Expanded Disability Status Scale; GM = gray matter; IQR = interquartile range; PIRA = progression independent of relapse activity; PPMS = primary progressive multiple sclerosis; PRL = paramagnetic rim lesions; pwMS = people with multiple sclerosis; RRMS = relapsing-remitting multiple sclerosis; SD = standard deviation; sNfL = serum neurofilament light chain; SPMS = secondary progressive multiple sclerosis; T2LV = T2-lesion volume; WM = white matter.

The median follow-up time was 3.5 years (IQR: 2.6; 4.2). Univariate associations between variables used in the Boruta models and outcome measures (i.e. EDSS, SDMT, disease phenotype, and time to PIRA) are visually represented in Figure 2.

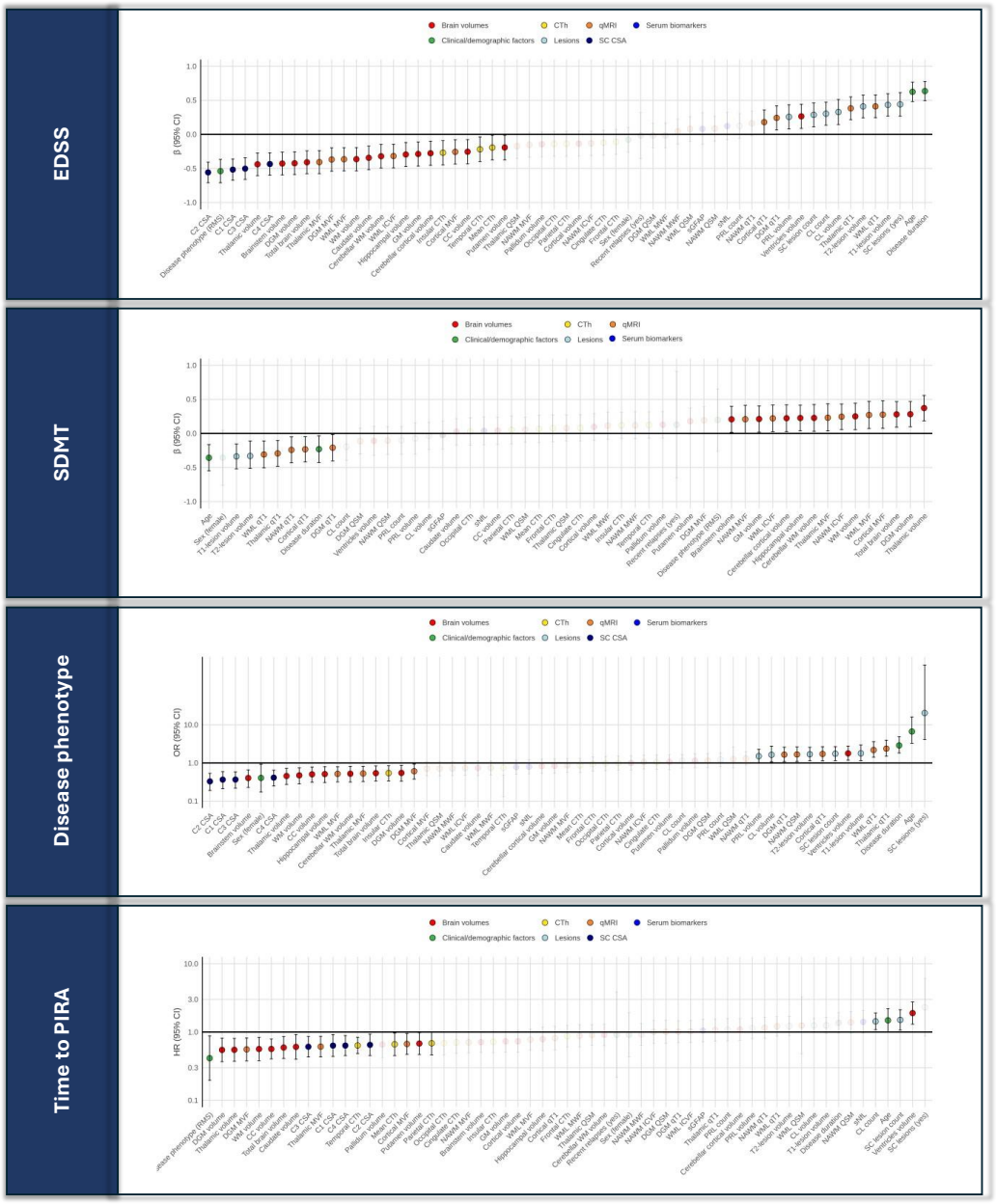

Figure 2. Univariate associations in Cohort 1

Abbreviations: CC, corpus callosum; CI, confidence interval; CL, cortical lesion; CSA, cross-sectional area; CTh, cortical thickness; DGM, deep gray matter; EDSS, Expanded Disability Status Scale; GM, gray matter; HR, hazard ratio; ICVF, intracellular volume fraction; MVF, myelin volume fraction; MWF, myelin water fraction; NAWM, normal-appearing white matter; PIRA, progression independent of relapse activity; PRL, paramagnetic rim lesions; qMRI, quantitative MRI; QSM, quantitative susceptibility mapping; qT1, quantitative T1; RMS, relapsing multiple sclerosis; SC, spinal cord; SDMT, Symbol Digit Modalities Test; sGFAP, serum glial fibrillary acidic protein; sNfL, serum neurofilament light chain; WM, white matter; WML, white matter lesions.

3.1.1. EDSS prediction

Twenty-four variables were identified by the Boruta model as significant predictors of the EDSS score, with age and disease duration being the strongest. Among biomarkers, spinal cord volumetric measurements emerged as the most critical, with C2, C1, C3, and C4 CSA contributing the most to the prediction model. Additional selected biomarkers included brain volumetric measurements, T1- and T2-WML burden, spinal cord and CL burden, and qMRI metrics in both lesions and normal-appearing GM (Figure 3). The model incorporating these predictors achieved a mean R^2 of 0.55.

The most relevant biomarkers for distinguishing patients with an EDSS score ≥3.0 (n=69) were thalamic qT1 and C2 CSA (model mean AUC = 0.91), while for differentiating those with an EDSS score ≥6.0 (n=24), the key biomarkers were C2 and C1 CSA (model mean AUC = 0.93) (eFigure 1).

3.1.2. SDMT prediction

Seven variables emerged as significant predictors of the SDMT z-score. These included, in order of importance, brain volumetric measurements (WM, thalamic, total brain, hippocampal, and DGM volumes), T1-WML burden, and DGM qT1 (Figure 3). The model incorporating these predictors achieved a mean R^2 of 0.31. In the sensitivity analysis, similar results, confirming the same volumetric variables, were observed when SDMT z-scores were recalculated based on the HC population rather than normative data (mean R^2 = 0.25) (eFigure 2).

3.1.3. Prediction of the disease phenotype

Sixteen variables significantly contributed to differentiating between PMS and RRMS, with age being the strongest predictor, followed by C2 CSA. Other selected biomarkers included T1-WML burden, C4, C3, and C1 CSA, qMRI metrics in both WMLs and normal-appearing tissue, and spinal cord lesion burden (Figure 3). The model incorporating these predictors achieved a mean AUC of 0.92. When EDSS was included as an additional predictor, it emerged as the strongest determinant, while the other selected biomarkers were largely consistent with the main analysis (mean AUC = 1.00) (eFigure 3).

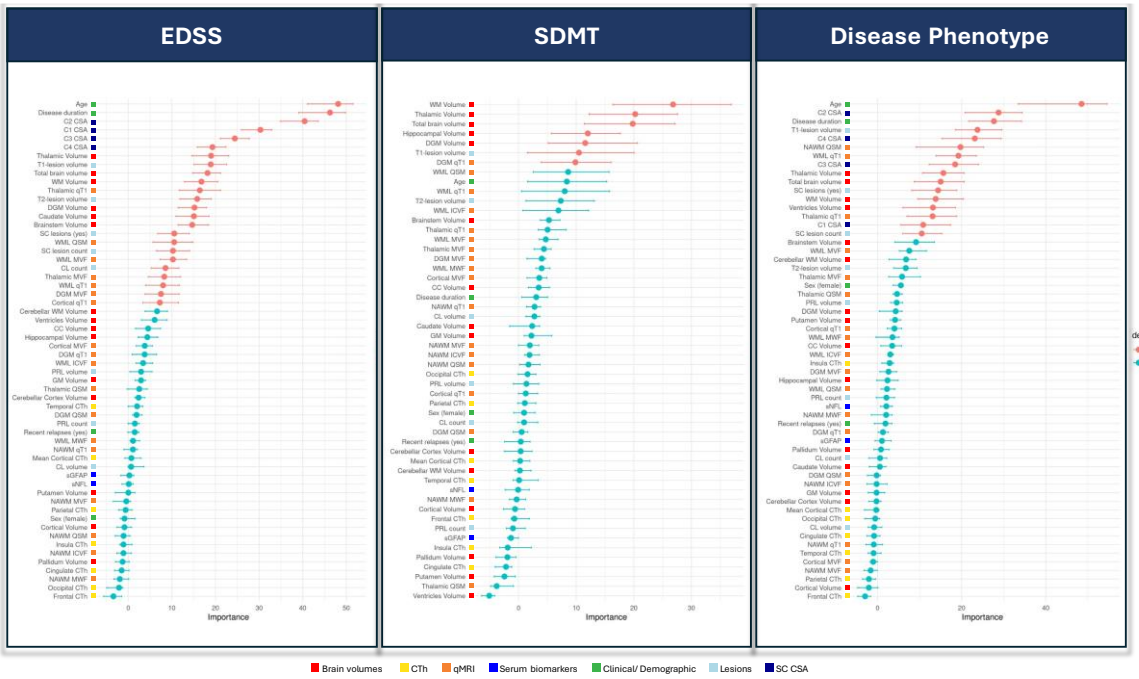

Figure 3. Selected predictors of the EDSS, SDMT, and disease phenotype in Cohort 1

Abbreviations: CC, corpus callosum; CL, cortical lesion; CSA, cross-sectional area; CTh, cortical thickness; DGM, deep gray matter; GM, gray matter; ICVF, intracellular volume fraction; MVF, myelin volume fraction; MWF, myelin water fraction; NAWM, normal-appearing white matter; PRL, paramagnetic rim lesions; qMRI, quantitative MRI; QSM, quantitative susceptibility mapping; qT1, quantitative T1; RMS, relapsing multiple sclerosis; SC, spinal cord; sGFAP, serum glial fibrillary acidic protein; sNfL, serum neurofilament light chain; WM, white matter; WML, white matter lesions.

3.1.4. Prediction of time to PIRA

During the follow-up period, 28 pwMS experienced PIRA and 26 pwMS experienced PIRMA. Among them, 16 patients with PIRA and 15 patients with PIRMA had an RRMS course. Only one patient experienced relapse-associated worsening.

Seven variables emerged as significant predictors of time to PIRA. These included, in order of importance, CTh in the temporal lobe, volumetric measurements of the ventricles, caudate, DGM and thalamus, and C3 and C4 CSA (Figure 4). The selected variables yielded a mean C-index of 0.67. Results remained consistent when including EDSS as an additional predictor (mean C-index = 0.70).

When predicting PIRMA events, five variables were selected: CTh in the temporal lobe, DGM volume, C1 CSA, ventricular volume, and thalamic volume (mean C-index = 0.70) (eFigure 4).

In the RRMS subgroup, CTh in the temporal lobe was the only significant predictor of both PIRA (mean C-index = 0.64) and PIRMA (mean C-index = 0.69) (eFigure 5).

In the propensity score-matched analysis, six variables were identified as discriminators between patients with and without PIRA, including measures of cortical damage (CL volume, CL count, and cortical qT1), neuroaxonal density within WMLs (ICVF), spinal cord C4 CSA, and sNfL levels (model mean AUC = 0.80) (Figure 4). Group characteristics before and after propensity score-matching are reported in eTable 5.

In SHAP dependence plots aimed at exploring the relationship between individual predictors and model-predicted PIRA risk, lower DGM volumes, reduced cervical CSA, and increased ventricular volume were associated with higher model-predicted PIRA risk. Temporal Cth displayed a non-linear association, with lower thickness corresponding to higher predicted PIRA risk (eFigure 6). The ridge Cox model confirmed the direction of associations observed in the SHAP analyses (eFigure 7).

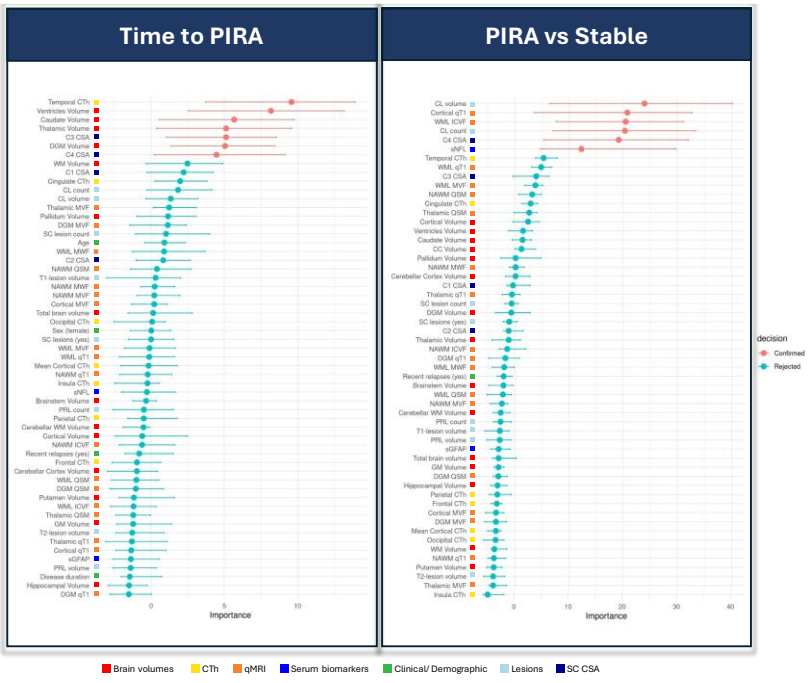

Figure 4. Selected predictors of PIRA in Cohort 1

Abbreviations: CC, corpus callosum; CL, cortical lesion; CSA, cross-sectional area; CTh, cortical thickness; DGM, deep gray matter; GM, gray matter; ICVF, intracellular volume fraction; MVF, myelin volume fraction; MWF, myelin water fraction; NAWM, normal-appearing white matter; PIRA, progression independent of relapse activity; PRL, paramagnetic rim lesions; qMRI, quantitative MRI; QSM, quantitative susceptibility mapping; qT1, quantitative T1; RMS, relapsing multiple sclerosis; SC, spinal cord; sGFAP, serum glial fibrillary acidic protein; sNfL, serum neurofilament light chain; WM, white matter; WML, white matter lesions.

3.2 Validation cohort

A total of 279 pwMS were included in Cohort 2; key characteristics are reported in Table 1. The median follow-up time was 7.3 years (IQR: 6.7; 7.9).

Eighteen variables were identified as significant predictors of the EDSS score. As in Cohort 1, spinal cord volumetric measurements – particularly CSA at all cervical levels – were among the strongest contributors. Additional selected biomarkers included T2- and T1-WML volume, sGFAP levels, and several brain volumetric measures, with thalamic volume again emerging as the most relevant (Figure 5). The model achieved a mean R^2 of 0.34. Models discriminating pwMS based on EDSS cut-offs of ≥3.0 and ≥6.0 achieved mean AUCs of 0.79 and 0.92, respectively (eFigure 8).

Eighteen variables also significantly contributed to distinguishing between RRMS and PMS. As in Cohort 1, spinal cord volumetric measures were the most important, alongside T1- and T2-WML volume, sGFAP values, and multiple brain volumetric metrics (model mean AUC = 0.87) (Figure 5).

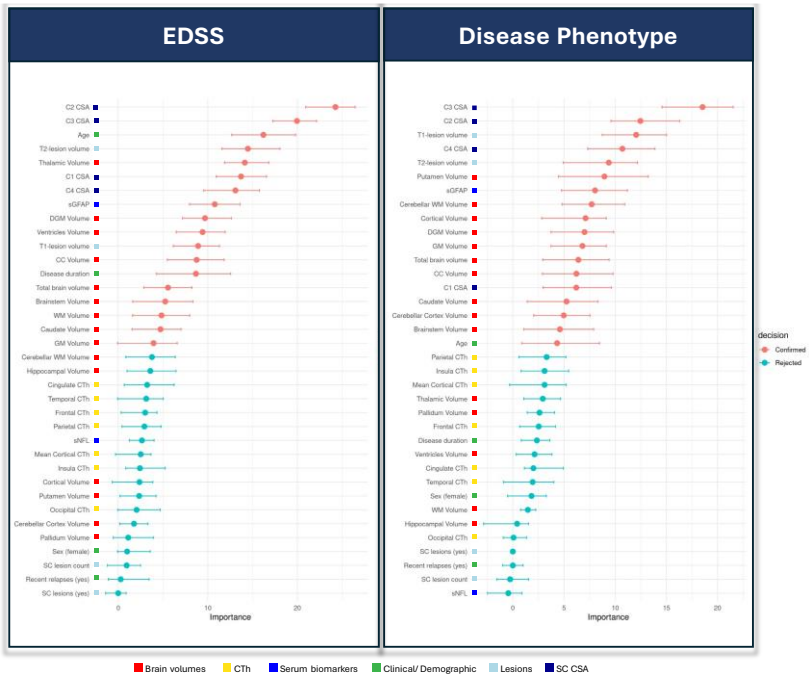

Figure 5. Selected predictors of the EDSS and disease phenotype in Cohort 2

Abbreviations: CC, corpus callosum; CI, confidence interval; CL, cortical lesion; CSA, cross-sectional area; CTh, cortical thickness; DGM, deep gray matter; GM, gray matter; SC, spinal cord; sGFAP, serum glial fibrillary acidic protein; sNfL, serum neurofilament light chain; WM, white matter; WML, white matter lesions.

During follow-up, 79 pwMS experienced PIRA. Seven variables were selected as predictors of time to PIRA. These included CSA at the C1, C2, and C3 levels, total brain volume, pallidum volume, and cingulate CTh (model mean C-index: 0.70) (Figure 6).

In the RRMS subgroup, the top predictors of time to PIRA, in order of importance, were C3 CSA, pallidum volume, thalamic volume, mean CTh, and caudate volume (model mean C-index: 0.76) (eFigure 9).

Fifty-six out of the 79 pwMS with PIRA fulfilled criteria for PIRMA. The same five variables – C3 CSA, pallidum volume, thalamic volume, mean CTh, and caudate volume – were selected as predictors of time to PIRMA (model mean C-index: 0.81) (eFigure 10).

In the propensity score-matched analysis, six variables emerged as discriminators between patients with and without PIRA. The most relevant was cingulate CTh, followed by C1 CSA, sGFAP levels, total brain volume, thalamic volume, and mean CTh (model mean AUC = 0.67) (Figure 6).

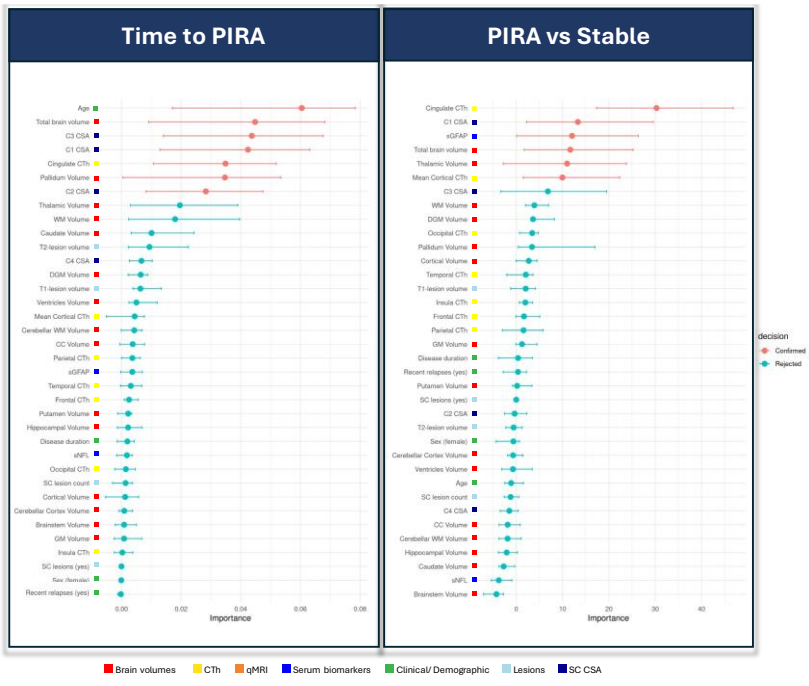

Figure 6. Selected predictors of PIRA in Cohort 2

Abbreviations: CC, corpus callosum; CI, confidence interval; CL, cortical lesion; CSA, cross-sectional area; CTh, cortical thickness; DGM, deep gray matter; GM, gray matter; SC, spinal cord; sGFAP, serum glial fibrillary acidic protein; sNfL, serum neurofilament light chain; WM, white matter; WML, white matter lesions.

Conditional Boruta in both cohorts produced findings that were overall comparable with the main analyses, although with a more parsimonious set of selected predictors (eFigures 11-14).

3.3 Derivation and validation of a clinically accessible PIRA risk score

To explore the feasibility of deriving a clinically applicable risk score for PIRA based on widely available MRI biomarkers, we developed a parsimonious prognostic score using ridge regression. From the subset of predictors identified by the Boruta analysis in Cohort 2, we selected variables with broad clinical availability, resulting in a model including age, C1 CSA, normalized total brain volume, and normalized thalamic volume. This score was derived in Cohort 2. In this cohort, the risk score was strongly associated with time to PIRA (hazard ratio [HR] 3.30, 95% CI 1.99–5.62; $p<0.0001$) and achieved a C-index of 0.64. Time-dependent AUCs calculated between 2 and 7 years were all statistically significant, ranging from 0.81 at 3 years to 0.61 at 7 years (eTable 6).

When applied to Cohort 1, the risk score showed consistent prognostic performance, with an HR of 3.60 (95% CI 1.57–8.25; $p=0.002$) and a C-index of 0.67 (eFigure 15). Time-dependent AUCs between 2 and 4 years were all significant, with values ranging from 0.68 at 2 years to 0.73 at 3 years (eTable 7).

4. Discussion

In this prospective cross-sectional and longitudinal study, we assessed the relative importance of conventional and advanced MRI biomarkers of brain and spinal cord damage, alongside serum biomarkers, in predicting key clinical outcomes in pwMS. A machine learning approach was employed to identify the variables most significantly contributing to clinical outcomes and to rank their importance. Our analysis suggested several predictors of neurological disability, cognitive impairment, as well as future disability progression, including spinal cord and brain volumetric metrics, qMRI parameters, and measures of lesion burden. Among the evaluated biomarkers, spinal cord atrophy emerged as a relevant determinant of disability severity and a distinguishing feature of patients with progressive disease. Cortical damage, encompassing both focal lesion burden and diffuse neurodegeneration, contributed to predicting the risk of PIRA. Notably, PIRA was also linked to markers of spinal cord and deep gray matter damage,

in addition to sNfL levels. The reproducibility of these findings was broadly consistent in an independent validation cohort of 279 pwMS with a longer follow-up. In this second cohort, spinal cord CSA measurements at all cervical levels again emerged as top predictors of EDSS, reinforcing their central role in determining physical disability. Thalamic volume, lesion burden, and sGFAP levels also contributed meaningfully to model performance. Consistent predictors of time to PIRA included spinal cord atrophy, deep gray matter volume, and cortical thickness, particularly in the cingulate cortex. These findings support the relevance of the selected biomarkers in capturing both cross-sectional disability and future disease progression.

Pathological changes in the spinal cord are a hallmark of MS, often manifesting early in the disease course and becoming particularly pronounced in PMS.[16] These changes include both focal demyelinating lesions and diffuse degeneration leading to atrophy. Spinal cord lesions are associated with an increased risk of disease progression,[162] while spinal cord atrophy has been consistently linked to clinical disability in several studies.[16,32] Atrophy reflects a complex interplay of microstructural changes, including demyelination, neuroaxonal loss, and gliosis,[30] and progresses partially independently of both spinal cord lesions and brain pathology.[31] Importantly, spinal cord atrophy has been shown to predict future clinical worsening,[163] including PIRA.[35,36] In this study, spinal cord atrophy emerged as the most significant marker of disability severity, with CSA at the four rostral cervical cord levels identified as primary predictors of the EDSS score. Among these, C2 CSA was the most informative biomarker for distinguishing PMS from RRMS. Furthermore, spinal cord CSA predicted disease progression due to PIRA. Notably, the influence of spinal cord CSA on disability severity and progression was independent of spinal cord lesion burden, which played a comparatively minor role. Collectively, these findings underscore spinal cord degeneration as a key determinant of MS severity. The validation cohort further reinforced these conclusions, with CSA at C1–C3 levels among the most important predictors of both overall disability and time to PIRA. Notably, C3 CSA was the strongest predictor of progression in the RRMS subgroup, supporting its robustness as a marker across disease phenotypes. Remarkably, these findings are noteworthy given that spinal cord CSA was derived directly from brain MRI scans. Although coverage was limited to the upper cervical cord and no specific spinal cord imaging protocol was available, the results indicate that meaningful and clinically relevant information can be obtained from cervical spinal cord segments that are commonly included in standard brain MRI examinations.

Measures of cortical damage also emerged as crucial predictors of clinical outcomes. Cortical degeneration, encompassing both focal lesions and diffuse atrophy reflected by volume loss and thinning, is a critical yet often underappreciated manifestation of MS pathology. Focal CLs, long overlooked due to imaging limitations, are now recognized as significant contributors to disease progression, linked to inflammation, demyelination, and neuronal loss.[82,164] Cortical atrophy correlates with cognitive decline and physical disability, progressing steadily and most prominently in progressive disease forms.[16,26] This degeneration arises from a complex interplay of primary neurodegenerative processes and secondary effects of white matter damage,[165] occurring in non-random clinically-relevant anatomical patterns.[81] Advances in imaging have enhanced the detection of cortical abnormalities, including both lesions and atrophy, providing valuable insights into their role as predictors of long-term disability and their potential as therapeutic targets.[58] In our study, while cortical damage was significantly associated with disease severity, its contribution was relatively lower than other MRI-based metrics. However, cortical damage was pivotal in predicting PIRA. Remarkably, CTh in the temporal lobe emerged as the strongest predictor of time to PIRA in Cohort 1, even in sensitivity analyses restricted to PIRMA events, and restricted to PIRA events that occurred in patients with a classical RRMS disease course. Cerebral cortex has previously been shown to exhibit accelerated thinning in patients experiencing PIRA as compared to stable patients.[26] Interestingly, our findings also suggest a potential connection with results from a large longitudinal study, which identified accelerated GM atrophy in the temporal lobe as the only volumetric measurement distinguishing patients with secondary progressive MS from those with RRMS.[79] In line with these findings, the validation cohort confirmed the predictive value of CTh – particularly cingulate and mean CTh – for PIRA and PIRMA.

Propensity score-matched analysis in Cohort 1 further underscored the importance of focal cortical degeneration in explaining disability accumulation due to PIRA. CLs showed the highest importance in distinguishing patients with PIRA from stable patients, with both CL volume and count being significant predictors. Interestingly, a previous study has likewise linked CL burden to the risk of conversion to secondary progressive MS.[82] Additionally, mean qT1 values in the normal appearing cerebral cortex significantly contributed to the classification, highlighting their relevance as a measure sensitive to tissue micro- and macrostructural integrity, influenced by myelin, water, and iron content.[50]

As expected, the biomarkers most associated with performance on the SDMT differed from those predicting physical disability. Subcortical volumetric measurements – including white matter, thalamus, hippocampus, and deep GM – emerged as the most relevant predictors. These findings align with prior studies emphasizing the importance of subcortical structures in explaining cognitive performance, particularly attention and information processing speed in pwMS.[166,167] The relevance of subcortical degeneration was further supported by the importance of qT1 values in the deep GM as a measure of tissue degeneration and loss of structural integrity.

The results of this study highlighted the complementary roles of brain and spinal cord volumetric measurements alongside measures of focal lesion burden. While CL load and T1-hypointense WMLs were significant predictors of the clinical outcomes under consideration, PRLs showed predictive value in univariate analyses but did not provide additional information in multivariate models. This finding may reflect the enhanced insights offered by advanced qMRI metrics, which capture WML microstructural changes with greater sensitivity. Alternatively, it could be partially attributable to the limited statistical power of the study, underscoring the need for further investigation with larger cohorts. Notably, qMRI metrics of normal-appearing tissue also significantly contributed to predicting disease severity and progression. Additionally, sNfL and sGFAP levels were useful in predicting PIRA. Elevated sNfL levels, a biomarker of neuroaxonal injury, are valuable for detecting acute and chronic neuronal damage. Existing literature has also shown the potential value of sNfL in predicting PIRA.[7,150,168] Given its increasing availability in clinical settings, sNfL is a promising biomarker; however, previous studies have highlighted sGFAP as a complementary marker that may offer greater specificity for smoldering disease activity and lower sensitivity to acute inflammation.[150,151] Indeed, in the validation cohort, sGFAP emerged as a significant predictor not only of disability severity and disease phenotype but also of PIRA occurrence.

In this study, we identified several predictors of PIRA, predominantly reflecting cortical degeneration, cervical spinal cord atrophy, and deep gray matter damage. These predictors yielded overall moderate performance in time-to-event models, with C-indices ranging from 0.64 to 0.81 across analyses. This finding is consistent with the known complexity of predicting an outcome such as PIRA, which is intrinsically challenging. Silent progression is influenced

by multiple, partially overlapping biological mechanisms. In addition, its identification and the determination of its onset are technically challenging due to reliance on EDSS-based definitions, measurement noise, variability in follow-up intervals, and the influence of confounding factors such as aging and comorbidities. Together, these factors likely contribute to the moderate discriminative performance observed, which is nonetheless comparable to - or in some cases higher than - previous investigations.[169–173] Importantly, a prediction score derived from a limited set of clinically accessible biomarkers achieved consistent performance and was corroborated across the two cohorts, suggesting that meaningful risk stratification is achievable to a certain extent. Such an approach may be particularly valuable for research applications and may also support clinical monitoring by facilitating the identification of individuals at potentially higher risk of silent progression.

A key strength of this study is the simultaneous evaluation of a diverse array of MRI and serum biomarkers, providing a comprehensive assessment of their relative contributions to clinical outcomes. The machine learning approach employed for feature selection reduced noise and overfitting while maintaining model interpretability, enabling the handling of complex, non-linear relationships. Models based on the predictors selected by Boruta showed high performance for disability classification and moderate performance for PIRA prediction, in line with the inherent complexity of this outcome. Importantly, results from the second cohort corroborated these overall patterns.

Nevertheless, the study has some limitations. First, PIRA was assessed exclusively through EDSS, which may underestimate subtle progression with still significant clinical impact. Second, the absence of spinal cord regional damage assessment is a limitation, especially considering recent studies showing that spinal cord GM atrophy outperforms whole CSA in explaining disability.[161,174] Third, although the inclusion of a validation cohort strengthens the robustness of our findings, several differences between cohorts should be acknowledged. The cohorts differed in follow-up duration - an important factor when studying outcomes such as PIRA - and in baseline clinical characteristics, with Cohort 1 including a higher proportion of progressive MS and higher baseline EDSS. These differences may partly explain discrepancies in the specific biomarkers selected across cohorts. In addition, fewer biomarkers were available in Cohort 2, and the absence of a matched healthy control cohort precluded adjustment of imaging biomarkers for physiological confounders using deviation-from-normal approaches. Despite these differences, we deliberately included the second cohort to enhance

generalizability, acknowledging that cohorts with an availability of advanced MRI metrics as extensive as Cohort 1 are exceptionally rare. Importantly, both cohorts consistently highlighted the relevance of cortical and spinal cord damage, and predictors of PIRA identified in Cohort 2 generalized well when applied to Cohort 1 for prognostication, supporting the robustness of the identified biomarkers across heterogeneous populations. Fourth, the disproportionate inclusion of a broad set of MRI-derived biomarkers compared to only two serum biomarkers (sNfL and sGFAP) may have introduced a bias toward the selection of MRI features in the variable importance ranking. Although serum biomarkers were associated with PIRA, the study was not powered to determine whether their addition to quantitative MRI metrics yields a statistically robust improvement in predictive performance, and further studies specifically designed to address this question will be required. Fifth, collinearity among some MRI-derived metrics may partially influence the interpretation of variable-importance estimates, although sensitivity analyses provided consistent results. Finally, despite the inclusion of two independent cohorts and a relatively long follow-up, it should be acknowledged that PIRA occurred only in a subset of patients, representing a common challenge in PIRA research. Consequently, the absolute number of PIRA events was limited, which may affect the generalizability of the findings. Nevertheless, the consistency of results across cohorts supports the robustness of the observed associations, while further confirmation in larger populations and additional settings is central to refine and validate these predictive approaches.

Despite these limitations, the findings are of potential clinical relevance. They highlight the crucial role of spinal cord and cortical degeneration as prognostic markers in MS, underscoring the potential value of their inclusion in clinical evaluations to bridge the gap between conventional MRI biomarkers and measures of disease severity and progression. These insights potentially pave the way for more refined and targeted approaches to understanding and managing MS.

8. Comparative Effectiveness of Teriflunomide and Ocrelizumab on Smoldering Activity in Multiple Sclerosis: An Observational Study in the Swiss Multiple Sclerosis Cohort

Authors: Alessandro Cagol[1,2,3,4], Sabine Schaedelin[1,5], Mario Ocampo-Pineda[1,2,3], Pascal Benkert[5], Lester Melie-Garcia[1,2,3], Ludovico Luchetti[21-22], Özgür Yaldizli[1,2,3], Johanna Oechtering[2,3], Marcus D'Souza[2,3], Bettina Fischer-Barnicol[2], Stefanie Müller[6], Sebastian Finkener[7], Jochen Vehoff[6], Giulio Disanto[8], Andrew Chan[9], Caroline Pot[10], Chiara Zecca[8,12], Tobias Derfuss[2,3], Johanna M. Lieb[13], Michael Diepers[14], Franca Wagner[15], Renaud Du Pasquier[10,16], Patrice H. Lalive[11], Emanuele Pravatà[8,12,17], Olaf Chan-Hi Kim[18], Robert Hoepner[9], Patrick Roth[19], Claudio Gobbi[8,12], David Leppert[2], Marco Battaglini[21-22], Ludwig Kappos[1,2], Maria Pia Sormani[4,20], Jens Kuhle,[2,3] & Cristina Granziera,[1,2,3] for the Swiss MS Cohort

Affiliations: 1. Translational Imaging in Neurology (ThINk) Basel, Department of Biomedical Engineering, Faculty of Medicine, University Hospital Basel and University of Basel, Hegenheimermattweg 167b, 4123, Allschwil, Basel, Switzerland. 2. Multiple Sclerosis Centre, Departments of Neurology, Clinical Research and Biomedicine, University Hospital Basel and University of Basel, Basel, Switzerland. 3. Research Center for Clinical Neuroimmunology and Neuroscience Basel (RC2NB), University Hospital Basel and University of Basel, Basel, Switzerland. 4. Dipartimento di Scienze della Salute, Università degli Studi di Genova, Genoa, Italy. 5. Department of Clinical Research, University Hospital Basel, University of Basel, Basel, Switzerland. 6. Clinic of Neurology, HOCH Health Ostschweiz, Cantonal Hospital St. Gallen, Academic and Research Hospital, St. Gallen, Switzerland. 7. Department of Neurology, Cantonal Hospital Aarau, Aarau, Switzerland. 8. Neurology Department, Neurocenter of Southern Switzerland, EOC, Lugano, Switzerland. 9. Department of Neurology, Inselspital, Bern University Hospital and University of Bern, Bern, Switzerland. 10. Division of Neurology, Department of Clinical Neurosciences, Lausanne University Hospital (CHUV) and University of Lausanne, Lausanne, Switzerland. 11. Department of Clinical Neurosciences, Division of

Neurology, Geneva University Hospitals and Faculty of Medicine, Geneva, Switzerland. 12. Faculty of Biomedical Sciences, Università della Svizzera Italiana, Lugano, Switzerland. 13. Division of Diagnostic and Interventional Neuroradiology, Clinic for Radiology and Nuclear Medicine, University Hospital Basel, University of Basel, Basel, Switzerland. 14. Department of Diagnostic and Interventional Neuroradiology, Cantonal Hospital Aarau, Aarau, Switzerland. 15. Department of Diagnostic and Interventional Neuroradiology, Inselspital, Bern University Hospital and University of Bern, Bern, Switzerland. 16. Division of Radiology, Lausanne University Hospital (CHUV) and University of Lausanne, Lausanne, Switzerland. 17. Department of Neuroscience, Imaging and Clinical Sciences, Institute of Advanced Biomedical Technologies, University of Chieti, 66100, Chieti, Italy. 18. Department of Radiology, Cantonal Hospital St. Gallen, St. Gallen, Switzerland. 19. Department of Neurology, University of Zurich, University Hospital of Zurich, Zurich, Switzerland. 20. IRCCS Ospedale Policlinico San Martino, Genoa, Italy. 21. Department of Medicine, Surgery and Neurosciences, University of Siena, Siena, Italy. 22. SIENA Imaging SRL, Siena, Italy.

Published in: J Neurol. 2025 Jul 2;272(8):491. doi: 10.1007/s00415-025-13221-x. PMID: 40603656; PMCID: PMC12222313.

Abstract

Background: This study aimed to compare the effects of teriflunomide and ocrelizumab on clinical and MRI endpoints related to smoldering activity in relapsing–remitting multiple sclerosis (RRMS).

Methods: In this observational, longitudinal, multicenter study, we included 128 people with RRMS (pwRRMS) treated with teriflunomide and 495 treated with ocrelizumab. Outcomes included time to progression independent of relapse activity (PIRA). In a subset, we also assessed brain volume loss (BVL), longitudinal changes in diffusion tensor imaging (DTI) metrics, and the burden of paramagnetic rim lesions (PRLs). Propensity score matching was used for between-group comparisons.

Results: Over a median follow-up of 3.1 years in the ocrelizumab group and 1.9 years in the teriflunomide group, there were no significant differences in the risk of PIRA (HR for teriflunomide vs. ocrelizumab: 0.80 [95%-CI:0.40–1.60]; p = 0.53). PwRRMS treated with

teriflunomide exhibited lower annualized rates of BVL (−0.80 [95%-CI: −0.91; −0.69] vs. −1.06 [95%-CI: −1.25; −0.86]; p = 0.025) and gray matter volume loss (−0.92 [95%-CI: −1.05; −0.79] vs. −1.20 [95%-CI: −1.43; −0.97]; p = 0.035). No differences were observed in DTI metrics or PRL count.

Conclusions: This real-world study suggests that teriflunomide shows similar efficacy to ocrelizumab on smoldering activity, with a potentially greater effect in reducing BVL. Further research is needed to confirm these findings and understand their long-term implications.

Introduction

Multiple sclerosis (MS) is an immune-mediated neurological disease characterized by inflammation, demyelination, and neurodegeneration, ultimately leading to progressive disability. Traditionally, relapsing–remitting MS (RRMS) was thought to be defined solely by acute inflammatory events interspersed with periods of stability. However, it is now increasingly recognized that smoldering disease processes play a critical role in RRMS.[4,5] A key concept in this evolving understanding is progression independent of relapse activity (PIRA), which refers to the gradual accumulation of disability driven by underlying disease processes that are unrelated to acute inflammatory events.[7] PIRA has been shown to occur frequently in people with RRMS (pwRRMS), where it is the primary determinant of disability accrual in the modern treatment era.[7,8]

The smoldering mechanisms underlying disease progression include non-resolving inflammation, neurodegeneration, oxidative stress, and mitochondrial dysfunction, which may occur independently or interact with each other.[4] In addition, the failure of compensatory mechanisms, such as remyelination and neuroplasticity, together with aging exacerbate these processes.[4] Some of these smoldering processes can be detected in vivo using advanced MRI biomarkers derived from both conventional and non-conventional techniques. These include the estimation of global and regional brain volume loss (BVL), particularly in gray matter structures, which serves as a proxy for the overall neurodegenerative burden of the disease.[16] Paramagnetic rim lesions (PRLs) are another important biomarker, gaining increasing importance for their ability to identify chronic active lesions, which are associated with worse clinical outcomes.[38] Diffusion MRI, which is sensitive to microstructural tissue integrity, provides indirect measures of demyelination and axonal loss.[74,108] Notably, all these MRI

measures have demonstrated sensitivity to the pathological changes occurring in patients with PIRA.[25,26,35,96,175]

Together, the smoldering neurodegenerative and chronic inflammatory processes shape the clinical trajectories of MS, emphasizing the need for therapeutic strategies that address the complex nature of the disease. The currently approved disease-modifying therapies (DMTs) vary in their efficacy in providing neuroprotection. Teriflunomide, an oral immunomodulator approved for the treatment of relapsing forms of MS, targets dihydroorotate dehydrogenase, a mitochondrial enzyme involved in pyrimidine synthesis, thereby reducing the activity of proliferating B and T cells. In phase II and phase III clinical trials, teriflunomide showed improvements over placebo in annualized relapse rate (ARR), MRI lesions, and disability accumulation.[176] Additionally, teriflunomide has been shown to reduce BVL in both clinical trials and real-world studies, suggesting a potential effect on neurodegenerative processes.[176] Ocrelizumab, a recombinant humanized anti-CD20 monoclonal antibody, is approved for the treatment of both relapsing forms of MS and primary progressive MS (PPMS). In RRMS, ocrelizumab has demonstrated efficacy in reducing ARR, MRI lesions, and disability accumulation as compared to interferon beta-1a.[177] However, while ocrelizumab demonstrated superiority over placebo in reducing BVL in patients with PPMS, it did not show greater efficacy compared to interferon beta-1a in pwRRMS.[177] Notably, a post-hoc analysis of the pooled OPERA I and II trials showed that ocrelizumab is effective in reducing the incidence of PIRA compared to interferon beta-1a.[3]

To date, no head-to-head comparisons have been conducted between teriflunomide and ocrelizumab, and the impact of these treatments on clinical and MRI measures of smoldering activity remains poorly explored.

In this study, we aimed to compare the association of teriflunomide and ocrelizumab with PIRA and MRI measures of smoldering disease activity in an observational multicenter cohort of pwRRMS.

Patients and methods

Participants and study design

In this observational study, participants were selected from the Swiss Multiple Sclerosis Cohort (SMSC), a prospective, multicenter study conducted across eight Swiss academic centers that

features standardized collection of demographic, clinical, and MRI data.[104] For our investigation, we retrospectively included all adult SMSC participants diagnosed with RRMS who were treated with either teriflunomide or ocrelizumab during follow-up. We analyzed all longitudinal clinical and MRI examinations for each patient from the initiation of teriflunomide or ocrelizumab treatment, censoring data at the last visit, or at treatment discontinuation. Patients who received both treatments during SMSC follow-up were included only with data corresponding to the first treatment chronologically.

Specific analysis sets, with propensity score matching between treatment groups, were defined for each study endpoint based on data availability. The study endpoints included:

1. Time to PIRA, analyzed in the entire study cohort.
2. Global and regional BVL, analyzed in participants with at least one brain MRI scan including three-dimensional (3D) magnetization-prepared rapid gradient echo (MPRAGE).
3. Longitudinal changes in diffusion tensor imaging (DTI) metrics within white matter lesions (WMLs), normal-appearing white matter (NAWM), and cerebral cortex, analyzed in participants with at least one brain MRI scan including diffusion-weighted imaging.
4. Longitudinal changes in paramagnetic rim lesion (PRL) burden, analyzed in participants with at least one brain MRI scan including 3D segmented echo planar imaging (EPI).

The study design is graphically displayed in Fig. 1. The study was approved by the local ethics committee, and all patients provided written informed consent before study entry.

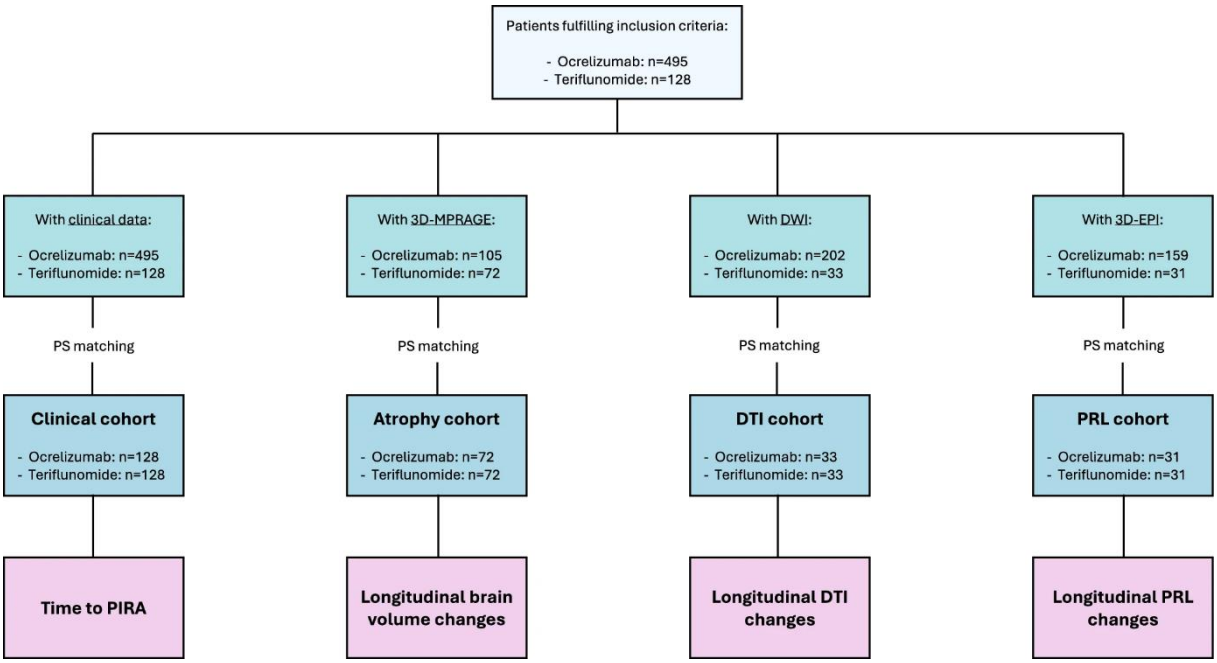

Study design. Abbreviations: 3D-EPI = three-dimensional echo planar imaging; 3D-MPRAGE = three-dimensional magnetization-prepared rapid gradient echo; DTI = diffusion tensor imaging; DWI = diffusion-weighted imaging; PIRA = progression independent of relapse activity; PRL = paramagnetic rim lesion; PS = propensity score.

Clinical data

All participants underwent regular clinical evaluations, conducted at least annually. Standardized assessments included the calculation of the Expanded Disability Status Scale (EDSS) score (https://www.neurostatus.net/), performed by certified raters.

The occurrence of PIRA during follow-up was defined as an increase in EDSS score (≥ 1.5, ≥ 1.0, or ≥ 0.5 points if baseline EDSS was 0, 1.0–5.5, or > 5.5, respectively) using a roving baseline,[152] confirmed at least after 6 months, in the absence of relapses (1) between the EDSS increase and the preceding reference visit (conducted ≥ 90 days before the EDSS increase) and (2) between the EDSS increase and its confirmation.[7]

MRI acquisition and analysis

Brain MRI scans were performed at each center with protocols optimized to ensure a homogeneous signal-to-noise ratio. Protocol details are provided in eTables 1–3.

Segmentation of T2-hyperintense WMLs on 3D fluid attenuated inversion recovery (FLAIR) images was performed using a deep learning-based tool,[105] followed by manual correction.

Brain volumetric measurements were obtained on 3D-MPRAGE images using the longitudinal pipeline of *SAMSEG*, with 3D-FLAIR images included as an additional input to optimize automatic segmentation.[178] The volumes of interest considered in the study included total brain volume, cortical volume, thalamic volume, and total gray matter volume. Total intracranial volume (TIV) was also calculated to account for between-subject differences in head size in the statistical analyses.

DTI metrics were derived from diffusion-weighted images after denoising and correction for ringing artifacts, eddy current distortions, misalignments, and bias field [21]. Fractional anisotropy (FA), radial diffusivity (RD), mean diffusivity (MD), and axial diffusivity (AD) maps were generated using *MRtrix*.[179] For each map, mean values within WMLs, NAWM, and cerebral cortex were derived.

The presence of PRLs was assessed by an experienced rater (A.Ca.), who was blinded to patient identity. PRLs were defined as discrete FLAIR-hyperintense lesions either completely or partially encircled by a rim of paramagnetic signal, clearly evident in at least one contrast between unwrapped phase and quantitative susceptibility mapping (QSM), as previously described.[35] High inter-rater agreement in PRL detection was previously demonstrated in the same cohort.[35]

In patients with PIRA, we assessed the accumulation of new or enlarged T2-hyperintense WMLs to identify events occurring without accompanying MRI activity, thereby fulfilling the criteria for progression independent of relapse and MRI activity (PIRMA).[7,10] This analysis was conducted using a semi-automated approach to systematically compare all 3D-FLAIR images acquired during routine follow-up in the SMSC.[107]

Statistical analysis

All statistical analyses were conducted using *R* (*version 4.3.1*).

To mitigate bias from the non-random assignment to treatments in the SMSC study, we performed 1:1 propensity score matching between treatment groups. The matching criteria included the following variables at baseline: age, sex, disease duration, number of previous DMTs, number and volume of WMLs, raw and Z score levels of serum neurofilament light chain (sNfL),[159] EDSS score, and time under current treatment. Separate matched sets were constructed for each endpoint to maximize sample size.

We compared the incidence of PIRA between groups using Cox proportional hazard models to assess time to PIRA. Longitudinal changes in brain volumes, DTI metrics, and PRL burden were analyzed using mixed-effect models. These models included an interaction term between treatment group and time to examine group differences in longitudinal changes, with participants included as random intercepts. When modeling BVL, scanner magnetic field strength and TIV were included as additional covariates. Time was log-transformed to derive the annualized percentage change (APC) in MRI metrics. Model assumptions were assessed through visual inspection of residuals.

For time to PIRA, the following sensitivity analyses were performed: (1) censoring patients at the same time as their matching pair rather than at their last observation (pairwise censoring); (2) including only PIRA episodes where the initial EDSS increase occurred after treatment initiation; and (3) exploring time to PIRMA.

For BVL, the following sensitivity analyses were conducted: (1) including baseline age, sex, and disease duration, along with their interaction with time, as covariates in the mixed-effect models; (2) including ARR during MRI follow-up, along with its interaction with time, as covariates in the mixed-effect models; (3) including only patients with at least two MRI scans for volumetric analysis; and (4) including only scans obtained at least 6 months after treatment initiation.

All statistical analyses were conducted by a statistician (S.S.) who was not involved in the MRI analyses, while the authors conducting the MRI analyses did not have access to patient information, including treatment details.

Results

A total of 623 pwRRMS met the inclusion criteria and were enrolled in the study. The key demographic and clinical characteristics are summarized in Table 1.

Table 1 Key baseline characteristics of the cohort

n	623
Age, mean (SD), years	43.1 (12.5)
Females, No. (%)	408 (65.5)
Disease duration, median [IQR], years	9.2 [3.6; 16.7]
EDSS, median [IQR]	2.5 [1.5; 3.5]
Number of previous DMTs, median [IQR]	1 [0; 3]
Time under current treatment, median [IQR], years	2.2 [0.0; 5.1]
sNfL, median [IQR], pg/ml	10.2 [7.3; 14.8]
sNfL Z-score, median [IQR]	0.8 [−0.1; 1.7]
T2LV, median [IQR], ml	7.4 [3.4; 14.2]
T2L count, median [IQR]	32.0 [21.7; 42.0]
SMSC centers	
– Aarau, No. (%)	71 (11.4)
– Basel, No. (%)	315 (50.6)
– Bern, No. (%)	17 (2.7)
– Geneva, No. (%)	64 (10.3)
– Lausanne, No. (%)	46 (7.4)
– Lugano, No. (%)	52 (8.3)
– St. Gallen, No. (%)	42 (6.7)
– Zurich, No. (%)	16 (2.6)

DMT disease modifying treatment, *EDSS* Expanded Disability Status Scale, *IQR* interquartile range, *SD* standard deviation, *SMSC* Swiss Multiple Sclerosis Cohort, *sNfL* serum neurofilament light chain, *T2L* T2-lesion, *T2LV* T2-lesion volume

Separate match sets were created for each outcome of interest, and the baseline MRI characteristics showed no significant differences between the propensity score-matched groups (Table 2).

Table 2 MRI characteristics at baseline

	Ocrelizumab	Teriflunomide	Comparison
Atrophy cohort			
n	72	72	
Brain parenchymal fraction, median [IQR]	0.69 [0.66;0.71]	0.68 [0.65;0.73]	[a]p = 0.85; SMD = 0.067
Cortical fraction, median [IQR]	0.31 [0.29;0.33]	0.31 [0.29;0.33]	[a]p = 0.99; SMD = 0.028
Thalamic fraction, median [IQR]	0.01 [0.01;0.01]	0.01 [0.01;0.01]	[a]p = 0.53; SMD = 0.217
Gray matter fraction, median [IQR]	0.40 [0.38;0.43]	0.41 [0.38;0.44]	[a]p = 0.56; SMD = 0.088
DTI cohort			
n	33	33	
AD WMLs, median [IQR], mm^2/s	0.00149 [0.00141;0.00158]	0.00145 [0.00141;0.00157]	[a]p = 0.77; SMD = 0.188
AD NAWM, median [IQR], mm^2/s	0.00106 [0.00105;0.00108]	0.00107 [0.00105;0.00109]	[a]p = 0.79; SMD = 0.023
AD Cortex, median [IQR], mm^2/s	0.00106 [0.00104;0.00109]	0.00106 [0.00103 0.00108]	[a]p = 0.69; SMD = 0.057
FA WMLs, median [IQR]	0.300 [0.277;0.320]	0.303 [0.287;0.340]	[a]p = 0.24; SMD = 0.364
FA NAWM, median [IQR]	0.376 [0.363;0.388]	0.386 [0.375;0.396]	[a]p = 0.12; SMD = 0.440
FA Cortex, median [IQR]	0.170 [0.158;0.175]	0.169 [0.163;0.173]	[a]p = 0.88; SMD = 0.237
MD WMLs, median [IQR], mm^2/s	0.00113 [0.00107;0.00121]	0.00109 [0.00103;0.00121]	[a]p = 0.31; SMD = 0.274
MD NAWM, median [IQR], mm^2/s	0.00074 [0.00073;0.00076]	0.00074 [0.00073;0.00076]	[a]p = 0.88; SMD = 0.201
MD Cortex, median [IQR], mm^2/s	0.00091 [0.00090;0.00093]	0.00091 [0.00088;0.00092]	[a]p = 0.39; SMD = 0.173
RD WMLs, median [IQR], mm^2/s	0.00095 [0.00091;0.00102]	0.00090 [0.00084;0.00102]	[a]p = 0.21; SMD = 0.307
RD NAWM, median [IQR], mm^2/s	0.00058 [0.00057;0.00060]	0.00057 [0.00056;0.00060]	[a]p = 0.57; SMD = 0.271
RD Cortex, median [IQR], mm^2/s	0.00083 [0.00082;0.00085]	0.00083 [0.00081;0.00085]	[a]p = 0.30; SMD = 0.214
PRL cohort			
n	31	31	
PRL count, median [IQR]	0 [0; 2]	1 [0; 3.25]	[a]p = 0.17; SMD = 0.036

Brain parenchymal fraction, cortical fraction, thalamic fraction, and gray matter fraction were obtained by dividing total brain volume, cortical volume, thalamic volume, and gray matter volume by the total intracranial volume

[a]Obtained with Mann–Whitney U test

AD axial diffusivity, *DTI* diffusion tensor imaging, *FA* fractional anisotropy, *IQR* interquartile range, *MD* mean diffusivity, *NAWM* normal-appearing white matter, *PRL* paramagnetic rim lesions, *RD* radial diffusivity, *SMD* standardized mean difference, *SD* standard deviation, *WMLs* white matter lesions

Incidence of PIRA

Baseline characteristics of the clinical cohort before and after propensity score matching are reported in eTable 4. A total of 128 pwRRMS per treatment group contributed to the analysis. The median (IQR) follow-up time was 3.1 (1.4; 4.6) years for the ocrelizumab group and 1.9 (1.0; 3.7) years for the teriflunomide group. During the observation period, there were 35 PIRA events, with 21 occurring in the ocrelizumab group and 14 in the teriflunomide group. The time to PIRA was not significantly different between treatment groups (hazard ratio [HR] for teriflunomide vs. ocrelizumab: 0.80 [95% CI: 0.40; 1.60]; p = 0.53). Kaplan–Meier curves for time to PIRA are displayed in Fig. 2.

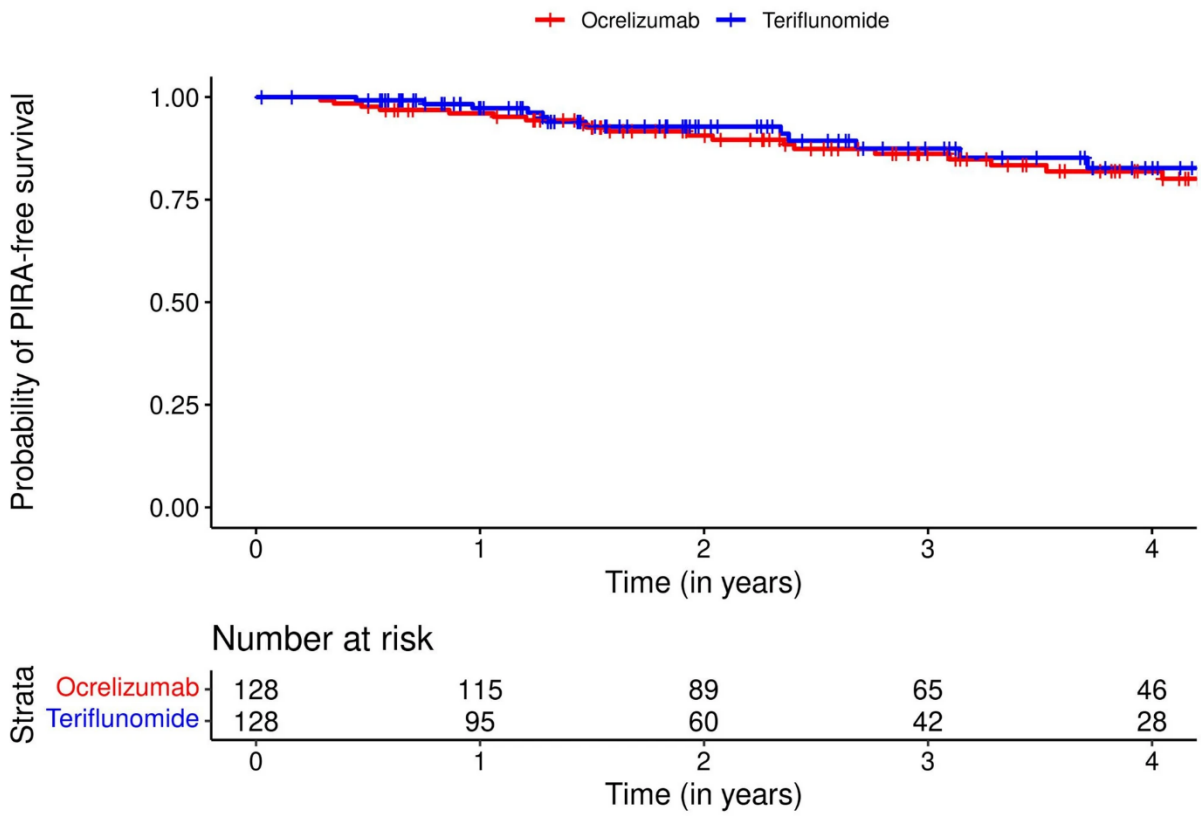

Fig. 2: Probability of PIRA-free survival. Abbreviations: PIRA = progression independent of relapse activity.

Results remained consistent in sensitivity analyses applying pairwise censoring (HR for teriflunomide vs. ocrelizumab: 0.90 [95% CI: 0.37; 2.21]; p = 0.82) and excluding PIRA events with onset before treatment initiation (HR for teriflunomide vs. ocrelizumab: 0.93 [95% CI: 0.43; 2.02]; p = 0.86). 32 out of 35 PIRA events qualified as PIRMA; the time to PIRMA was not different between treatment groups (HR for teriflunomide vs. ocrelizumab: 0.75 [95% CI: 0.36; 1.56]; p = 0.44).

Brain volume loss

Baseline characteristics of the brain atrophy cohort before and after propensity score matching are reported in eTable 5. A total of 72 pwRRMS per treatment group contributed to the analysis. The median (IQR) follow-up time was 1.7 (0.6; 2.5) years for the ocrelizumab group and 1.0 (0.0; 3.8) years for the teriflunomide group. Compared to pwRRMS treated with ocrelizumab, those treated with teriflunomide exhibited reduced rates of total BVL (APC: −0.80 [95% CI: −0.91; −0.69] vs. −1.06 [95% CI: −1.25; −0.86]; p = 0.025) and gray matter volume loss (APC: −0.92 [95% CI: −1.05; −0.79] vs. −1.20 [95% CI: −1.43; −0.97]; p = 0.035) during the

observation period (Fig. 3). There were no significant differences in the rates of cortical volume and thalamic volume loss between groups (Table 3).

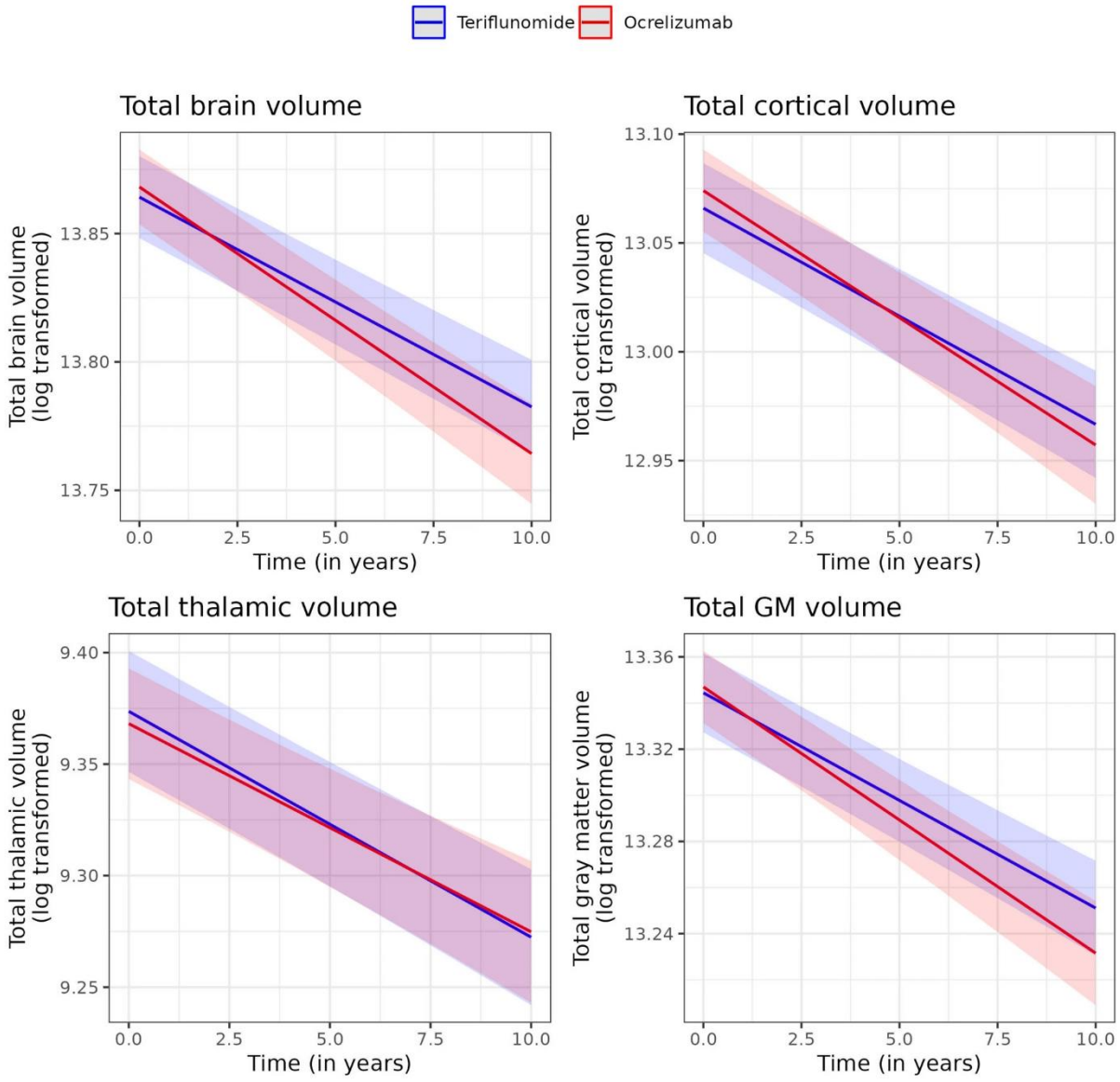

***Fig. 3**: Between group comparison of brain volume loss rates*

Table 3 Longitudinal changes in MRI metrics

	Ocrelizumab (APC)	Teriflunomide (APC)	Comparison
Atrophy cohort			
n	72	72	
Total brain volume change, mean (95% CI)	−1.06 (−1.25; −0.86)	−0.80 (−0.91; −0.69)	[a]**p = 0.025**
Cortical volume change, mean (95% CI)	−1.24 (−1.51; −0.97)	−0.97 (−1.12, −0.82)	[a]p = 0.09
Thalamic volume change, mean (95% CI)	−0.97 (−1.23; −0.71)	−1.04 (−1.19; −0.90)	[a]p = 0.64
Gray matter volume change, mean (95% CI)	−1.20 (−1.43; −0.97)	−0.92 (−1.05; −0.79)	[a]**p = 0.035**
No. of MRI follow-ups, median [IQR]	2.5 [2.0;3.0]	2.0 [1.0;4.3]	[b]p = 0.81; SMD = 0.295
Follow-up time, median [IQR], years	1.7 [0.6; 2.5]	1.0 (0.0; 3.8)	[b]p = 0.83; SMD = 0.246
DTI cohort			
n	33	33	
AD WMLs change, mean (95% CI)	−0.05 (−0.72; 0.62)	0.79 (0.15; 1.44)	[a]p = 0.08
AD NAWM change, mean (95% CI)	0.10 (−0.18; 0.38)	−0.00 (−0.27; 0.26)	[a]p = 0.60
AD Cortex change, mean (95% CI)	−0.30 (−0.68; 0.09)	0.08 (−0.28; 0.44)	[a]p = 0.17
FA WMLs change, mean (95% CI)	−0.04 (−1.29; 1.20)	0.23 (−0.94; 1.41)	[a]p = 0.76
FA NAWM change, mean (95% CI)	0.62 (−0.11; 1.34)	−0.27 (−0.95; 0.40)	[a]p = 0.08
FA Cortex change, mean (95% CI)	−0.43 (−1.36; 0.52)	0.33 (−0.58; 1.24)	[a]p = 0.26
MD WMLs change, mean (95% CI)	0.14 (−0.65; 0.93)	0.84 (0.08; 1.60)	[a]p = 0.21
MD NAWM change, mean (95% CI)	−0.11 (−0.55; 0.33)	0.10 (−0.31; 0.51)	[a]p = 0.50
MD Cortex change, mean (95% CI)	−0.24 (−0.56; 0.09)	0.01 (−0.30; 0.32)	[a]p = 0.29
RD WMLs change, mean (95% CI)	0.30 (−0.69; 1.30)	0.89 (−0.07; 1.85)	[a]p = 0.41
RD NAWM change, mean (95% CI)	−0.29 (−0.92; 0.34)	0.19 (−0.40; 0.79)	[a]p = 0.28
RD Cortex change, mean (95% CI)	−0.20 (−0.52; 0.12)	−0.06 (−0.36; 0.25)	[a]p = 0.52
No. of MRI follow-ups, median [IQR]	3 [2; 4]	3 [2; 4]	[b]p = 0.75; SMD = 0.050
Follow-up time, median [IQR], years	2.0 [1.7; 2.9]	2.0 [1.0; 2.9]	[b]p = 0.91; SMD = 0.104
PRL cohort			
n	31	31	
Longitudinal changes over follow-up:			
– Subjects with new PRLs, No (%)	1 (3)	2 (6)	[a]p = 0.96
– Subjects with resolving PRLs, No (%)	0 (0)	0 (0)	
No. of MRI follow-ups, median [IQR]	2 [2; 3]	3 [2; 4]	[b]p = 0.25; SMD = 0.171
Follow-up time, median [IQR], years	1.5 [1.0; 2.2]	2.0 [1.2; 2.9]	[b]p = 0.07; SMD = 0.452

[a]Obtained from the mixed-effect models

[b]Obtained with Mann–Whitney U test

AD axial diffusivity, *APC* annualized percentage change, *DTI* diffusion tensor imaging, *FA* fractional anisotropy, *IQR* interquartile range, *MD* mean diffusivity, *MRI* magnetic resonance imaging, *NAWM* normal-appearing white matter, *PRL* paramagnetic rim lesions, *RD* radial diffusivity, *SMD* standardized mean difference, *SD* standard deviation, *WMLs* white matter lesions

Significant *p*-values are displayed in bold

A significantly lower rate of BVL in patients treated with teriflunomide was confirmed in sensitivity analyses adjusting for baseline age, sex, and disease duration, as well as for ARR during the observation period, and in the subset of patients with at least 2 MRI time points (eTables 6–8). When including only scans performed at least 6 months after treatment initiation, the between-group differences in rates of BVL lost statistical significance (eTable 9).

DTI metrics

Baseline characteristics of the DTI cohort before and after propensity score matching are reported in eTable 10. A total of 33 pwRRMS per treatment group contributed to the analysis.

The median (IQR) follow-up time was 2.0 (1.7; 2.9) years for the ocrelizumab group and 2.0 (1.0; 2.9) years for the teriflunomide group. No significant differences were observed in the rates of DTI metrics changes across any of the regions of interest during the observation period (Table 3).

PRL count

Baseline characteristics of the PRL cohort before and after propensity score matching are reported in eTable 11. A total of 31 pwRRMS per treatment group contributed to the analysis. The median (IQR) follow-up time was 1.5 (1.0; 2.2) years for the ocrelizumab group and 2.0 (1.2; 2.9) years for the teriflunomide group. During the observation period, three pwRRMS exhibited an increase in PRL count: two treated with teriflunomide and one with ocrelizumab. No patients showed resolution of PRLs. Longitudinal changes in PRL count did not differ between treatment groups ($p = 0.96$) (Table 3).

Discussion

In this large observational study, we found no differences in the incidence of PIRA between pwRRMS treated with teriflunomide or ocrelizumab. Similarly, longitudinal changes in PRL burden and DTI metrics did not differ between the two groups. However, pwRRMS treated with teriflunomide exhibited reduced rates of whole brain and gray matter volume loss compared to those treated with ocrelizumab.

PIRA, a relatively recent clinical concept, has garnered considerable attention for highlighting that disability can accumulate independently of clinical relapses, even in pwRRMS with short disease duration and low disability.[3,7,8] This understanding has driven research into mechanisms underlying disease progression and underscored the urgent need for treatments targeting these processes.[4,5] This is relevant as PIRA is associated with unfavorable long-term outcomes, particularly when it occurs early in the disease course.[6]

Currently, data on the impact of DMTs on PIRA incidence remain limited. A pivotal analysis of the pooled OPERA I and II trials demonstrated that ocrelizumab reduced the risk of PIRA by 22% compared to interferon beta-1a.[3] Post-hoc analyses of the ASCLEPIOS I and II trials found teriflunomide significantly inferior to ofatumumab, which reduced the risk of PIRA by 56%.[92] However, comparative data on teriflunomide versus ocrelizumab have been lacking. Our study

addresses this gap in an observational real-world cohort using propensity score-matched treatment groups and reveals no differences in PIRA incidence between the two treatments, suggesting comparable impacts on the mechanisms underlying disability progression. Despite potential biases in implementing the PIRA concept in observational studies, our study benefitted from regular clinical follow-up and used a specific definition for PIRA optimized for providing high specificity in the context of observational studies.[7]

During follow-up, patients treated with teriflunomide exhibited significantly reduced BVL compared to those treated with ocrelizumab. In randomized controlled trials, teriflunomide has proved superior to placebo,[180] not significantly different from ofatumumab and ublituximab,[181,182] and inferior to ponesimod[183] in reducing BVL. Ocrelizumab, on the other hand, demonstrated superiority over placebo in PPMS,[184] though differences compared to interferon beta-1a were non-confirmatory in the OPERA I trial and non-significant in the OPERA II trial.[185] In our study, whole brain and gray matter atrophy rates were significantly higher in the ocrelizumab group. Conversely, regional analyses showed no differences in cortex or thalamus atrophy rates. While the results were robust after adjusting for additional confounders, statistical significance was lost in sensitivity analyses restricted to scans obtained after six months of treatment initiation. This loss of significance may suggest a potential influence of pseudoatrophy on the observed results. However, it is important to acknowledge that the sensitivity analyses were limited by reduced statistical power due to a smaller dataset, making direct comparisons challenging. Collectively, these findings suggest teriflunomide may exert a greater impact on reducing neurodegenerative processes leading to macroscopic BVL, though further data are needed to confirm this observation. Supporting our findings, a recent network meta-analysis of clinical trials found teriflunomide to be superior to placebo in reducing BVL, while this was not the case for ocrelizumab. Moreover, monoclonal antibodies overall did not appear to outperform most other DMTs in this domain.[186]

No significant differences in DTI metrics were observed between treatment groups. Diffusion imaging examines the dynamics of water molecules, offering indirect insights into the microstructural organization of tissues.[74,108] Among diffusion MRI approaches, DTI is the simplest model, providing measures sensitive to both macrostructural and microstructural tissue integrity, which reflect processes such as demyelination and axonal damage.[74] Despite its limitations—such as an inability to accurately model complex tissue architectures, particularly in regions with crossing fibers—DTI has been widely utilized in MS research. Quantitative maps derived from DTI have demonstrated clinical relevance, serving as biomarkers at both the

lesional level and in normal-appearing tissue.[58] The lack of significant differences in longitudinal DTI metrics between treatment groups aligns with the observed lack of differences in clinical outcomes.

Similarly, there were no differences in PRL burden changes between groups. Data on DMT effects on PRLs remain limited, with existing studies suggesting that current DMTs have minimal impact on PRL resolution.[43] Observational studies have shown no reduction in PRL count with teriflunomide[187] or anti-CD20 therapies, including ocrelizumab.[96] Our findings are therefore consistent with these observations.

Our study has several limitations. First, its observational design and the non-random allocation of patients to treatments introduce potential bias. While we attempted to mitigate this by performing propensity score matching, incorporating various demographic, clinical, and paraclinical factors, the study design cannot eliminate residual bias, particularly given the differing characteristics of patients treated with teriflunomide and ocrelizumab in clinical practice. Moreover, some relevant clinical variables, such as the burden of spinal cord lesions, could not be included as matching criteria. Additionally, we did not include pre-enrollment ARR as a criterion for matching, opting instead for sNfL levels as a potentially more sensitive marker of inflammatory activity. Second, although the overall cohort size was large, the number of patients included in certain MRI analyses was relatively small, with a relatively short follow-up period; this limitation is due to the recent introduction of systematic 3D-EPI and diffusion MRI data collection in the SMSC study. Third, due to the limited sample size, we were unable to stratify patients further based on prior treatment sequences or systematically account for potential temporal lags in reaching treatment nadir. Fourth, given the exploratory nature of this study, we chose not to adjust for multiple comparisons, which may have increased the risk of type I errors. Fifth, PIRA was defined exclusively by changes in EDSS scores, without incorporating additional measures such as upper and lower limb dexterity, potentially overlooking treatment-specific impacts on these outcomes. Sixth, the follow-up period was unbalanced between groups in some analyses; however, to address this potential bias, we used mixed-effect models specifically designed to account for differences in follow-up duration.

Despite these limitations, our findings are of potential clinical relevance, demonstrating that teriflunomide is non-inferior to ocrelizumab in clinical and MRI measures reflecting smoldering disease activity in patients with RRMS. However, further data are needed to confirm these findings and better understand their long-term implications.

9. The Effect of Disease-Modifying Therapies on Brain Volume Loss and Disability Accumulation in Multiple Sclerosis: A Systematic Review and Network Meta-Analysis

Authors: Alessandro Cagol[1,2,3,4], Sabine Schaedelin[5], Roxanne Pretzsch[1,2,3], Ludwig Kappos[1,2,3], Maria Pia Sormani[4,5], Cristina Granziera[1,2,3*]*

**These authors share last authorship*

Affiliations: 1. Translational Imaging in Neurology (ThINk) Basel, Department of Biomedical Engineering, Faculty of Medicine, University Hospital Basel and University of Basel, Basel, Switzerland. 2 Multiple Sclerosis Centre, Departments of Neurology, Clinical Research and Biomedicine, University Hospital and University Basel, Switzerland. 3. Research Center for Clinical Neuroimmunology and Neuroscience Basel (RC2NB), University Hospital Basel and University of Basel, Basel, Switzerland. 4. Dipartimento di Scienze della Salute, Università degli Studi di Genova, Genova, Italy. 5. Department of Clinical Research, University Hospital Basel, University of Basel, Basel, Switzerland. 6. IRCCS Ospedale Policlinico San Martino, Genova, Italy.

Published in: Lancet Reg Health Eur. 2025 Sep 27;59:101476. doi: 10.1016/j.lanepe.2025.101476. PMID: 41080911; PMCID: PMC12509907.

Summary

Background: Multiple treatments have demonstrated efficacy in preventing brain volume loss (BVL) in randomized controlled trials (RCTs) for multiple sclerosis (MS). However, assessing their relative effectiveness remains challenging due to limited head-to-head comparisons. Additionally, the relationship between treatment effects on BVL and disability accumulation is not established for newer therapies. This study aimed to compare the efficacy of approved disease-modifying therapies (DMTs) in reducing BVL in MS and to investigate the association between treatment effects on BVL and disability accumulation.

Methods: In this systematic review and network meta-analysis, we included all RCTs enrolling adults with MS that evaluated FDA-approved DMTs and reported BVL outcomes over at least one year. We searched PubMed, Embase, and Cochrane from inception to September 2024. Following PRISMA guidelines, two reviewers independently extracted data on BVL, MRI lesion activity, and disability progression. We conducted a mixed-effects network meta-analysis with placebo as the reference group. Meta-regression analyses examined the association between treatment effects on BVL and disability progression, adjusting for MRI lesion activity.

The primary outcome was BVL. Secondary outcomes included MRI lesion accumulation and risk of confirmed disability progression. Effect sizes were reported as the ratio of means (ROM) and hazard ratios (HRs), with 95% confidence intervals (CIs). This study is registered with PROSPERO (CRD420251034936).

Findings: We included 33 RCTs evaluating 16 DMTs and 26,247 patients. Eight DMTs significantly reduced BVL compared to placebo, including ponesimod (ROM = 0.52; 95%-CI: 0.35–0.77), ofatumumab (ROM = 0.58; 95%-CI: 0.40–0.83), alemtuzumab (ROM = 0.63; 95%-CI: 0.49–0.83), teriflunomide (ROM = 0.71; 95%-CI: 0.52–0.97), ozanimod (ROM = 0.74; 95%-CI: 0.56–0.98), natalizumab (ROM = 0.77; 95%-CI: 0.61–0.96), siponimod (ROM = 0.77; 95%-CI: 0.60–0.98), and fingolimod (ROM = 0.83; 95%-CI: 0.71–0.96). The treatment effect on BVL was associated with the treatment effect on disability accumulation ($\beta = 0.466$; $p = 0.008$), and this association remained significant independently of the treatment effect on MRI activity ($\beta = 0.422$; $p = 0.005$).

Interpretation: Several DMTs—including newer therapies—significantly reduce BVL, and this effect correlates with reduced disability accumulation. These findings support BVL as a meaningful treatment target in MS.

Funding: None.

Research in context

Evidence before this study: Multiple sclerosis (MS) involves both inflammatory and neurodegenerative mechanisms, with brain volume loss (BVL) serving as a key marker of neurodegeneration and a predictor of long-term disability. Although many disease-modifying therapies (DMTs) have demonstrated the ability to reduce BVL, direct comparisons of their relative effects remain limited, partly due to the scarcity of head-to-head randomized trials.

Earlier studies used placebo controls, while more recent trials rely on active comparators, complicating cross-study comparisons. A meta-analysis from 2014 identified an association between treatment effects on BVL and disability progression but did not include several DMTs approved in subsequent years. As a result, a comprehensive, up-to-date synthesis of the comparative impact of all approved DMTs on BVL—and how these effects relate to disability accumulation—is lacking. We searched PubMed, Embase, and Cochrane from inception to September 2024, without language restrictions, using terms for multiple sclerosis ("Multiple Sclerosis", "MS"), trial design ("Randomized Controlled Trial", "RCT"), and the following DMTs: alemtuzumab, cladribine, dimethyl fumarate, diroximel fumarate, fingolimod, glatiramer acetate, interferon beta-1a, interferon beta-1b, natalizumab, ocrelizumab, ofatumumab, ozanimod, peg-interferon beta-1a, ponesimod, siponimod, teriflunomide, and ublituximab. Eligible trials enrolled adults, assessed treatment effects on BVL over ≥1 year, and excluded pediatric populations, combination therapies, and open-label or extension studies.

Added value of this study: This study provides a thorough network meta-analysis of 33 randomized controlled trials encompassing over 26,000 patients, systematically evaluating the efficacy of 16 approved DMTs on BVL, MRI lesion activity, and disability progression. Eight therapies showed significant superiority over placebo in reducing BVL, while all reduced MRI lesion accumulation, and six significantly delayed disability worsening. Meta-regression analyses revealed that reductions in BVL were associated with decreased disability accumulation, independent of changes in MRI lesion activity. By integrating both direct and indirect evidence, this work advances prior knowledge by robustly establishing BVL reduction as an independent and clinically meaningful predictor of long-term disability outcomes across a broad spectrum of modern treatments.

Implications of all the available evidence: These findings underscore that multiple DMTs—including newer agents—effectively reduce BVL in MS. The demonstrated link between treatment effects on BVL and disability accumulation, independent of inflammatory lesion activity, suggests that some therapies may provide neuroprotective benefits beyond MRI lesion control. Furthermore, these results strengthen the role of BVL as a clinically relevant biomarker and a meaningful therapeutic target in MS management.

Introduction

Multiple sclerosis (MS) is a chronic, immune-mediated disease of the central nervous system (CNS), characterized by the coexistence of inflammatory and neurodegenerative processes.[188] While a wide range of disease-modifying therapies (DMTs) is now available, these treatments primarily target the inflammatory component, especially in patients with relapsing-remitting MS. In contrast, the neurodegenerative component—recognized as the primary driver of long-term disability[189]—remains less effectively addressed.[188]

Inflammatory activity in MS manifests clinically as relapses and radiologically as the accumulation of focal lesions. Neurodegeneration, by contrast, can be quantified through brain volume loss (BVL), a process that occurs at a pathologically accelerated rate in MS.[17] Notably, increased BVL is consistently observed across all disease phases, including its early stages.[16] At the population level, BVL correlates strongly with greater disability severity and is a predictor of future disease progression, associated with both physical and cognitive impairment.[16,190–192] Beyond its prognostic value, BVL offers critical insights into the mechanisms driving progression and has been proposed as a key outcome measure in clinical trials investigating neuroprotective therapies.[16]

Although several DMTs have demonstrated efficacy in reducing BVL in MS,[193] systematic comparisons of their effects remain challenging due to the limited availability of head-to-head trials. Evolution in trial design, with older clinical trials primarily assessing treatment effects against placebo and more recent studies using active comparators, further complicates the interpretation of relative treatment effects.

Furthermore, the extent to which reductions in BVL correlate with improvements in disease trajectories in terms of disability progression, remains incompletely understood. A meta-analysis published in 2014 established a link between treatment effects on BVL and disability accumulation.[102] However, the approval of several new DMTs since then necessitates an updated and comprehensive analysis. Such an effort could not only further validate BVL as a clinically meaningful measure of disease progression but also enhance our understanding of how treatment-induced reductions in BVL influence long-term outcomes.

To address these gaps, we conducted a study with two complementary components: 1) a network meta-analysis (NMA), a statistical approach that integrates direct evidence from head-to-head trials and indirect evidence from trials with a common comparator, to systematically compare the effects of DMTs on BVL. This method enables the estimation of relative treatment

effects even when direct comparisons between treatments are unavailable;[194] 2) a meta-regression, designed to investigate the association between treatment effects on BVL and disability accumulation. Meta-regression is a statistical approach that enables the exploration of relationships between outcomes of study-level characteristics across trials.

Methods

The study adhered to the Preferred Reporting Items for Systematic Reviews and Meta-analyses (PRISMA) guidelines for NMAs.[195]

Search strategy and selection criteria

We included randomized controlled trials (RCTs) on adult patients with MS reporting treatment effect on BVL over a period of at least one year for any of the following FDA-approved DMTs: alemtuzumab, cladribine, dimethyl fumarate, diroximel fumarate, fingolimod, glatiramer acetate, interferon beta-1a, interferon beta-1b, natalizumab, ocrelizumab, ofatumumab, ozanimod, peg-interferon beta-1a, ponesimod, siponimod, teriflunomide, and ublituximab. RCTs involving pediatric populations, DMT combinations, or open-label or extension phases were excluded.

A comprehensive search of PubMed, Embase, and the Cochrane Registry of Clinical Trials was conducted from database inception to September 2024, without language restrictions. Detailed search strategies are provided in eMethods, and the screening process is summarized in the PRISMA flow diagram in Fig. 1.

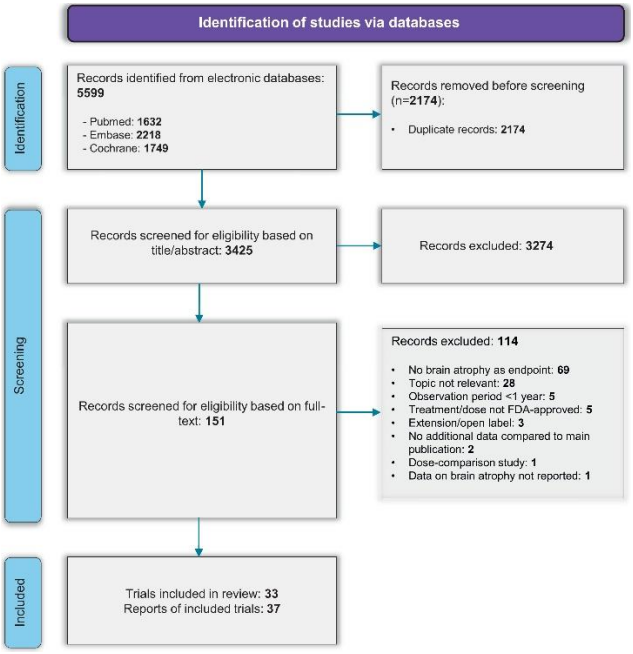

***Fig. 1**: PRISMA flow diagram.*

Data analysis

Two reviewers (A.C. and R.P.) independently extracted data, resolving discrepancies by consensus. For each trial, we recorded publication year, number of randomized patients, and key demographic and clinical characteristics. Outcomes of interest included treatment effects on BVL, MRI lesions, and probability of disability progression. These were evaluated as the ratio of mean (ROM) or median brain volume change, the ratio of cumulative active T2-lesions counts, and the ratio of disability progression probability between the intervention and control arms.[9] BVL estimates excluding the first 6 (or 12) months of observation were used to account for pseudoatrophy effects where available. Further details are provided in eMethods.

All statistical analyses were conducted using *R* (version 4.2.1; R Core Team, 2022), with a significance threshold set at $p < 0.05$. Treatment effects on the outcomes of interest were analyzed using NMAs with the *netmeta* package,[196] employing mixed-effects models with placebo as the reference group. Risk of bias was assessed systematically (eTable 1), model inconsistency was evaluated by comparing indirect effects with direct effects where available (eFigures 1–3), and publication bias was assessed with funnel plots and Egger's test (eFigures 4–6). Sensitivity analyses included: 1) Bayesian NMA models with evaluation of treatment rankings using surface under the cumulative ranking (SUCRA) values. SUCRA provides a summary score for each treatment, indicating the probability of being among the most effective

options, with values closer to 100% reflecting better performance; 2) analyses restricted to patients with relapsing MS (RMS); 3) analyses restricted to BVL estimates obtained with Structural Image Evaluation using Normalization of Atrophy (SIENA) software;[197] 4) analyses using the longest BVL observation period; 5) analyses limited to studies excluding the initial 6 (or 12) months for BVL estimation; 6) exclusion of RCTs in which measures of uncertainty could only be imputed; and 7) analyses restricted to RCTs reporting disability accumulation confirmed at 3 months.

Meta-regression analyses were conducted using linear regression models to assess the association between the treatment effect on BVL and the treatment effect on disability progression. The association was explored both in a univariable analysis and including the treatment effect on MRI lesions as an additional covariate. Each trial was given a weight based on the number of participants and the length of the observation period, as previously proposed.[102] The coefficient of determination (R^2) was used to assess the goodness of fit for each model. Models were applied using both the treatment effects derived from the original RCTs, as well as the estimates derived from the NMAs. Sensitivity analyses were conducted: 1) excluding each individual trial, 2) using unweighted regression, 3) in patients with RMS only and in patients with RRMS only, 4) using BVL estimate referred to the longest observation period, 5) in models adjusted for the software used to estimate BVL, and 6) in models accounting for cohort age, sex, and expanded disability status scale (EDSS) score (eTables 2–5). In addition, we performed a causal mediation analysis to explore the extent to which the association between treatment effects on BVL and disability progression was mediated by changes in MRI lesion accumulation. The analysis was implemented using the *mediation* R package with nonparametric bootstrapping (1000 simulations).

Role of the funding source

There was no funding source for this study.

Results

The systematic literature review identified 37 eligible studies for data extraction, including primary RCT publications and post-hoc analyses. These studies were derived from 33 unique RCTs evaluating 16 different DMTs and included a total of 26,247 patients with MS: 21,309 with RMS, and 4938 with progressive MS (PMS). When multiple publications originated from the same RCT, we included only non-overlapping data for each outcome of interest to avoid

duplication of participant populations. All steps of the study selection process are detailed in the PRISMA flow diagram shown in Fig. 1. Among studies on RMS, the weighted mean (SD) age was 36.8 (1.6) years, the proportion of female participants was 68.4% (3.4), and the mean EDSS was 2.6 (0.2). In studies on PMS, the weighted mean (SD) age was 46.6 (2.6) years, the proportion of female participants was 56.7% (6.2), and the mean EDSS was 5.2 (0.4). Additional details are reported in Table 1 and eTable 6.

Trial	Experimental arm	N experimental arm	Control arm	N control arm	Mean age experimental arm	% Females experimental arm	Mean EDSS experimental arm	MS phenotype
MSCRG (1996)[14,15]	Interferon β-1a	158	Placebo	143	36.7	75	2.4	RRMS
IFNβ-1b European Study Group (1998)[16,17]	Interferon β-1b	360	Placebo	358	41.1	58	5.1	SPMS
AFFIRM (2006)[18,19]	Natalizumab	627	Placebo	315	35.6	72	2.3	RRMS
REGARD (2008)[20]	Interferon β-1a	386	Glatiramer acetate	378	36.7	69	2.4	RRMS
CAMMS223 (2008)[21]	Alemtuzumab	112	Interferon β-1a	111	31.9	64	1.9	RRMS
BEYOND (2009)[22]	Interferon β-1b	897	Glatiramer acetate	448	35.8	70	2.4	RRMS
Montalban et al. (2009)[23]	Interferon β-1b	36	Placebo	37	48.8	39	5.3	PPMS
FREEDOMS I (2010)[24]	Fingolimod	425	Placebo	418	36.6	70	2.3	RRMS
TRANSFORMS (2010)[25]	Fingolimod	431	Interferon β-1a	435	36.7	65	2.2	RRMS
TEMSO (2011)[26,27]	Teriflunomide	359	Placebo	363	37.8	71	2.7	RRMS
CONFIRM (2012)[28,29]	Dimethyl fumarate	359	Placebo	363	37.8	68	2.6	RRMS
	Glatiramer acetate	350			36.7	71	2.6	RRMS
CARE-MS I (2012)[30]	Alemtuzumab	376	Interferon β-1a	187	33.0	65	2.0	RRMS
CARE-MS II (2012)[31]	Alemtuzumab	426	Interferon β-1a	202	34.8	66	2.7	RRMS
GALA (2013)[32]	Glatiramer acetate	943	Placebo	461	37.4	68	2.8	RRMS
DEFINE (2014)[33,34]	Dimethyl fumarate	410	Placebo	408	38.1	72	2.4	RRMS
ADVANCE (2014)[35]	Peginterferon β-1a	512	Placebo	500	36.9	71	2.5	RRMS
FREEDOMS II (2014)[36]	Fingolimod	358	Placebo	355	40.6	77	2.4	RRMS
INFORMS (2016)[37]	Fingolimod	336	Placebo	487	49.0	49	4.7	PPMS
OPERA I (2017)[38]	Ocrelizumab	410	Interferon β-1a	411	37.1	66	2.9	RRMS
OPERA II (2017)[38]	Ocrelizumab	417	Interferon β-1a	418	37.2	65	2.8	RRMS
ORATORIO (2017)[39]	Ocrelizumab	488	Placebo	244	44.7	49	4.7	PPMS
CLARITY (2018)[40,41]	Cladribine	433	Placebo	437	37.9	69	2.8	RRMS
EXPAND (2018)[42]	Siponimod	1105	Placebo	546	48.0	61	5.4	SPMS
ASCEND (2018)[43]	Natalizumab	439	Placebo	448	47.3	62	6.0[a]	SPMS
SUNBEAM (2019)[44]	Ozanimod	447	Interferon β-1a	448	34.8	63	2.6	RMS
RADIANCE (2019)[45]	Ozanimod	433	Interferon β-1a	441	36.0	67	2.6	RMS
ASCLEPIOS I (2020)[46]	Ofatumumab	465	Teriflunomide	462	38.9	68	3.0	RMS
ASCLEPIOS II (2020)[46]	Ofatumumab	481	Teriflunomide	474	38.0	66	2.9	RMS
ASSESS (2020)[47]	Fingolimod	352	Glatiramer acetate	342	40.3	75	2.7	RRMS
OPTIMUM (2021)[48]	Ponesimod	567	Teriflunomide	566	36.7	64	2.6	RRMS
FUMAPMS (2021)[49]	Dimethyl fumarate	27	Placebo	27	55.7	37	4.3	PPMS
ULTIMATE I (2022)[50]	Ublituximab	271	Teriflunomide	274	36.2	61	3.0	RMS
ULTIMATE II (2022)[50]	Ublituximab	272	Teriflunomide	272	34.5	65	2.8	RMS
Total								

Abbreviations: RMS, relapsing multiple sclerosis; RRMS, relapsing-remitting multiple sclerosis; PPMS, primary-progressive multiple sclerosis; SPMS, secondary-progressive multiple sclerosis. [a]Median.

Table 1: **Characteristics of included trials.**

References: MSCRG[198,199]; IFNb-1b European Study Group[200,201]; AFFIRM[202,203]; REGARD[204]; CAMMS223[205]; BEYOND[206]; Montalban et al, 2009[207]; FREEDOMS I[208]; TRANSFORMS[209]; TEMSO[210,211]; CONFIRM[212,213]; CARE-MS I[214]; CARE-MS II[215]; GALA[216]; DEFINE[217,218]; ADVANCE[219]; FREEDOMS II[220]; INFORMS[221]; OPERA I[185]; OPERA II[185]; ORATORIO[184]; CLARITY[222,223]; EXPAND[224]; ASCEND[225]; SUNBEAM[226]; RADIANCE[227]; ASCLEPIOS I[181]; ASCLEPIOS II[181]; ASSESS[228]; OPTIMUM[183]; FUMAPMS[229]; ULTIMATE I[182]; ULTIMATE II[182].

Treatment effect on BVL

All included RCTs reported data on BVL, as per inclusion criteria. The median (IQR) observation time was 24 (18–24) months. BVL was estimated using SIENA in 18 RCTs, with other or unspecified software used in the remaining 15. Results of the NMA are reported in Fig. 2a. Eight DMTs showed significant superiority over placebo in reducing BVL, including ponesimod (ROM = 0.52; 95%-CI: 0.35–0.77), ofatumumab (ROM = 0.58; 95%-CI: 0.40–0.83), alemtuzumab (ROM = 0.63; 95%-CI: 0.49–0.83), teriflunomide (ROM = 0.71; 95%-CI: 0.52–0.97), ozanimod (ROM = 0.74; 95%-CI: 0.56–0.98), natalizumab (ROM = 0.77; 95%-CI: 0.61–0.96), siponimod (ROM = 0.77; 95%-CI: 0.60–0.98), and fingolimod (ROM = 0.83; 95%-CI: 0.71–0.96). Bayesian NMA yielded similar results (eFigure 7).

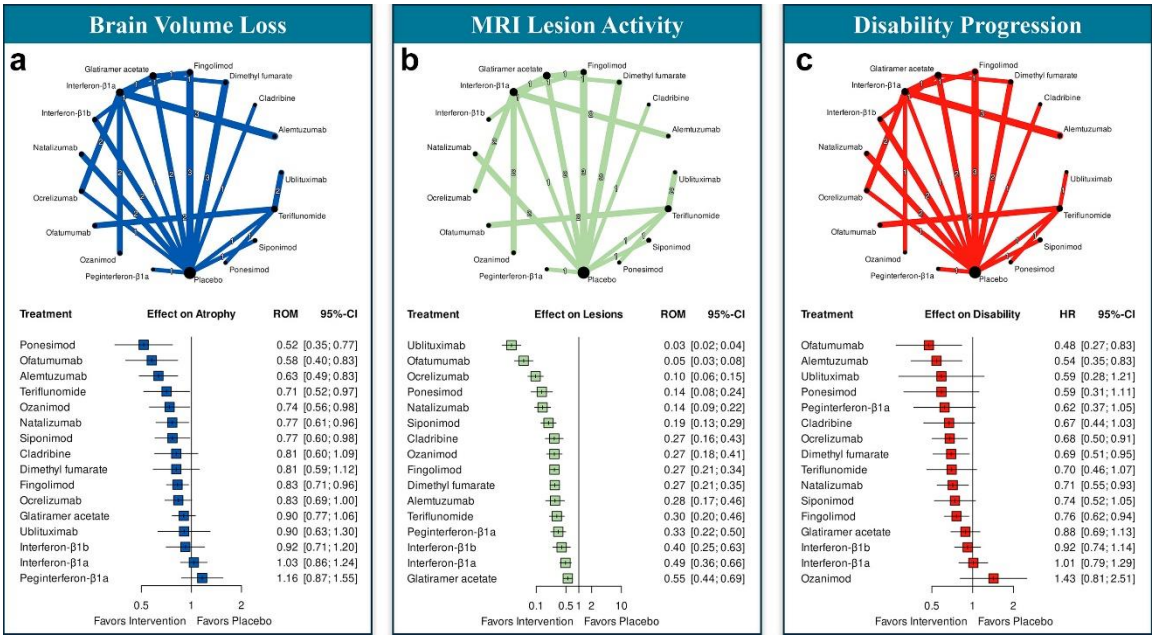

Fig. 2 Results of the network meta-analyses. a: treatment effect on brain volume loss; b: treatment effect on MRI lesion activity; c: treatment effect on disability progression. *Each panel includes two elements: 1) Top: A network diagram summarizing direct comparisons between disease-modifying treatments across randomized controlled trials. Each node represents a treatment, with node size proportional to the total number of participants receiving that treatment. Edges indicate direct comparisons, with thickness reflecting the number of contributing trials, and the exact number of trials labeled at the midpoint of each edge; 2) Bottom: Forest plots displaying treatment effects estimated from NMA models, compared to placebo. For brain volume loss and MRI lesion activity (Panels a and b), results are reported as ratios of means (ROM); for disability progression (Panel c), effects are reported as hazard ratios (HR). Squares represent point estimates, and horizontal lines represent 95% confidence intervals. Results of the corresponding sensitivity analyses are presented with analogous network diagrams and forest plots in eFigures 8–15. Abbreviations: ROM, ratio of means; HR, hazard ratio.*

In the sensitivity analysis estimating BVL based on the longest observation period, six DMTs were superior to placebo in reducing BVL, including ponesimod (ROM = 0.52; 95%-CI: 0.35–0.77), ofatumumab (ROM = 0.58; 95%-CI: 0.40–0.83), alemtuzumab (ROM = 0.64; 95%-CI: 0.49–0.83), teriflunomide (ROM = 0.71; 95%-CI: 0.52–0.97), ozanimod (ROM = 0.75; 95%-CI: 0.57–0.98), and fingolimod (ROM = 0.82; 95%-CI: 0.71–0.95) (eFigure 8). Results of sensitivity analyses are reported in eFigures 8–15. In sensitivity analyses, results were largely consistent with those of the main analyses. Among DMTs tested in the RMS population, as well as in purely RRMS population, those showing significant effect on BVL in the main analyses were confirmed in these subgroups. When the NMA was restricted to RCTs reporting BVL estimates with rebaselining, ocrelizumab also demonstrated a significant effect on BVL. Conversely, when longer observation periods were prioritized over the rebaselining time frame, the primary change was a loss of significance for natalizumab. Results were consistent when excluding RCTs in which measures of uncertainty had to be imputed.

Treatment effect on MRI lesion activity

MRI lesion activity was measured by the count of active T2-lesions (i.e., new or enlarging T2-lesions) in 27 RCTs, and by the count of combined unique active lesions (i.e., new or enlarging T2-lesions or gadolinium-enhancing lesions) in 2 studies. The median (IQR) observation time was 24 (24–24) months. In the NMA, all DMTs demonstrated significant superiority over placebo in preventing MRI lesion activity, with ROM ranging from 0.03 to 0.55 (Fig. 2b). Bayesian NMA yielded similar results (eFigure 16).

Treatment effect on disability accumulation

Data on confirmed disability progression were available for 31 RCTs, with hazard ratio (HR) reported in 23 RCTs and risk ratio (RR) in 8. The median (IQR) observation time was 24 (24–24) months. In the NMA, six DMTs showed significant superiority over placebo in preventing disability accumulation, including ofatumumab (HR = 0.48; 95%-CI: 0.27–0.83), alemtuzumab (HR = 0.54; 95%-CI: 0.35–0.83), ocrelizumab (HR = 0.68; 95%-CI: 0.50–0.91), dimethyl fumarate (HR = 0.69; 95%-CI: 0.51–0.95), natalizumab (HR = 0.71; 95%-CI: 0.55–0.93), and fingolimod (HR = 0.76; 95%-CI: 0.62–0.94) (Fig. 2c). Bayesian NMA yielded similar results (eFigure 17).

Association between treatment effects on BVL and disability

In the weighted meta-regression, the treatment effect on BVL was significantly associated with the treatment effect on disability progression ($\beta = 0.466$; $p = 0.008$; $R^2 = 0.217$) (Fig. 3a). This

association remained significant in a multivariable model adjusting for treatment effect on MRI lesion activity (β = 0.422; p = 0.005; R^2 = 0.560) with minimal change in the strength of association between treatment effect on BVL and disability when adjusting for treatment effect on MRI lesions (β decreased from 0.466 to 0.422, indicating that less than 10% of the relationship between treatment effect on BVL and disability is mediated by the effect on MRI lesions). Adjustment for treatment effect on MRI lesions had a relevant effect on the explained variance (R^2 increased from 0.217 to 0.560, indicating a complementary and independent effect of MRI lesions on disability effect). Similar results were obtained when using treatment effect estimates derived from the NMA models (univariable regression: β = 0.582; p = 0.0006; R^2 = 0.339; multivariable regression accounting for MRI lesion activity: β = 0.392; p = 0.012; R^2 = 0.549) (Fig. 3b). Results were confirmed in sensitivity analyses (eTables 2–5). The variance in treatment effect on disability progression explained by the treatment effect on BVL was increased in sensitivity analyses restricted to specific subsets of RCTs: RCTs conducted in RRMS populations (R^2 = 0.435), those using SIENA or brain parenchymal fraction (BPF) for BVL estimation (R^2 = 0.431), and those reporting BVL with rebaselining (R^2 = 0.503) (eTable 3). A causal mediation analysis indicated that the association between treatment effects on BVL and disability accumulation was not significantly mediated by MRI lesion accumulation (eTable 7). For all three outcomes of interest, assessment of funnel plot asymmetry and Egger's test revealed no substantial evidence of publication bias (eFigures 4–6).

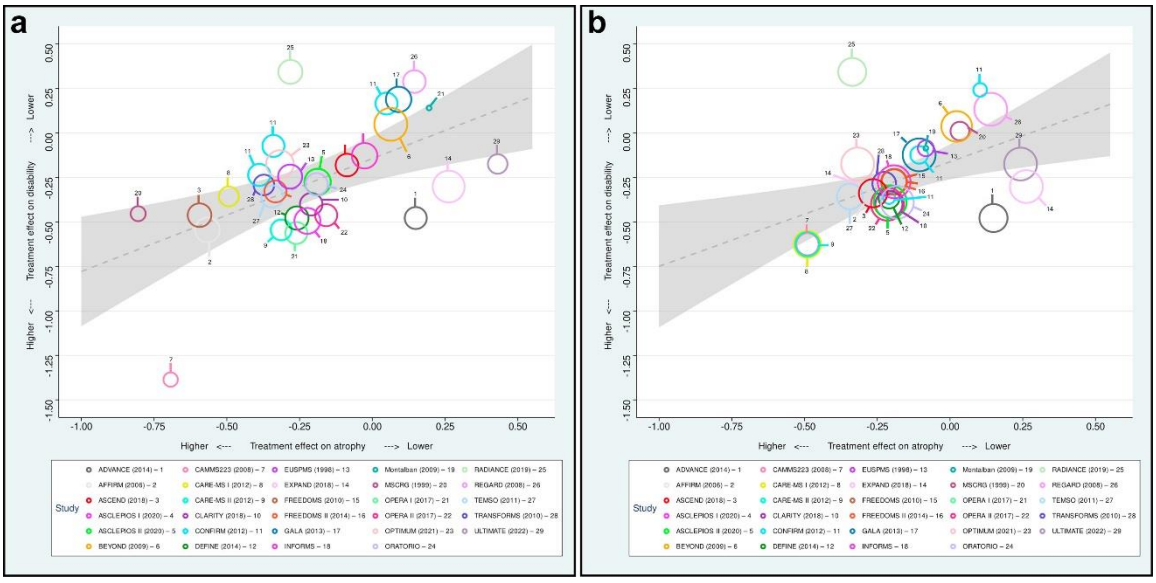

Fig. 3 Association between treatments effects on brain volume loss and disability accumulation. *Panel a: Weighted regression model using treatment estimates derived from the original RCTs. Panel b: Weighted regression model using treatment estimates derived from the NMAs. The circle size reflects the weight of the study in the weighted regression.*

Discussion

Using a meta-analytical approach, we showed that multiple DMTs significantly reduce the rate of BVL in patients with MS compared to placebo. Additionally, multiple treatments decreased the risk of confirmed disability progression, while all approved DMTs effectively reduced the accumulation of MRI lesions, a key marker of focal inflammatory activity. Notably, the reduction in BVL was associated with decreased disability accumulation, with this relationship being independent of the treatments' effects on MRI lesions. These findings suggest that certain DMTs may impact neurodegenerative processes in MS beyond their impact on neuroinflammation.

Among the 16 DMTs analyzed, eight demonstrated a significant effect in reducing BVL. These included sphingosine 1-phosphate (S1P) modulators (ponesimod, ozanimod, siponimod, fingolimod), monoclonal antibodies (ofatumumab, alemtuzumab, natalizumab), and teriflunomide. Additionally, ocrelizumab showed a trend toward statistical significance. Notably, more recently approved DMTs were generally more effective in mitigating BVL, reflecting advancements in therapeutic development. Among these, ponesimod exhibited the greatest efficacy, nearly halving the rate of atrophy compared to placebo.

Six DMTs also significantly reduced the risk of disability accumulation compared to placebo, including monoclonal antibodies (ofatumumab, alemtuzumab, ocrelizumab, natalizumab), S1P modulators (fingolimod), and dimethyl fumarate. Ofatumumab exhibited the most substantial effect, lowering disability accumulation risk by over 50%. As expected, all DMTs effectively decreased MRI lesion accumulation, with reductions ranging from 45% for glatiramer acetate to an almost complete suppression (97%) observed with ublituximab. Bayesian analyses yielded largely concordant results, with the added advantage of providing SUCRA values—a summary measure that reflects the probability (expressed as a percentage) that a treatment ranks among the most effective in the network, thereby supporting its potential value in treatment decision-making. Notably, the observed effects of DMTs on BVL remained largely consistent across sensitivity analyses. Analyses restricted to relapsing populations confirmed the significant impact on BVL of DMTs identified in the main analysis. Results were also consistent when considering different time frames for BVL estimation. The main difference was the loss of a significant effect for natalizumab when prioritizing longer observation periods over the rebaselining time frame, likely reflecting the influence of pseudoatrophy. Importantly, natalizumab is known to produce a pronounced pseudoatrophy effect.[16,202] Conversely, when restricting the analysis to trials without rebaselining, ocrelizumab emerged as having a

significant effect on BVL, suggesting a true treatment effect that may have been obscured in more heterogeneous trial settings.

These findings were derived using a network meta-analytic framework that integrates both direct and indirect comparisons across approved DMTs. While multiple head-to-head RCTs were available, they covered only a limited subset of treatment pairs: specifically, 22 unique direct comparisons for BVL, 20 for MRI lesion accumulation, and 21 for disability progression. The majority of the possible pairwise comparisons (n = 136) for each outcome were therefore informed indirectly through the network structure. In this context, NMA enabled a unified assessment of relative treatment effects across all outcomes, extending beyond the capabilities of conventional pairwise meta-analyses.

Meta-regression analyses showed a positive association between the treatment effects on BVL and disability progression, even after accounting for the treatment effects on MRI activity, a known contributor to brain atrophy. This analysis is in accordance with one earlier meta-analysis[102] reporting that the treatment effect on BVL influences disability progression independently and complements the treatment effect on MRI lesions. This suggests that certain DMTs may exert effects on neurodegenerative processes in MS independent of their effects of acute inflammation. This consideration is particularly relevant given the growing recognition of progression independent of relapse activity (PIRA) as a major driver of disability accumulation in MS,[3,8] even in patients with typical relapsing-remitting phenotype.[3,6,7] Remarkably, recent studies have shown that patients with PIRA still exhibit accelerated BVL,[25,26] even when both clinical and MRI inflammatory activity are completely suppressed.[26] Although PIRA has not yet been included as an outcome measure in MS trials, DMT use has been shown to delay reaching disability milestones in patients experiencing PIRA.[8] Additionally, post-hoc analyses of ocrelizumab, ofatumumab, and ponesimod trials have supported a positive impact of these treatments in reducing the incidence of PIRA.[3,7,92]

The impact of treatment effect on neurodegeneration, along with the reduced risk of relapse-associated worsening, may explain the observed improvement in clinical trajectories in the treatment era compared to earlier periods. In fact, several observational studies have shown that the rates of disability accrual and progression to secondary progressive MS are now substantially lower compared to previous natural history studies.[230] Additionally, early initiation of high-efficacy therapies is especially linked to better long-term outcomes.[231]

Remarkably, our study found that the treatment effect on BVL accounted for nearly 22% (R^2 = 0.217) of the variability in the effect on disease progression, highlighting the potential involvement of other biological mechanisms. Factors such as non-resolving inflammation in chronic active lesions,[35,40,47] leptomeningeal inflammation,[232] cortical lesions,[82,233] diffuse microglial activation, chronic demyelination, oxidative stress, mitochondrial dysfunction, and the failure of compensatory mechanisms[4] have all been proposed as contributors to disease progression. Importantly, these mechanisms may not always manifest with measurable atrophy. Additionally, spinal cord atrophy plays a pivotal role in explaining disability progression,[34–36] as do regional thalamic and cortical atrophy,[16,79–81,190,234] showing a stronger correlation with disease severity than total brain atrophy.[16] However, their routine quantification in clinical trials remains limited, primarily due to technical challenges.[16,94] The heterogeneity of biological processes underlying disability progression but also BVL may explain the dissociation between treatment effects on BVL and disability progression seen with certain treatments, as recently observed with the Bruton tyrosine kinase (BTK) inhibitor tolebrutinib.[235,236]

The proportion of variance in treatment effect on disability accumulation explained by BVL was lower than previously reported by Sormani et al.[16,94,102] However, that study applied more restrictive inclusion criteria, focusing on RCTs conducted in RRMS populations, lasting at least 24 months, using SIENA or BPF for BVL estimation, and including rebaselined BVL measures. When similar criteria were applied in our sensitivity analyses, the explanatory power of BVL increased substantially, reaching up to 70% (R^2 = 0.703).

The results of this study should be interpreted with caution, as NMA relies on several critical assumptions that may not have been fully satisfied in this context. These include homogeneity (expecting similar results across studies comparing the same treatments), transitivity (ensuring comparability of treatment effect across studies), consistency (agreement between direct and indirect evidence), and similarity across study designs, populations, and outcomes. Since our analysis prioritized maximizing data inclusion to provide a comprehensive overview of treatment effects, this approach may have increased the risk of bias that we tried to address with some of the sensitivity analyses.

Several potential sources of bias and violations of these assumptions warrant careful consideration. First, technical variability in MRI acquisition protocols and sequence parameters may have introduced inconsistencies. Additionally, different post-processing methods were used to estimate BVL: while most RCTs employed SIENA, others used alternative tools with

varying sensitivity to detect neurodegenerative changes and differing susceptibility to measurement error.[237]

Second, outcome definitions and reporting practices varied across studies. For BVL, some studies reported annualized percentage change, while others presented absolute change over differing time frames. Definitions of MRI lesion accumulation also differed, with some studies including only new or enlarging T2 lesions and others incorporating gadolinium-enhancing lesions. For disability accumulation, outcome measures ranged from time-to-event analyses to binary outcomes reported as risk ratios, complicating direct comparisons.

Third, study duration varied widely, which may have influenced the ability to detect treatment effects and introduced variability in outcome sensitivity. In some cases, time frames differed across outcomes within the same study, further limiting comparability.

Fourth, differences in study populations may have challenged the transitivity assumption. Inclusion criteria varied in terms of disease duration, baseline EDSS, prior treatment exposure—including RCTs restricted to treatment-naive patients—and pre-enrollment relapse rates. Additionally, we intentionally included RCTs involving both relapsing and progressive MS populations. Although BVL rates have been reported as similar between these phenotypes, their inclusion may still affect transitivity.

Fifth, due to data limitations, we were unable to systematically exclude the initial observation period in all trials when quantifying BVL, potentially introducing bias related to the pseudoatrophy effect.

Sixth, studies differed in their statistical methodologies, with some reporting adjusted treatment effects and others providing unadjusted outcomes, limiting direct comparability.

Finally, although we formally tested for publication bias—including enough studies to allow such assessment—and found no significant evidence of its presence, its potential influence cannot be entirely ruled out, as is common in meta-analysis.

While extensive sensitivity analyses were conducted to address these limitations and evaluate the robustness of our findings, residual bias may remain. These concerns are particularly relevant given the limited number of direct comparisons available for each outcome, meaning that many estimates relied primarily on indirect evidence. However, in cases where both direct and indirect evidence were available, the estimates derived from the NMA were largely consistent with those from head-to-head RCTs, providing reassurance regarding the internal

coherence of the model.[94,201,237] Another important limitation lies in the inherent observational nature of NMA. As such, it cannot establish causality and does not replace direct head-to-head comparisons, which remain the gold standard for evaluating treatment efficacy.

It is also important to emphasize that the associations observed in the meta-regression analyses are based on group-level data, not individual-level data. These associations do not establish causality but indicate that the effects of treatment on the studied outcomes occur concurrently. As such, they are subject to ecological bias, whereby group-level associations may not reflect true relationships at the individual level. Moreover, meta-regression is inherently limited by the number of available studies, resulting in reduced statistical power and the ability to detect only large associations. Additionally, most studies included in this work had a follow-up of 24 months or less, limiting the ability to capture long-term disability accumulation and neurodegeneration. This constrains the interpretation of the BVL–disability accumulation relationship, particularly for DMTs whose effects may evolve over time. As a result, potential changes in long-term effects on both BVL and disability accumulation may be underestimated.

From a methodological perspective, the use of ROMs as the effect size metric assumes an underlying log-normal distribution of outcomes, which may not always hold. Moreover, while ROMs offer advantages in terms of comparability across trials, their interpretability is less intuitive than that of more commonly used metrics, such as standardized mean difference.

Despite these limitations, this study offers valuable insights by demonstrating that several DMTs substantially reduce BVL in MS, with this being linked to reduced disability progression. These findings collectively highlight the importance of assessing BVL in trials targeting long-term disability accrual, reinforcing its significance as a meaningful therapeutic target.

10. Discussion

This thesis focused on the mechanisms, imaging correlates, and treatment of disability progression in MS, with a particular emphasis on PIRA and on MRI markers that capture neurodegenerative and smoldering disease processes beyond conventional inflammatory measures. Across five complementary studies, we addressed disease progression from different angles: (1) investigating microstructural WM correlates of PIRA using DTI; (2) characterizing in vivo thalamic pathology using multiparametric qMRI over longitudinal follow-up; (3) assessing the relative contribution of a wide array of MRI and serum biomarkers in predicting disability, cognition, and future PIRA using machine learning; (4) comparing real-world effectiveness of two widely used DMTs (teriflunomide and ocrelizumab) on PIRA incidence and MRI outcomes, including markers of chronic inflammatory activity; and (5) conducting a network meta-analysis of randomized trials to quantify the impact of approved DMTs on BVL and how this effect relates to the efficacy in preventing disease progression.

Despite their distinct designs, the studies converge on several conclusions. First, progression in MS – captured clinically as PIRA – is consistently associated with diffuse tissue injury that extends beyond focal lesions and can be detected using clinically available MRI approaches. Second, neurodegeneration is regionally heterogeneous: spinal cord atrophy and cortical damage emerge as key determinants of disability and PIRA risk, while thalamic degeneration represents a central hub of macro- and microstructural damage with strong clinical correlates and measurable longitudinal degeneration, particularly in progressive phenotypes. Third, integrating conventional MRI, advanced qMRI, and serum biomarkers improves phenotyping and risk stratification, but the predictive performance for PIRA remains moderate, reflecting both biological complexity and limitations of current clinical definitions. Finally, treatment effects on progression-related outcomes appear only partially explained by suppression of focal inflammatory activity, and changes in BVL provide complementary information that is linked to disability accumulation at the trial level, though with relevant heterogeneity across therapies and study designs.

The first study presented in this thesis (**chapter 5**) showed that pwMS who experience PIRA exhibit significantly greater microstructural damage in major WM tracts compared with matched counterparts without PIRA, despite similarity in demographic and conventional MRI characteristics. Between-group differences were consistent across DTI-derived maps, including

alterations suggestive of both axonal and myelin injury. Importantly, the pattern remained evident when restricting analyses to patients with PIRMA, strengthening the concept that the observed WM injury is not merely an effect of focal inflammatory activity.

These findings expand the evidence linking PIRA to diffuse neurodegenerative processes. While prior work has associated disability progression with structural brain and spinal cord atrophy and with PRLs,[25,26,35,36] the present study provides support for the concept that silent progression is also associated with microstructural damage in normal-appearing WM. The observed DTI pattern is compatible with mechanisms such as Wallerian degeneration and network disconnection and aligns with the idea that focal pathology can propagate along major tracts.

At the same time, interpretation of DTI metrics remains intrinsically limited. DTI is sensitive to neuroaxonal and myelin damage but not specific, and its interpretation is challenging in areas with crossing fibers and complex tissue geometry. The study mitigated this by focusing on major WM tracts with predominant orientations, yet ambiguity remains regarding the relative contributions of demyelination, axonal loss, edema, and gliosis. In addition, DTI maps were available at a single time point following the follow-up period in which PIRA was defined, which limits inference regarding timing.

Despite these limitations, this study supports the view that PIRA associates with detectable tract-level imaging correlates and provides a rationale for incorporating microstructural WM measures – potentially with more specific diffusion models in future work – into studies aiming to characterize silent progression.

The second study (**chapter 6**) investigated thalamic pathology using an in vivo multiparametric qMRI protocol probing complementary tissue properties, comprehensively capturing macroscopic atrophy and microstructural alterations linked to demyelination, neuroaxonal loss, and changes in iron homeostasis. The findings showed substantial thalamic abnormalities in pwMS compared with healthy controls, accelerated thalamic degeneration over two years, and especially more severe alterations in progressive MS. Notably, qMRI changes were not confined to focal thalamic lesions but extended diffusely into normal-appearing tissue, supporting the concept of widespread tissue dysfunction not visible on conventional MRI.

A key contribution of this work is the demonstration that thalamic damage in MS can be decomposed into multiple interpretable microstructural dimensions. Prolonged qT1 – highly

sensitive to a broad spectrum of pathological changes – was present both in lesions and in normal-appearing thalamic tissue, suggesting diffuse microstructural disruption. Reduced MVF values pointed to macromolecular loss and demyelination, with particularly marked effects in progressive phenotypes. NDI alterations within lesions supported neuroaxonal loss, while decreased QSM values suggested disruption in iron homeostasis, possibly reflecting iron depletion from oligodendrocytes in the context of chronic microglial activation. Importantly, the clinical relevance of these measures was supported by robust associations with EDSS, cognitive measures, and MRI markers of disease burden.

Beyond cross-sectional characterization, the study emphasized the value of longitudinal qMRI trajectories. People with MS, especially presenting with progressive phenotypes, exhibited accelerated thalamic atrophy and longitudinal worsening of qMRI markers. qT1 in particular emerged as a useful discriminator between active RRMS and inactive PMS, suggesting that microstructural qMRI may capture progression-relevant changes that are not reflected by volumetric measures alone.
Interestingly, the regional predominance of changes close to CSF aligns with the notion of a surface-in gradient of thalamic injury,[238] potentially reflecting toxic CSF-mediated mechanisms, while the association with lesion burden within thalamocortical projections supports an additional role of disconnection and secondary degeneration.

Limitations largely reflect the challenges of longitudinal advanced imaging studies. Follow-up was not available for all participants, and disease progression was defined based on two EDSS time points, which may have increased misclassification and did not allow formal identification of PIRA events. Multiple comparisons correction was selectively applied to balance type I and type II error risks in an exploratory multiparametric framework; nonetheless, some reported associations warrant replication.

Collectively, this study strengthens the role of the thalamus as a clinically meaningful hub of MS pathology and highlights the added value of qMRI for disentangling and tracking neurodegenerative processes over time, particularly those relevant to progressive disease biology.

The third study (**chapter 7**) evaluated the relative importance of a broad panel of conventional and advanced MRI metrics and serum biomarkers for predicting cross-sectional disability, cognitive performance, and future progressive outcomes including PIRA. Using a machine

learning framework for feature selection and ranking, and validating findings in an independent cohort, the study provides an integrative view of which biomarkers best capture clinically meaningful outcomes.

A key finding across cohorts was the central relevance of spinal cord atrophy as a determinant of physical disability and a marker distinguishing progressive from relapsing phenotypes. Cervical CSA derived from standard brain MRI emerged among the most informative predictors for EDSS and disease phenotype, and was also predictive of time to PIRA. This reinforces the concept that spinal cord degeneration plays a fundamental role in MS disability, partly independent of lesion burden. In parallel, cortical pathology – both focal (with cortical lesions) and diffuse (with cortical thinning and qT1 alterations) – emerged as pivotal for predicting PIRA. Deep GM volume, thalamic measures, lesion burden, and serum biomarkers contributed meaningfully, supporting the idea that progression risk is multifactorial and cannot be captured by any single domain.

A key strength of this work is the explicit comparison of biomarker domains within a unified analytical framework and the effort to corroborate findings across two cohorts with different characteristics. The overall predictive performance for disability classification was high, whereas the discriminative performance for PIRA prediction was moderate. This performance is consistent with the conceptual and technical challenges of predicting PIRA, an outcome influenced by overlapping mechanisms and limited by the precision of EDSS-based definitions. Interestingly, the work suggests that a parsimonious panel of accessible biomarkers can enable meaningful risk stratification, supporting potential translatability to the clinical setting.

Limitations of the study include that the two cohorts differed in follow-up duration, baseline severity, and available imaging markers. In addition, the imbalance between the large number of MRI variables and the limited serum biomarker panel may bias selection toward MRI markers. Furthermore, the limited number of PIRA events – common in studies addressing disease progression – constrains generalizability and calls for replication in larger studies.

Despite these limitations, this study positions spinal cord atrophy and cortical degeneration as robust indicators of progression and supports multimodal biomarker strategies to better capture heterogeneity in disability trajectories.

The fourth study (**chapter 8**) used a propensity score-matched real-world cohort to compare teriflunomide and ocrelizumab in people with RRMS, focusing on PIRA incidence and on MRI

markers reflecting smoldering disease activity, including PRL burden and DTI metrics. The key finding was the absence of differences in PIRA incidence, PRL changes, and longitudinal DTI metrics between treatment groups, suggesting comparable impact on progression-related mechanisms within the observed follow-up window. Interestingly, teriflunomide was associated with reduced rates of whole brain and GM volume loss compared with ocrelizumab, although this effect was attenuated in sensitivity analyses restricted to scans acquired after six months from treatment initiation, raising the possibility of a confounding effect of pseudoatrophy.

This work contributes in two ways. First, it addresses a clinically relevant comparative question that is difficult to study in randomized settings, given the lack of direct teriflunomide-ocrelizumab trials, especially addressing PIRA. Second, it reinforces the observation that MRI markers of chronic activity such as PRLs may be relatively insensitive to currently available DMT classes, consistent with emerging literature suggesting limited impact of many therapies on PRL resolution.

Limitations of the study are those inherent to observational comparative studies. Non-random treatment allocation results in potential residual confounding even with propensity matching, particularly given real-world differences in patient profiles and unmeasured variables. MRI analyses had limited sample sizes and relatively short follow-up, limiting the ability to assess longer-term divergence in progression trajectories. Additionally, PIRA was based exclusively on EDSS, potentially missing treatment effects on other disability domains.

In summary, the study supports the interpretation that teriflunomide is non-inferior to ocrelizumab – an established highly effective DMT – with respect to PIRA incidence, underscoring the need for further real-world studies specifically focused on treatment effects on disability progression to better inform therapeutic strategies.

The fifth study (**chapter 9**) synthesized randomized trial evidence using a network meta-analytic approach to quantify the effects of approved DMTs on BVL, and to examine the relationship between treatment effects on neurodegeneration and clinical worsening beyond inflammatory activity. The analyses showed that multiple DMTs significantly reduce BVL compared with placebo, several reduce the risk of confirmed disability progression, and all reduce MRI lesion accumulation. Importantly, meta-regression indicated that treatment effects on BVL are associated with reduced disability accumulation independent of effects on MRI

lesion activity, supporting the concept that atrophy captures progression-relevant processes that are not fully explained by focal inflammatory suppression.

This study reinforces the clinical relevance of BVL as a therapeutic target and outcome measure in MS trials, particularly in an era where relapse and lesion suppression are increasingly achievable. It also highlights relevant heterogeneity across therapies: some DMTs showed strong effects in BVL, others on disability progression, and the relationship between these domains was substantial but incomplete. The moderate proportion of variance in disability progression explained by BVL underscores that progression is multifactorial, with contributions from mechanisms that may not manifest as global atrophy. Sensitivity analyses showed that the explanatory power of BVL increases in more homogeneous trial subsets, consistent with the idea that methodological heterogeneity dilutes the observed relationships.

At the same time, the interpretation of network meta-analytic results requires caution. Network meta-analysis relies on assumptions of transitivity, consistency, and homogeneity that may be challenged by factors such as heterogeneity in MRI acquisition, post-processing tools, outcome definitions and reporting, study duration, baseline disease characteristics, prior treatment exposure, and inclusion of both relapsing and progressive populations. Moreover, many treatment comparisons were informed indirectly due to limited head-to-head randomized controlled trial coverage, and meta-regression operated at the group level, with the risk of ecological bias.

Despite these limitations, the network meta-analysis provides an integrative and clinically relevant synthesis: multiple DMTs reduce BVL and disability progression, and BVL captures an important component of treatment effect that is not reducible to lesion suppression alone.

11. Conclusions

The five studies reported in this thesis coherently indicate that disability progression in MS reflects a complex interplay of focal inflammatory injury and diffuse, compartmentalized, and neurodegenerative processes that are variably captured by different biomarkers.

The clinical construct of PIRA is supported by imaging evidence across modalities – microstructural WM tract damage, regional patterns of spinal cord atrophy, cortical degeneration, and deep GM damage. The thalamus appears as a particularly informative structure where macrostructural atrophy and microstructural qMRI provide complementary information and progress measurably over time, with clinical relevance and marked severity in progressive phenotypes. Spinal cord CSA consistently emerges as a key marker of physical disability and a robust predictor of progression-related outcomes, reinforcing the need to integrate spinal cord metrics into both research and clinical protocols, even when only limited upper cervical coverage is available from brain MRI.

From a therapeutic perspective, the thesis supports the notion that current DMTs – while highly effective at suppressing focal inflammatory activity – may have variable and sometimes modest impact on markers of smoldering disease activity and neurodegeneration. Observational comparisons suggest that differences in PIRA incidence between therapies may be smaller than expected, at least in the short term, and PRL burden may remain largely unaffected. Meanwhile, trial evidence indicates that reducing BVL is related to reducing disability accumulation independently of lesion suppression, suggesting that atrophy metrics retain value as therapeutic endpoints even as inflammatory activity becomes more controlled. However, the incomplete overlap between BVL and disability effects, and the moderate ability to predict PIRA, highlight that progression biology remains only partially captured by measures of BVL and likely requires additional biomarkers sensitive to chronic inflammation, failure of repair, and regionally specific neurodegeneration, particularly in the deep GM and spinal cord.

12. Bibliography

1. Stadelmann C, Wegner C, Brück W. Inflammation, demyelination, and degeneration - Recent insights from MS pathology. *Biochim Biophys Acta Mol Basis Dis.Biochim Biophys Acta*. 2011;1812(2):275-282. doi:10.1016/j.bbadis.2010.07.007

2. Kobelt G, Thompson A, Berg J, Gannedahl M, Eriksson J. New insights into the burden and costs of multiple sclerosis in Europe. *Multiple Sclerosis*. 2017;23(8):1123-1136. doi:10.1177/1352458517694432

3. Kappos L, Wolinsky JS, Giovannoni G, et al. Contribution of Relapse-Independent Progression vs Relapse-Associated Worsening to Overall Confirmed Disability Accumulation in Typical Relapsing Multiple Sclerosis in a Pooled Analysis of 2 Randomized Clinical Trials. *JAMA Neurol*. 2020;77(9):1132-1140. doi:10.1001/jamaneurol.2020.1568

4. Kuhlmann T, Moccia M, Coetzee T, et al. Multiple sclerosis progression: time for a new mechanism-driven framework. *Lancet Neurol*. 2023;22(1):78-88. doi:10.1016/S1474-4422(22)00289-7

5. Scalfari A, Traboulsee A, Oh J, et al. Smouldering-Associated Worsening in Multiple Sclerosis: An International Consensus Statement on Definition, Biology, Clinical Implications, and Future Directions. *Ann Neurol*. 2024;96(5). doi:10.1002/ANA.27034

6. Tur C, Carbonell-Mirabent P, Cobo-Calvo Á, et al. Association of Early Progression Independent of Relapse Activity With Long-term Disability After a First Demyelinating Event in Multiple Sclerosis. *JAMA Neurol*. 2022;80(2). doi:10.1001/jamaneurol.2022.4655

7. Müller J, Cagol A, Lorscheider J, et al. Harmonizing Definitions for Progression Independent of Relapse Activity in Multiple Sclerosis: A Systematic Review. *JAMA Neurol*. 2023;80(11):1232-1245. doi:10.1001/jamaneurol.2023.3331

8. Lublin FD, Häring DA, Ganjgahi H, et al. How patients with multiple sclerosis acquire disability. *Brain*. Published online February 1, 2022. doi:10.1093/brain/awac016

9. Portaccio E, Bellinvia A, Fonderico M, et al. Progression is independent of relapse activity in early multiple sclerosis: a real-life cohort study. *Brain*. 2022;145(8):2796-2805. doi:10.1093/brain/awac111

10. Ciccarelli O, Barkhof F, Calabrese M, et al. Using the Progression Independent of Relapse Activity Framework to Unveil the Pathobiological Foundations of Multiple Sclerosis. *Neurology*. 2024;103(1). doi:10.1212/WNL.0000000000209444/SUPPL_FILE/SUPPLEMENTARY_TABLE1.PDF

11. Trapp BD, Peterson J, Ransohoff RM, Rudick R, Mörk S, Bö L. Axonal Transection in the Lesions of Multiple Sclerosis. *New England Journal of Medicine*. 1998;338(5):278-285. doi:10.1056/nejm199801293380502

12. Lucchinetti CF, Brück W, Rodriguez M, Lassmann H. Distinct Patterns of Multiple Sclerosis Pathology Indicates Heterogeneity in Pathogenesis. *Brain Pathol*. 1996;6(3):259. doi:10.1111/J.1750-3639.1996.TB00854.X

13. Kutzelnigg A, Lucchinetti CF, Stadelmann C, et al. Cortical demyelination and diffuse white matter injury in multiple sclerosis. *Brain*. 2005;128(11):2705-2712. doi:10.1093/BRAIN/AWH641

14. Lucchinetti CF, Popescu BFG, Bunyan RF, et al. Inflammatory Cortical Demyelination in Early Multiple Sclerosis. *New England Journal of Medicine*. 2011;365(23):2188-2197. doi:10.1056/nejmoa1100648

15. Popescu V, Klaver R, Versteeg A, et al. Postmortem validation of MRI cortical volume measurements in MS. *Hum Brain Mapp*. 2016;37(6):2223-2233. doi:10.1002/hbm.23168

16. Sastre-Garriga J, Pareto D, Battaglini M, et al. MAGNIMS consensus recommendations on the use of brain and spinal cord atrophy measures in clinical practice. *Nat Rev Neurol*. 2020;16(3):171-182. doi:10.1038/s41582-020-0314-x

17. De Stefano N, Stromillo ML, Giorgio A, et al. Establishing pathological cut-offs of brain atrophy rates in multiple sclerosis. *J Neurol Neurosurg Psychiatry*. 2016;87(1):93-99. doi:10.1136/jnnp-2014-309903

18. Battaglini M, Gentile G, Luchetti L, et al. Lifespan normative data on rates of brain volume changes. *Neurobiol Aging*. 2019;81:30-37. doi:10.1016/j.neurobiolaging.2019.05.010

19. De Stefano N, Giorgio A, Battaglini M, et al. Assessing brain atrophy rates in a large population of untreated multiple sclerosis subtypes. *Neurology*. Published online 2010. doi:10.1212/WNL.0b013e3181e24136

20. Amato MP, Hakiki B, Goretti B, et al. Association of MRI metrics and cognitive impairment in radiologically isolated syndromes. *Neurology*. 2012;78(5):309-314. doi:10.1212/WNL.0B013E31824528C9

21. De Meo E, Portaccio E, Giorgio A, et al. Identifying the Distinct Cognitive Phenotypes in Multiple Sclerosis. *JAMA Neurol*. 2021;78(4):414-425. doi:10.1001/JAMANEUROL.2020.4920

22. Pérez-Miralles F, Sastre-Garriga J, Tintoré M, et al. Clinical impact of early brain atrophy in clinically isolated syndromes. *Multiple Sclerosis Journal*. 2013;19(14):1878-1886. doi:10.1177/1352458513488231

23. Filippi M, Preziosa P, Copetti M, et al. Gray matter damage predicts the accumulation of disability 13 years later in MS. *Neurology*. 2013;81(20):1759-1767. doi:10.1212/01.wnl.0000435551.90824.d0

24. Fisniku LK, Chard DT, Jackson JS, et al. Gray matter atrophy is related to long-term disability in multiple sclerosis. *Ann Neurol*. Published online 2008. doi:10.1002/ana.21423

25. Cree BAC, Hollenbach JA, Bove R, et al. Silent progression in disease activity–free relapsing multiple sclerosis. *Ann Neurol*. 2019;85(5):653-666. doi:10.1002/ana.25463

26. Cagol A, Schaedelin S, Barakovic M, et al. Association of Brain Atrophy With Disease Progression Independent of Relapse Activity in Patients With Relapsing Multiple Sclerosis. *JAMA Neurol*. 2022;79(7). doi:10.1001/jamaneurol.2022.1025

27. Eshaghi A, Marinescu R V., Young AL, et al. Progression of regional grey matter atrophy in multiple sclerosis. *Brain*. 2018;141(6):1665-1677. doi:10.1093/BRAIN/AWY088

28. Valsasina P, Benedetti B, Rovaris M, Sormani MP, Comi G, Filippi M. Evidence for progressive gray matter loss in patients with relapsing-remitting MS. *Neurology*. Published online 2005. doi:10.1212/01.wnl.0000178982.53965.70

29. Jasperse B. Spinal Cord Imaging in Multiple Sclerosis and Related Disorders. *Neuroimaging Clin N Am*. 2024;34(3):385-398. doi:10.1016/j.nic.2024.03.011

30. Bot JCJ, Blezer ELA, Kamphorst W, et al. The spinal cord in multiple sclerosis: relationship of high-spatial-resolution quantitative MR imaging findings to histopathologic results. *Radiology*. 2004;233(2):531-540. doi:10.1148/RADIOL.2332031572

31. Evangelou N, DeLuca GC, Owens T, Esiri MM. Pathological study of spinal cord atrophy in multiple sclerosis suggests limited role of local lesions. *Brain*. 2005;128(1):29-34. doi:10.1093/BRAIN/AWH323

32. Casserly C, Seyman EE, Alcaide-Leon P, et al. Spinal Cord Atrophy in Multiple Sclerosis: A Systematic Review and Meta-Analysis. 2018;28(6):556-586. Accessed September 5, 2022. https://pubmed.ncbi.nlm.nih.gov/30102003/

33. Biberacher V, Boucard CC, Schmidt P, et al. Atrophy and structural variability of the upper cervical cord in early multiple sclerosis. *Multiple Sclerosis*. 2015;21(7):875-884. doi:10.1177/1352458514546514

34. Tsagkas C, Magon S, Gaetano L, et al. Spinal cord volume loss: A marker of disease progression in multiple sclerosis. *Neurology*. 2018;91(4):e349-e358. doi:10.1212/WNL.0000000000005853

35. Cagol A, Benkert P, Melie-Garcia L, et al. Association of Spinal Cord Atrophy and Brain Paramagnetic Rim Lesions With Progression Independent of Relapse Activity in People With MS. *Neurology*. 2024;102(1). doi:10.1212/WNL.0000000000207768

36. Bischof A, Papinutto N, Keshavan A, et al. Spinal Cord Atrophy Predicts Progressive Disease in Relapsing Multiple Sclerosis. *Ann Neurol*. 2022;91(2):268-281. doi:10.1002/ana.26281

37. Kuhlmann T, Ludwin S, Prat A, Antel J, Brück W, Lassmann H. An updated histological classification system for multiple sclerosis lesions. *Acta Neuropathol*. 2017;133(1):13-24. doi:10.1007/S00401-016-1653-Y

38. Bagnato F, Sati P, Hemond CC, et al. Imaging chronic active lesions in multiple sclerosis: a consensus statement. *Brain*. 2024;147(9):2913-2933. doi:10.1093/BRAIN/AWAE013

39. Calvi A, Tur C, Chard D, et al. Slowly expanding lesions relate to persisting black-holes and clinical outcomes in relapse-onset multiple sclerosis. *Neuroimage Clin*. 2022;35. doi:10.1016/j.nicl.2022.103048

40. Dal-Bianco A, Grabner G, Kronnerwetter C, et al. Slow expansion of multiple sclerosis iron rim lesions: pathology and 7 T magnetic resonance imaging. *Acta Neuropathol*. 2017;133(1):25. doi:10.1007/S00401-016-1636-Z

41. Absinta M, Maric D, Gharagozloo M, et al. A lymphocyte–microglia–astrocyte axis in chronic active multiple sclerosis. *Nature*. 2021;597(7878):709-714. doi:10.1038/s41586-021-03892-7

42. Rahmanzadeh R, Lu PJ, Barakovic M, et al. Myelin and axon pathology in multiple sclerosis assessed by myelin water and multi-shell diffusion imaging. *Brain*. 2021;144(6):1684-1696. doi:10.1093/BRAIN/AWAB088

43. Martire MS, Moiola L, Rocca MA, Filippi M, Absinta M. What is the potential of paramagnetic rim lesions as diagnostic indicators in multiple sclerosis? *Expert Rev Neurother*. Published online November 8, 2022:1-9. doi:10.1080/14737175.2022.2143265

44. Clarke MA, Pareto D, Pessini-Ferreira L, et al. Value of 3T Susceptibility-Weighted Imaging in the Diagnosis of Multiple Sclerosis. *American Journal of Neuroradiology*. 2020;41(6):1001-1008. doi:10.3174/AJNR.A6547

45. Montalban X, Lebrun-Frénay C, Oh J, et al. Diagnosis of multiple sclerosis: 2024 revisions of the McDonald criteria. *Lancet Neurol*. 2025;24(10):850-865. doi:10.1016/S1474-4422(25)00270-4

46. Maggi P, Kuhle J, Schädelin S, et al. Chronic White Matter Inflammation and Serum Neurofilament Levels in Multiple Sclerosis. *Neurology*. 2021;97(6):e543-e553. doi:10.1212/WNL.0000000000012326

47. Absinta M, Sati P, Masuzzo F, et al. Association of Chronic Active Multiple Sclerosis Lesions With Disability In Vivo. *JAMA Neurol*. 2019;76(12):1474. doi:10.1001/JAMANEUROL.2019.2399

48. Barkhof F. The clinico-radiological paradox in multiple sclerosis revisited. *Curr Opin Neurol*. 2002;15(3):239-245. doi:10.1097/00019052-200206000-00003

49. Tranfa M, Pontillo G, Petracca M, et al. *Quantitative MRI in Multiple Sclerosis: From Theory to Application*. Vol 43. AJNR Am J Neuroradiol; 2022:1688-1695. Accessed January 9, 2023. https://pubmed.ncbi.nlm.nih.gov/35680161/

50. Granziera C, Wuerfel J, Barkhof F, et al. Quantitative magnetic resonance imaging towards clinical application in multiple sclerosis. *Brain*. 2021;144(5):1296-1311. doi:10.1093/brain/awab029

51. Helms G. Tissue Properties from Quantitative MRI. In: *Brain Mapping: An Encyclopedic Reference*. Vol 1. Academic Press; 2015:287-294. doi:10.1016/B978-0-12-397025-1.00297-9

52. Mottershead JP, Schmierer K, Clemence M, et al. High field MRI correlates of myelin content and axonal density in multiple sclerosis: A post-mortem study of the spinal cord. *J Neurol*. 2003;250(11):1293-1301. doi:10.1007/s00415-003-0192-3

53. Schmierer K, Scaravilli F, Altmann DR, Barker GJ, Miller DH. Magnetization transfer ratio and myelin in postmortem multiple sclerosis brain. 2004;56(3):407-415. Accessed November 13, 2023. https://pubmed.ncbi.nlm.nih.gov/15349868/

54. Van Waesberghe JHTM, Kamphorst W, De Groot CJA, et al. Axonal loss in multiple sclerosis lesions: Magnetic resonance imaging insights into substrates of disability. *Ann Neurol*. 1999;46(5):747-754. doi:10.1002/1531-8249(199911)46:5<747::AID-ANA10>3.0.CO;2-4

55. Moccia M, Van De Pavert S, Eshaghi A, et al. Pathologic correlates of the magnetization transfer ratio in multiple sclerosis. *Neurology*. 2020;95(22):E2965-E2976. doi:10.1212/WNL.0000000000010909

56. Vavasour IM, Laule C, Li DKB, Traboulsee AL, MacKay AL. Is the magnetization transfer ratio a marker for myelin in multiple sclerosis? *Journal of Magnetic Resonance Imaging*. 2011;33(3):710-718. doi:10.1002/jmri.22441

57. Helms G, Dathe H, Kallenberg K, Dechent P. High-resolution maps of magnetization transfer with inherent correction for RF inhomogeneity and T1 relaxation obtained from 3D FLASH MRI. *Magn Reson Med*. 2008;60(6):1396-1407. doi:10.1002/mrm.21732

58. Cagol A, Tsagkas C, Granziera C. Advanced Brain Imaging in Central Nervous System Demyelinating Diseases. *Neuroimaging Clinics*. 2024;0(0). doi:10.1016/J.NIC.2024.03.003

59. Lee J, Hyun JW, Lee J, et al. So You Want to Image Myelin Using MRI: An Overview and Practical Guide for Myelin Water Imaging. *Journal of Magnetic Resonance Imaging.John Wiley & Sons, Ltd*. 2021;53(2):360-373. doi:10.1002/jmri.27059

60. MacKay AL, Laule C. Magnetic Resonance of Myelin Water: An in vivo Marker for Myelin. *Brain Plasticity*. 2016;2(1):71-91. doi:10.3233/bpl-160033

61. Laule C, Leung E, Li DKB, et al. Myelin water imaging in multiple sclerosis: Quantitative correlations with histopathology. *Multiple Sclerosis*. 2006;12(6):747-753. doi:10.1177/1352458506070928

62. Laule C, Kozlowski P, Leung E, Li DKB, MacKay AL, Moore GRW. Myelin water imaging of multiple sclerosis at 7 T: Correlations with histopathology. *Neuroimage*. 2008;40(4):1575-1580. doi:10.1016/j.neuroimage.2007.12.008

63. Liu C, Wei H, Gong NJ, Cronin M, Dibb R, Decker K. Quantitative Susceptibility Mapping: Contrast Mechanisms and Clinical Applications. *Tomography*. 2015;1(1):3-17. doi:10.18383/j.tom.2015.00136

64. Harada T, Kudo K, Fujima N, et al. Quantitative Susceptibility Mapping: Basic Methods and Clinical Applications. *Radiographics*. 2022;42(4):1161-1176. doi:10.1148/rg.210054

65. Duyn JH, Schenck J. Contributions to magnetic susceptibility of brain tissue. *NMR Biomed.NIH Public Access*. 2017;30(4). doi:10.1002/nbm.3546

66. Hametner S, Endmayr V, Deistung A, et al. The influence of brain iron and myelin on magnetic susceptibility and effective transverse relaxation - A biochemical and histological validation study. *Neuroimage*. 2018;179:117-133. doi:10.1016/j.neuroimage.2018.06.007

67. Pontillo G, Petracca M, Monti S, et al. Unraveling deep gray matter atrophy and iron and myelin changes in multiple sclerosis. *American Journal of Neuroradiology*. 2021;42(7):1223-1230. doi:10.3174/ajnr.A7093

68. Schweser F, Hagemeier J, Dwyer MG, et al. Decreasing brain iron in multiple sclerosis: The difference between concentration and content in iron MRI. *Hum Brain Mapp*. 2021;42(5):1463-1474. doi:10.1002/hbm.25306

69. Zivadinov R, Schweser F, Dawes C, et al. A multicentre study of quantitative susceptibility mapping in sub-cortical deep gray matter structures in relapsing multiple sclerosis. *Mult Scler*. 2016;22:222. doi:10.1177/1352458516663081

70. Schweser F, Raffaini Duarte Martins AL, Hagemeier J, et al. Mapping of Thalamic Magnetic Susceptibility in Multiple Sclerosis Indicates Decreasing Iron with Disease Duration: A Proposed Mechanistic Relationship between Inflammation and Oligodendrocyte Vitality. *Neuroimage*. 2018;167:438. doi:10.1016/J.NEUROIMAGE.2017.10.063

71. Rahmanzadeh R, Galbusera R, Lu PJ, et al. A New Advanced MRI Biomarker for Remyelinated Lesions in Multiple Sclerosis. *Ann Neurol*. 2022;92(3):486-502. doi:10.1002/ana.26441

72. Pierpaoli C, Jezzard P, Basser PJ, Barnett A, Di Chiro G. Diffusion tensor MR imaging of the human brain. *Radiology*. 1996;201(3):637-648. doi:10.1148/radiology.201.3.8939209

73. Jones DK, Cercignani M. Twenty-five pitfalls in the analysis of diffusion MRI data. *NMR Biomed*. 2010;23(7):803-820. doi:10.1002/nbm.1543

74. Schmierer K, Wheeler-Kingshott CAM, Boulby PA, et al. Diffusion tensor imaging of post mortem multiple sclerosis brain. *Neuroimage*. 2007;35(2):467-477. doi:10.1016/j.neuroimage.2006.12.010

75. Song SK, Yoshino J, Le TQ, et al. Demyelination increases radial diffusivity in corpus callosum of mouse brain. *Neuroimage*. 2005;26(1):132-140. doi:10.1016/j.neuroimage.2005.01.028

76. Guo AC, Jewells VL, Provenzale JM. Analysis of normal-appearing white Matter in multiple sclerosis: Comparison of diffusion tensor MR imaging and magnetization transfer imaging. *American Journal of Neuroradiology*. 2001;22(10):1893-1900.

77. Martinez-Heras E, Grussu F, Prados F, Solana E, Llufriu S. Diffusion-Weighted Imaging: Recent Advances and Applications. *Seminars in Ultrasound, CT and MRI*. 2021;42(5):490-506. doi:10.1053/j.sult.2021.07.006

78. Ontaneda D, Raza PC, Mahajan KR, et al. Deep grey matter injury in multiple sclerosis: A NAIMS consensus statement. *Brain*. 2021;2021. doi:10.1093/brain/awab132

79. Eshaghi A, Prados F, Brownlee WJ, et al. Deep gray matter volume loss drives disability worsening in multiple sclerosis. *Ann Neurol*. 2018;83(2):210-222. doi:10.1002/ana.25145

80. Azevedo CJ, Cen SY, Khadka S, et al. Thalamic atrophy in multiple sclerosis: A magnetic resonance imaging marker of neurodegeneration throughout disease. *Ann Neurol*. Published online 2018. doi:10.1002/ana.25150

81. Steenwijk MD, Geurts JJG, Daams M, et al. Cortical atrophy patterns in multiple sclerosis are non-random and clinically relevant. *Brain*. 2016;139(1):115-126. doi:10.1093/brain/awv337

82. Scalfari A, Romualdi C, Nicholas RS, et al. The cortical damage, early relapses, and onset of the progressive phase in multiple sclerosis. *Neurology*. 2018;90(24):e2099-e2106. doi:10.1212/WNL.0000000000005685

83. Lazzarotto A, Hamzaoui M, Tonietto M, et al. Time is myelin: early cortical myelin repair prevents atrophy and clinical progression in multiple sclerosis. *Brain*. 2024;147(4):1331-1343. doi:10.1093/BRAIN/AWAE024

84. Reich DS, Lucchinetti CF, Calabresi PA. Multiple Sclerosis. *New England Journal of Medicine*. 2018;378(2):169-180. doi:10.1056/NEJMRA1401483;PAGEGROUP:STRING:PUBLICATION

85. Giovannoni G. Disease-modifying treatments for early and advanced multiple sclerosis: A new treatment paradigm. *Curr Opin Neurol*. 2018;31(3):233-243. doi:10.1097/WCO.0000000000000561

86. Hauser SL, Kappos L, Arnold DL, et al. Five years of ocrelizumab in relapsing multiple sclerosis: OPERA studies open-label extension. *Neurology*. 2020;95(13):E1854-E1867. doi:10.1212/WNL.0000000000010376

87. Buron MD, Chalmer TA, Sellebjerg F, et al. Initial high-efficacy disease-modifying therapy in multiple sclerosis: A nationwide cohort study. *Neurology*. 2020;95(8):E1041-E1051. doi:10.1212/WNL.0000000000010135;PAGE:STRING:ARTICLE/CHAPTER

88. He A, Merkel B, Brown JWL, et al. Timing of high-efficacy therapy for multiple sclerosis: a retrospective observational cohort study. *Lancet Neurol*. 2020;19(4):307-316. doi:10.1016/S1474-4422(20)30067-3

89. Graf J, Leussink VI, Soncin G, et al. Relapse-independent multiple sclerosis progression under natalizumab. *Brain Commun*. 2021;3(4). doi:10.1093/BRAINCOMMS/FCAB229

90. Kapica-Topczewska K, Collin F, Tarasiuk J, et al. Assessment of Disability Progression Independent of Relapse and Brain MRI Activity in Patients with Multiple Sclerosis in Poland. *J Clin Med*. 2021;10(4):1-15. doi:10.3390/JCM10040868

91. von Wyl V, Benkert P, Moser A, et al. Disability progression in relapse-free multiple sclerosis patients on fingolimod versus interferon-beta/glatiramer acetate. *Mult Scler*. 2021;27(3):439-448. doi:10.1177/1352458520918489

92. Gärtner J, Hauser SL, Bar-Or A, et al. Efficacy and safety of ofatumumab in recently diagnosed, treatment-naive patients with multiple sclerosis: Results from ASCLEPIOS I and II. *Mult Scler*. 2022;28(10):1562-1575. doi:10.1177/13524585221078825

93. Montobbio N, Bovis F, Signori A, et al. Uncovering a bias in estimated treatment effects on PIRA in multiple sclerosis clinical trials. *EBioMedicine*. 2025;117. doi:10.1016/j.ebiom.2025.105802

94. Sastre-Garriga J, Pareto D, Rovira À. Brain Atrophy in Multiple Sclerosis: Clinical Relevance and Technical Aspects. *Neuroimaging Clin N Am*. 2017;27(2):289-300. doi:10.1016/j.nic.2017.01.002

95. Reeves JA, Mohebbi M, Wicks T, et al. Paramagnetic rim lesions predict greater long-term relapse rates and clinical progression over 10 years. *Mult Scler*. 2024;30(4-5):535-545. doi:10.1177/13524585241229956

96. Maggi P, Bulcke C Vanden, Pedrini E, et al. B cell depletion therapy does not resolve chronic active multiple sclerosis lesions. *EBioMedicine*. 2023;94. doi:10.1016/j.ebiom.2023.104701

97. Nakamura K, Thoomukuntla B, Bena J, Cohen JA, Fox RJ, Ontaneda D. Ibudilast reduces slowly enlarging lesions in progressive multiple sclerosis. *Multiple Sclerosis Journal*. 2024;30(3):369-380. doi:10.1177/13524585231224702;PAGE:STRING:ARTICLE/CHAPTER

98. Arnold DL, Elliott C, Martin EC, Hyvert Y, Tomic D, Montalban X. Effect of Evobrutinib on Slowly Expanding Lesion Volume in Relapsing Multiple Sclerosis: A Post Hoc Analysis of a Phase 2 Trial. *Neurology*. 2024;102(5). doi:10.1212/WNL.0000000000208058

99. York EN, Thrippleton MJ, Meijboom R, Hunt DPJ, Waldman AD. Quantitative magnetization transfer imaging in relapsing-remitting multiple sclerosis: A systematic review and meta-analysis. *Brain Commun.Oxford Academic*. 2022;4(2). doi:10.1093/braincomms/fcac088

100. Kolind S, Abel S, Taylor C, et al. Myelin water imaging in relapsing multiple sclerosis treated with ocrelizumab and interferon beta-1a. *Neuroimage Clin*. 2022;35. doi:10.1016/j.nicl.2022.103109

101. Caverzasi E, Papinutto N, Cordano C, et al. MWF of the corpus callosum is a robust measure of remyelination: Results from the ReBUILD trial. *Proc Natl Acad Sci U S A*. 2023;120(20):e2217635120. doi:10.1073/PNAS.2217635120;PAGE:STRING:ARTICLE/CHAPTER

102. Sormani MP, Arnold DL, De Stefano N. Treatment effect on brain atrophy correlates with treatment effect on disability in multiple sclerosis. *Ann Neurol*. 2014;75(1):43-49. doi:10.1002/ana.24018

103. Lublin FD, Reingold SC, Cohen JA, et al. Defining the clinical course of multiple sclerosis: the 2013 revisions. *Neurology*. 2014;83(3):278-286. doi:10.1212/WNL.0000000000000560

104. Disanto G, Benkert P, Lorscheider J, et al. The Swiss Multiple Sclerosis Cohort-Study (SMSC): A prospective Swiss wide investigation of key phases in disease evolution and new treatment options. *PLoS One*. 2016;11(3). doi:10.1371/journal.pone.0152347

105. La Rosa F, Abdulkadir A, Fartaria MJ, et al. Multiple sclerosis cortical and WM lesion segmentation at 3T MRI: a deep learning method based on FLAIR and MP2RAGE. *Neuroimage Clin*. 2020;27. doi:10.1016/j.nicl.2020.102335

106. Hua K, Zhang J, Wakana S, et al. Tract probability maps in stereotaxic spaces: Analyses of white matter anatomy and tract-specific quantification. *Neuroimage*. 2008;39(1):336-347. doi:10.1016/j.neuroimage.2007.07.053

107. Todea AR, Melie-Garcia L, Barakovic M, et al. A Multicenter Longitudinal MRI Study Assessing LeMan-PV Software Accuracy in the Detection of White Matter Lesions in Multiple Sclerosis Patients. *Journal of Magnetic Resonance Imaging*. 2023;58(3):864-876. doi:10.1002/jmri.28618

108. Caranova M, Soares JF, Batista S, Castelo-Branco M, Duarte JV. A systematic review of microstructural abnormalities in multiple sclerosis detected with NODDI and DTI models of diffusion-weighted magnetic resonance imaging. *Magn Reson Imaging.Elsevier*. 2023;104:61-71. doi:10.1016/j.mri.2023.09.010

109. Lopez-Soley E, Martinez-Heras E, Solana E, et al. Diffusion tensor imaging metrics associated with future disability in multiple sclerosis. *Sci Rep*. 2023;13(1):1-10. doi:10.1038/s41598-023-30502-5

110. Geurts JJ, Barkhof F. Grey matter pathology in multiple sclerosis. *Lancet Neurol.Elsevier*. 2008;7(9):841-851. doi:10.1016/S1474-4422(08)70191-1

111. Mehndiratta A, Treaba CA, Barletta V, et al. Characterization of thalamic lesions and their correlates in multiple sclerosis by ultra-high-field MRI. *Multiple Sclerosis Journal*. 2021;27(5):674-683. doi:10.1177/1352458520932804

112. Fadda G, Brown RA, Magliozzi R, et al. A surface-in gradient of thalamic damage evolves in pediatric multiple sclerosis. *Ann Neurol*. 2019;85(3):340-351. doi:10.1002/ana.25429

113. Magliozzi R, Fadda G, Brown RA, et al. "Ependymal-in" Gradient of Thalamic Damage in Progressive Multiple Sclerosis. *Ann Neurol*. 2022;92(4):670-685. doi:10.1002/ana.26448

114. De Meo E, Storelli L, Moiola L, et al. In vivo gradients of thalamic damage in paediatric multiple sclerosis: A window into pathology. *Brain*. 2021;144(1):186-197. doi:10.1093/brain/awaa379

115. Liu Z, Pardini M, Yaldizli Ö, et al. Magnetization transfer ratio measures in normal-appearing white matter show periventricular gradient abnormalities in multiple sclerosis. *Brain*. 2015;138(5):1239-1246. doi:10.1093/brain/awv065

116. Witte ME, Mahad DJ, Lassmann H, van Horssen J. Mitochondrial dysfunction contributes to neurodegeneration in multiple sclerosis. *Trends Mol Med.Trends Mol Med*. 2014;20(3):179-187. doi:10.1016/j.molmed.2013.11.007

117. Haider L, Simeonidou C, Steinberger G, et al. Multiple sclerosis deep grey matter: The relation between demyelination, neurodegeneration, inflammation and iron. *J Neurol Neurosurg Psychiatry*. 2014;85(12):1386-1395. doi:10.1136/jnnp-2014-307712

118. Houtchens MK, Benedict RHB, Killiany R, et al. Thalamic atrophy and cognition in multiple sclerosis. *Neurology*. 2007;69(12):1213-1223. doi:10.1212/01.wnl.0000276992.17011.b5

119. Geurts JJG, Reuling IEW, Vrenken H, et al. MR spectroscopic evidence for thalamic and hippocampal, but not cortical, damage in multiple sclerosis. *Magn Reson Med*. 2006;55(3):478-483. doi:10.1002/mrm.20792

120. Cifelli A, Arridge M, Jezzard P, Esiri MM, Palace J, Matthews PM. Thalamic neurodegeneration in multiple sclerosis. *Ann Neurol*. 2002;52(5):650-653. doi:10.1002/ana.10326

121. Louapre C, Govindarajan ST, Giannì C, et al. Heterogeneous pathological processes account for thalamic degeneration in multiple sclerosis: Insights from 7 T imaging. *Multiple Sclerosis Journal*. 2018;24(11):1433-1444. doi:10.1177/1352458517726382

122. Henkelman RM, Stanisz GJ, Graham SJ. Magnetization transfer in MRI: A review. *NMR Biomed.NMR Biomed*. 2001;14(2):57-64. doi:10.1002/nbm.683

123. Kaden E, Kelm ND, Carson RP, Does MD, Alexander DC. Multi-compartment microscopic diffusion imaging. *Neuroimage*. 2016;139:346-359. doi:10.1016/j.neuroimage.2016.06.002

124. Thompson AJ, Banwell BL, Barkhof F, et al. Diagnosis of multiple sclerosis: 2017 revisions of the McDonald criteria. *Lancet Neurol.Elsevier*. 2018;17(2):162-173. doi:10.1016/S1474-4422(17)30470-2

125. Von Elm E, Altman DG, Egger M, Pocock SJ, Gøtzsche PC, Vandenbrouckef JP. The Strengthening the Reporting of Observational Studies in Epidemiology (STROBE) Statement: Guidelines for reporting observational studies. *Bull World Health Organ.World Health Organization*. 2007;85(11):867-872. doi:10.2471/BLT.07.045120

126. Kurtzke JF. Rating neurologic impairment in multiple sclerosis: An expanded disability status scale (EDSS). *Neurology*. 1983;33(11):1444-1452. doi:10.1212/wnl.33.11.1444

127. Smith A. Symbol digit modalities test. Published online 1973. Accessed November 24, 2021. https://www.communicate-ed.org.uk/assets/downloads/SDMT_Formula_Chart_Communicate-ed_2.pdf

128. C Helmstaedter, M Lendt SL. VLMT: Verbaler Lern-und Merkfähigkeitstest. Preprint posted online 2001.

129. Calabrese P, Kalbe E, Kessler J. Ein neuropsychologisches screening zur erfassung kognitiver störungen bei MS-patienten: Das Multiple Sklerose Inventarium Cognition (MUSIC). *PsychoNeuro.Karl Demeter Verlag GmbH*. 2004;30(7):384-388. doi:10.1055/s-2004-831083

130. Rahmanzadeh R, Weigel M, Lu PJ, et al. A comparative assessment of myelin-sensitive measures in multiple sclerosis patients and healthy subjects. *Neuroimage Clin*. 2022;36. doi:10.1016/j.nicl.2022.103177

131. Marques JP, Kober T, Krueger G, van der Zwaag W, Van de Moortele PF, Gruetter R. MP2RAGE, a self bias-field corrected sequence for improved segmentation and T1-mapping at high field. *Neuroimage*. 2010;49(2):1271-1281. doi:10.1016/j.neuroimage.2009.10.002

132. Helms G, Dathe H, Dechent P. Quantitative FLASH MRI at 3T using a rational approximation of the Ernst equation. *Magn Reson Med*. 2008;59(3):667-672. doi:10.1002/mrm.21542

133. Helms G, Dechent P. Increased SNR and reduced distortions by averaging multiple gradient echo signals in 3D FLASH imaging of the human brain at 3T. *J Magn Reson Imaging*. 2009;29(1):198-204. doi:10.1002/JMRI.21629

134. Cercignani M, Giulietti G, Dowell NG, et al. Characterizing axonal myelination within the healthy population: a tract-by-tract mapping of effects of age and gender on the fiber g-ratio. *Neurobiol Aging*. 2017;49:109-118. doi:10.1016/j.neurobiolaging.2016.09.016

135. Mancini M, Giulietti G, Dowell N, et al. Introducing axonal myelination in connectomics: A preliminary analysis of g-ratio distribution in healthy subjects. *Neuroimage*. 2018;182:351-359. doi:10.1016/j.neuroimage.2017.09.018

136. Liu T, Xu W, Spincemaille P, Avestimehr AS, Wang Y. Accuracy of the morphology enabled dipole inversion (MEDI) algorithm for quantitative susceptibility mapping in MRI. 2012;31(3):816-824. doi:10.1109/TMI.2011.2182523

137. Patenaude B, Smith SM, Kennedy DN, Jenkinson M. A Bayesian model of shape and appearance for subcortical brain segmentation. *Neuroimage*. 2011;56(3):907-922. doi:10.1016/j.neuroimage.2011.02.046

138. de Sitter A, Burggraaff J, Bartel F, et al. Development and evaluation of a manual segmentation protocol for deep grey matter in multiple sclerosis: Towards accelerated semi-automated references. *Neuroimage Clin*. 2021;30. doi:10.1016/j.nicl.2021.102659

139. Su JH, Thomas FT, Kasoff WS, et al. Thalamus Optimized Multi Atlas Segmentation (THOMAS): fast, fully automated segmentation of thalamic nuclei from structural MRI. *Neuroimage*. 2019;194:272-282. doi:10.1016/j.neuroimage.2019.03.021

140. Cerri S, Puonti O, Meier DS, et al. A contrast-adaptive method for simultaneous whole-brain and lesion segmentation in multiple sclerosis. *Neuroimage*. 2021;225:117471. doi:10.1016/j.neuroimage.2020.117471

141. Eshaghi A, Wottschel V, Cortese R, et al. Gray matter MRI differentiates neuromyelitis optica from multiple sclerosis using random forest. *Neurology*. 2016;87(23). doi:10.1212/WNL.0000000000003395

142. Vrenken H, Geurts JJG, Knol DL, et al. Whole-brain T1 mapping in multiple sclerosis: Global changes of normal-appearing gray and white matter. *Radiology*. 2006;240(3):811-820. doi:10.1148/radiol.2403050569

143. Tranfa M, Pontillo G, Petracca M, et al. Quantitative MRI in Multiple Sclerosis: From Theory to Application. *AJNR Am J Neuroradiol*. 2022;43(12):1688-1695. doi:10.3174/ajnr.A7536

144. Zivadinov R, Tavazzi E, Bergsland N, et al. Brain iron at quantitative MRI is associated with disability in multiple sclerosis. *Radiology*. 2018;289(2):487-496. doi:10.1148/radiol.2018180136

145. Blyau S, Koubiyr I, Saranathan M, et al. Differential vulnerability of thalamic nuclei in multiple sclerosis. *Multiple Sclerosis Journal*. 2023;29(2):295-300. doi:10.1177/13524585221114247

146. Koubiyr I, Yamamoto T, Blyau S, et al. Vulnerability of Thalamic Nuclei at CSF Interface During the Entire Course of Multiple Sclerosis. *Neurology(R) neuroimmunology & neuroinflammation*. 2024;11(3):e200222. doi:10.1212/NXI.0000000000200222

147. Calabrese M, Filippi M, Gallo P. Cortical lesions in multiple sclerosis. *Nature Reviews Neurology 2010 6:8*. 2010;6(8):438-444. doi:10.1038/nrneurol.2010.93

148. Bagnato F, Sati P, Hemond CC, et al. Imaging chronic active lesions in multiple sclerosis: a consensus statement. *Brain*. 2012;139(4):16-17. doi:10.1093/BRAIN/AWAE013

149. Di Filippo M, Gaetani L, Centonze D, et al. Fluid biomarkers in multiple sclerosis: from current to future applications. *The Lancet Regional Health - Europe*. 2024;44. doi:10.1016/J.LANEPE.2024.101009/ASSET/4ABD497E-32E3-4286-804E-A99D1F5F7E9D/MAIN.ASSETS/GR2.JPG

150. Meier S, Willemse EAJ, Schaedelin S, et al. Serum Glial Fibrillary Acidic Protein Compared With Neurofilament Light Chain as a Biomarker for Disease Progression in Multiple Sclerosis. *JAMA Neurol*. Published online February 6, 2023. doi:10.1001/jamaneurol.2022.5250

151. Benkert P, Maleska Maceski A, Schaedelin S, et al. Serum Glial Fibrillary Acidic Protein and Neurofilament Light Chain Levels Reflect Different Mechanisms of Disease Progression under B-Cell Depleting Treatment in Multiple Sclerosis. *Ann Neurol*. Published online 2024. doi:10.1002/ANA.27096

152. Kappos L, Butzkueven H, Wiendl H, et al. Greater sensitivity to multiple sclerosis disability worsening and progression events using a roving versus a fixed reference value in a prospective cohort study. *Multiple Sclerosis Journal*. 2018;24(7):963-973. doi:10.1177/1352458517709619

153. Montobbio N, Carmisciano L, Signori A, et al. Creating an automated tool for a consistent and repeatable evaluation of disability progression in clinical studies for multiple sclerosis. *Multiple Sclerosis Journal*. Published online August 1, 2024. doi:10.1177/13524585241243157/SUPPL_FILE/SJ-DOCX-1-MSJ-10.1177_13524585241243157.DOCX

154. Cagol A, Cortese R, Barakovic M, et al. Diagnostic Performance of Cortical Lesions and the Central Vein Sign in Multiple Sclerosis. *JAMA Neurol*. 2024;81(2):143-153. doi:10.1001/JAMANEUROL.2023.4737

155. Puonti O, Iglesias JE, Van Leemput K. Fast and sequence-adaptive whole-brain segmentation using parametric Bayesian modeling. *Neuroimage*. 2016;143:235-249. doi:10.1016/j.neuroimage.2016.09.011

156. De Leener B, Lévy S, Dupont SM, et al. SCT: Spinal Cord Toolbox, an open-source software for processing spinal cord MRI data. *Neuroimage*. 2017;145(Pt A):24-43. doi:10.1016/j.neuroimage.2016.10.009

157. Nguyen TD, Deh K, Monohan E, et al. Feasibility and reproducibility of whole brain myelin water mapping in 4 minutes using fast acquisition with spiral trajectory and adiabatic T2prep (FAST-T2) at 3T. *Magn Reson Med*. 2016;76(2):456-465. doi:10.1002/mrm.25877

158. Zhang H, Schneider T, Wheeler-Kingshott CA, Alexander DC. NODDI: Practical in vivo neurite orientation dispersion and density imaging of the human brain. *Neuroimage*. 2012;61(4):1000-1016. doi:10.1016/j.neuroimage.2012.03.072

159. Benkert P, Meier S, Schaedelin S, et al. Serum neurofilament light chain for individual prognostication of disease activity in people with multiple sclerosis: a retrospective modelling and validation study. *Lancet Neurol*. 2022;21(3):246-257. doi:10.1016/S1474-4422(22)00009-6

160. Kursa MB, Rudnicki WR. Feature Selection with the Boruta Package. *J Stat Softw*. 2010;36(11):1-13. doi:10.18637/JSS.V036.I11

161. Morozumi T, Preziosa P, Meani A, et al. Brain and cervical spinal cord MRI correlates of sensorimotor impairment in patients with multiple sclerosis. *https://doi.org/101177/13524585241260145*. Published online June 24, 2024. doi:10.1177/13524585241260145

162. Brownlee WJ, Altmann DR, Prados F, et al. Early imaging predictors of long-term outcomes in relapse-onset multiple sclerosis. *Brain*. 2019;142(8):2276-2287. doi:10.1093/BRAIN/AWZ156

163. Rocca MA, Valsasina P, Meani A, et al. Spinal cord lesions and brain grey matter atrophy independently predict clinical worsening in definite multiple sclerosis: a 5-year, multicentre study. *J Neurol Neurosurg Psychiatry*. 2022;94(1):10-18. doi:10.1136/JNNP-2022-329854,

164. Calabrese M, Rocca MA, Atzori M, et al. A 3-year magnetic resonance imaging study of cortical lesions in relapse-onset multiple sclerosis. *Ann Neurol*. 2010;67(3):376-383. doi:10.1002/ANA.21906

165. Treaba CA, Herranz E, Barletta VT, et al. The relevance of multiple sclerosis cortical lesions on cortical thinning and their clinical impact as assessed by 7.0-T MRI. *J Neurol*. 2021;268(7):2473-2481. doi:10.1007/S00415-021-10400-4

166. Bisecco A, Stamenova S, Caiazzo G, et al. Attention and processing speed performance in multiple sclerosis is mostly related to thalamic volume. *Brain Imaging Behav*. 2018;12(1):20-28. doi:10.1007/S11682-016-9667-6/TABLES/5

167. Koenig KA, Sakaie KE, Lowe MJ, et al. Hippocampal volume is related to cognitive decline and fornicial diffusion measures in multiple sclerosis. *Magn Reson Imaging*. 2014;32(4):354-358. doi:10.1016/j.mri.2013.12.012

168. Abdelhak A, Benkert P, Schaedelin S, et al. Neurofilament Light Chain Elevation and Disability Progression in Multiple Sclerosis. *JAMA Neurol*. 2023;80(12):1317-1325. doi:10.1001/JAMANEUROL.2023.3997

169. Coll L, Pareto D, Aparicio-Serrano F, et al. Deep learning to predict progression independent of relapse activity at a first demyelinating event. *Brain Commun*. 2025;7(4). doi:10.1093/BRAINCOMMS/FCAF243

170. Lauerer M, Wiltgen T, Brückner C, et al. Predictors of early disability accumulation in newly diagnosed multiple sclerosis: clinical, imaging and cerebrospinal fluid measures. *J Neurol Neurosurg Psychiatry*. 2025;96(9):900-907. doi:10.1136/JNNP-2024-335037

171. Monreal E, Fernández-Velasco JI, García-Sánchez MI, et al. Association of Serum Neurofilament Light Chain Levels at Disease Onset with Disability Worsening in Patients with a First Demyelinating Multiple Sclerosis Event Not Treated with High-Efficacy Drugs. *JAMA Neurol*. 2023;80(4):397-403. doi:10.1001/JAMANEUROL.2023.0010,

172. Poretto V, Endrizzi W, Betti M, et al. Machine Learning Analysis Applied to Prediction of Early Progression Independent of Relapse Activity in Multiple Sclerosis Patients. *Eur J Neurol*. 2025;32(12):e70417. doi:10.1111/ENE.70417;SUBPAGE:STRING:FULL

173. Marastoni D, Colato E, Foschi M, et al. Intrathecal Inflammatory Profile and Gray Matter Damage Predict Progression Independent of Relapse Activity in Early Multiple Sclerosis. *Neurology(R) neuroimmunology & neuroinflammation*. 2025;12(4). doi:10.1212/NXI.0000000000200399

174. Tsagkas C, Huck-Horvath A, Cagol A, et al. Anterior horn atrophy in the cervical spinal cord: A new biomarker in progressive multiple sclerosis. *Mult Scler*. 2023;29(6):702-718. doi:10.1177/13524585221139152

175. Ocampo-Pineda M, Cagol A, Benkert P, et al. White Matter Tract Degeneration in Multiple Sclerosis Patients With Progression Independent of Relapse Activity. *Neurology(R) neuroimmunology & neuroinflammation*. 2025;12(3). doi:10.1212/NXI.0000000000200388

176. Miller AE. An Updated Review of teriflunomide's Use in Multiple Sclerosis. *Neurodegener Dis Manag*. 2021;11(5):387-409. doi:10.2217/NMT-2021-0014

177. Lamb YN. Ocrelizumab: A Review in Multiple Sclerosis. *Drugs*. 2022;82(3):323-334. doi:10.1007/S40265-022-01672-9

178. Cerri S, Greve DN, Hoopes A, et al. An open-source tool for longitudinal whole-brain and white matter lesion segmentation. *Neuroimage Clin*. 2023;38:103354. doi:10.1016/j.nicl.2023.103354

179. Tournier JD, Smith R, Raffelt D, et al. MRtrix3: A fast, flexible and open software framework for medical image processing and visualisation. *Neuroimage.Academic Press*. 2019;202:116137. doi:10.1016/j.neuroimage.2019.116137

180. Radue EW, Sprenger T, Gaetano L, et al. Teriflunomide slows BVL in relapsing MS: A reanalysis of the TEMSO MRI data set using SIENA. *Neurol Neuroimmunol Neuroinflamm*. Published online 2017.

181. Hauser SL, Bar-Or A, Cohen JA, et al. Ofatumumab versus Teriflunomide in Multiple Sclerosis. *New England Journal of Medicine*. 2020;383(6):546-557. doi:10.1056/nejmoa1917246

182. Steinman L, Fox E, Hartung HP, et al. Ublituximab versus Teriflunomide in Relapsing Multiple Sclerosis. *New England Journal of Medicine*. 2022;387(8):704-714. doi:10.1056/nejmoa2201904

183. Kappos L, Fox RJ, Burcklen M, et al. Ponesimod Compared with Teriflunomide in Patients with Relapsing Multiple Sclerosis in the Active-Comparator Phase 3 OPTIMUM Study: A Randomized Clinical Trial. *JAMA Neurol*. 2021;78(5):558-567. doi:10.1001/jamaneurol.2021.0405

184. Montalban X, Hauser SL, Kappos L, et al. Ocrelizumab versus Placebo in Primary Progressive Multiple Sclerosis. *N Engl J Med*. 2017;376(3):209-220. doi:10.1056/NEJMoa1606468

185. Hauser SL, Bar-Or A, Comi G, et al. Ocrelizumab versus Interferon Beta-1a in Relapsing Multiple Sclerosis. *New England Journal of Medicine*. 2017;376(3):221-234. doi:10.1056/nejmoa1601277

186. Zivadinov R, Keenan AJ, Le HH, et al. Brain volume loss in relapsing multiple sclerosis: indirect treatment comparisons of available disease-modifying therapies. *BMC Neurology 2024 24:1*. 2024;24(1):1-12. doi:10.1186/S12883-024-03888-6

187. Tan H, Li X, Li Y, et al. Real-world experience of teriflunomide in relapsing multiple sclerosis: paramagnetic rim lesions may play a role. *Front Immunol*. 2024;15:1343531. doi:10.3389/FIMMU.2024.1343531/BIBTEX

188. Thompson AJ, Baranzini SE, Geurts J, Hemmer B, Ciccarelli O. Multiple sclerosis. *The Lancet.Elsevier*. 2018;391(10130):1622-1636. doi:10.1016/S0140-6736(18)30481-1

189. Correale J, Gaitán MI, Ysrraelit MC, Fiol MP. Progressive multiple sclerosis: from pathogenic mechanisms to treatment. *Brain*. 2017;140(3):527-546. doi:10.1093/BRAIN/AWW258

190. Perez-Miralles F, Sastre-Garriga J, Tintore M, et al. Clinical impact of early brain atrophy in clinically isolated syndromes. *Mult Scler*. 2013;19(14):1878-1886. doi:10.1177/1352458513488231

191. Minneboo A, Jasperse B, Barkhof F, et al. Predicting short-term disability progression in early multiple sclerosis: Added value of MRI parameters. *J Neurol Neurosurg Psychiatry*. 2008;79(8):917-923. doi:10.1136/jnnp.2007.124123

192. Rocca MA, Sormani MP, Rovaris M, et al. Long-term disability progression in primary progressive multiple sclerosis: A 15-year study. *Brain*. 2017;140(11):2814-2819. doi:10.1093/brain/awx250

193. Branger P, Parienti JJ, Sormani MP, Defer G. The Effect of Disease-Modifying Drugs on Brain Atrophy in Relapsing-Remitting Multiple Sclerosis: A Meta-Analysis. *PLoS One*. 2016;11(3). doi:10.1371/JOURNAL.PONE.0149685

194. Sormani MP. Indirect comparisons of treatment effects: Network meta-analyses. *Mult Scler*. 2017;23(4):510-512. doi:10.1177/1352458517690272

195. Hutton B, Salanti G, Caldwell DM, et al. The PRISMA extension statement for reporting of systematic reviews incorporating network meta-analyses of health care interventions: checklist and explanations. *Ann Intern Med*. 2015;162(11):777-784. doi:10.7326/M14-2385

196. Balduzzi S, Rücker G, Nikolakopoulou A, et al. netmeta: An R Package for Network Meta-Analysis Using Frequentist Methods. *J Stat Softw*. 2023;106(2):1-40. doi:10.18637/JSS.V106.I02

197. Smith SM, Zhang Y, Jenkinson M, et al. Accurate, robust, and automated longitudinal and cross-sectional brain change analysis. *Neuroimage*. Published online 2002. doi:10.1006/nimg.2002.1040

198. Jacobs LD, Cookfair DL, Rudick RA, et al. Intramuscular interferon beta-1a for disease progression in relapsing multiple sclerosis. *Ann Neurol*. 1996;39(3):285-294. doi:10.1002/ana.410390304

199. Rudick RA, Fisher E, Lee JC, Simon J, Jacobs L. Use of the brain parenchymal fraction to measure whole brain atrophy in relapsing-remitting MS. *Neurology*. 1999;53(8):1698-1704. doi:10.1212/wnl.53.8.1698

200. Kappos L, Polman C, Pozzilli C, Thompson A, Dahlke F. Placebo-controlled multicentre randomised trial of interferon β-1b in treatment of secondary progressive multiple sclerosis. *Lancet*. 1998;352(9139):1491-1497. doi:10.1016/S0140-6736(98)10039-9 LK - https://basel.swisscovery.org/openurl/41SLSP_UBS/41SLSP_UBS:live?sid=EMBASE&sid=EMBASE&issn=01406736&id=doi:10.1016%2FS0140-6736%2898%2910039-9&atitle=Placebo-controlled+multicentre+randomised+trial+of+interferon+%CE%B2-1b+in+treatment+of+secondary+progressive+multiple+sclerosis&stitle=Lancet&title=Lancet&volume=352&issue=9139&spage=1491&epage=1497&aulast=Kappos&aufirs

t=Ludwig&auinit=L.&aufull=Kappos+L.&coden=LANCA&isbn=&pages=1491-1497&date=1998&auinit1=L&aui

201. Molyneux PD, Kappos L, Polman C, et al. The effect of interferon beta-1b treatment on MRI measures of cerebral atrophy in secondary progressive multiple sclerosis. *Brain*. 2000;123(11):2256-2263. doi:10.1093/brain/123.11.2256

202. Miller DH, Soon D, Fernando KT, et al. MRI outcomes in a placebo-controlled trial of natalizumab in relapsing MS. *Neurology*. 2007;68(17):1390-1401. doi:10.1212/01.wnl.0000260064.77700.fd

203. Polman CH, O'Connor PW, Havrdova E, et al. A Randomized, Placebo-Controlled Trial of Natalizumab for Relapsing Multiple Sclerosis. *New England Journal of Medicine*. 2006;354(9):899-910. doi:10.1056/nejmoa044397

204. Mikol DD, Barkhof F, Chang P, et al. Comparison of subcutaneous interferon beta-1a with glatiramer acetate in patients with relapsing multiple sclerosis (the REbif vs Glatiramer Acetate in Relapsing MS Disease [REGARD] study): a multicentre, randomised, parallel, open-label trial. *Lancet Neurol*. 2008;7(10):903-914. doi:10.1016/S1474-4422(08)70200-X

205. Coles AJ, Compston DAS, Selmaj KW, et al. Alemtuzumab vs. interferon beta-1a in early multiple sclerosis. *N Engl J Med*. 2008;359(17):1786-1801. doi:10.1056/NEJMoa0802670

206. O'Connor P, Filippi M, Arnason B, et al. 250 Mg or 500 Mg Interferon Beta-1B Versus 20 Mg Glatiramer Acetate in Relapsing-Remitting Multiple Sclerosis: a Prospective, Randomised, Multicentre Study. *Lancet Neurol*. 2009;8(10):889-897. doi:10.1016/S1474-4422(09)70226-1

207. Montalban X, Sastre-Garriga J, Tintoré M, et al. A single-center, randomized, double-blind, placebo-controlled study of interferon beta-1b on primary progressive and transitional multiple sclerosis. *Mult Scler*. 2009;15(10):1195-1205. doi:10.1177/1352458509106937

208. Kappos L, Radue EW, O'Connor P, et al. A Placebo-Controlled Trial of Oral Fingolimod in Relapsing Multiple Sclerosis. *New England Journal of Medicine*. Published online 2010. doi:10.1056/nejmoa0909494

209. Cohen JA, Barkhof F, Comi G, et al. Oral Fingolimod or Intramuscular Interferon for Relapsing Multiple Sclerosis. *New England Journal of Medicine*. 2010;362(5):402-415. doi:10.1056/nejmoa0907839

210. O'Connor P, Wolinsky JS, Confavreux C, et al. Randomized Trial of Oral Teriflunomide for Relapsing Multiple Sclerosis. *New England Journal of Medicine*. 2011;365(14):1293-1303. doi:10.1056/nejmoa1014656

211. Radue EWEW, Sprenger T, Gaetano L, et al. Teriflunomide slows BVL in relapsing MS. *Neurol Neuroimmunol Neuroinflamm*. 2017;4(5). doi:10.1212/NXI.0000000000000390

212. Miller DH, Fox RJ, Phillips JT, et al. Effects of delayed-release dimethyl fumarate on MRI measures in the phase 3 CONFIRM study. *Neurology*. 2015;84(11):1145-1152. doi:10.1212/WNL.0000000000001360

213. Fox RJ, Miller DH, Phillips JT, et al. Placebo-controlled phase 3 study of oral BG-12 or glatiramer in multiple sclerosis. *N Engl J Med*. 2012;367(12):1087-1097. doi:10.1056/NEJMoa1206328

214. Cohen JA, Coles AJ, Arnold DL, et al. Alemtuzumab versus interferon beta 1a as first-line treatment for patients with relapsing-remitting multiple sclerosis: A randomised controlled phase 3 trial. *The Lancet*. 2012;380(9856):1819-1828. doi:10.1016/S0140-6736(12)61769-3

215. Coles AJ, Twyman CL, Arnold DL, et al. Alemtuzumab for patients with relapsing multiple sclerosis after disease-modifying therapy: A randomised controlled phase 3 trial. *The Lancet*. Published online 2012. doi:10.1016/S0140-6736(12)61768-1

216. Khan O, Rieckmann P, Boyko A, Selmaj K, Zivadinov R. Three times weekly glatiramer acetate in relapsing-remitting multiple sclerosis. *Ann Neurol*. 2013;73(6):705-713. doi:10.1002/ana.23938

217. Gold R, Kappos L, Arnold DL, et al. Placebo-Controlled Phase 3 Study of Oral BG-12 for Relapsing Multiple Sclerosis. *New England Journal of Medicine*. 2012;367(12):1098-1107. doi:10.1056/nejmoa1114287

218. Arnold DL, Gold R, Kappos L, et al. Effects of delayed-release dimethyl fumarate on MRI measures in the Phase 3 DEFINE study. *J Neurol*. 2014;261(9):1794-1802. doi:10.1007/s00415-014-7412-x

219. Calabresi PA, Kieseier BC, Arnold DL, et al. Pegylated interferon beta-1a for relapsing-remitting multiple sclerosis (ADVANCE): A randomised, phase 3, double-blind study. *Lancet Neurol*. 2014;13(7):657-665. doi:10.1016/S1474-4422(14)70068-7

220. Calabresi PA, Radue EW, Goodin D, et al. Safety and efficacy of fingolimod in patients with relapsing-remitting multiple sclerosis (FREEDOMS II): A double-blind, randomised, placebo-controlled, phase 3 trial. *Lancet Neurol*. 2014;13(6):545-556. doi:10.1016/S1474-4422(14)70049-3

221. Lublin F, Miller DH, Freedman MS, et al. Oral fingolimod in primary progressive multiple sclerosis (INFORMS): A phase 3, randomised, double-blind, placebo-controlled trial. *The Lancet*. 2016;387(10023):1075-1084. doi:10.1016/S0140-6736(15)01314-8

222. Giovannoni G, Comi G, Cook S, et al. A placebo-controlled trial of oral cladribine for relapsing multiple sclerosis. *N Engl J Med*. 2010;362(5):416-426. doi:10.1056/NEJMoa0902533

223. De Stefano N, Giorgio A, Battaglini M, et al. Reduced brain atrophy rates are associated with lower risk of disability progression in patients with relapsing multiple sclerosis treated with cladribine tablets. *Multiple Sclerosis*. 2018;24(2):222-226. doi:10.1177/1352458517690269

224. Kappos L, Bar-Or A, Cree BAC, et al. Siponimod versus placebo in secondary progressive multiple sclerosis (EXPAND): a double-blind, randomised, phase 3 study. *Lancet*. 2018;391(10127):1263-1273. doi:10.1016/S0140-6736(18)30475-6

225. Kapoor R, Ho PR, Campbell N, et al. Effect of natalizumab on disease progression in secondary progressive multiple sclerosis (ASCEND): a phase 3, randomised, double-blind, placebo-controlled trial with an open-label extension. *Lancet Neurol*. 2018;17(5):405-415. doi:10.1016/S1474-4422(18)30069-3

226. Comi G, Kappos L, Selmaj KW, et al. Safety and efficacy of ozanimod versus interferon beta-1a in relapsing multiple sclerosis (SUNBEAM): a multicentre, randomised, minimum 12-month, phase 3 trial. *Lancet Neurol*. 2019;18(11):1009-1020. doi:10.1016/S1474-4422(19)30239-X

227. Cohen JA, Comi G, Selmaj KW, et al. Safety and efficacy of ozanimod versus interferon beta-1a in relapsing multiple sclerosis (RADIANCE): a multicentre, randomised, 24-month, phase 3 trial. *Lancet Neurol*. 2019;18(11):1021-1033. doi:10.1016/S1474-4422(19)30238-8

228. Cree BAC, Goldman MD, Corboy JR, et al. Efficacy and Safety of 2 Fingolimod Doses vs Glatiramer Acetate for the Treatment of Patients With Relapsing-Remitting Multiple Sclerosis: a Randomized Clinical Trial. *JAMA Neurol*. 2020;78(1):1-13. doi:10.1001/jamaneurol.2020.2950

229. Højsgaard Chow H, Talbot J, Lundell H, et al. Dimethyl Fumarate Treatment in Patients With Primary Progressive Multiple Sclerosis: A Randomized, Controlled Trial. *Neurology(R) neuroimmunology & neuroinflammation*. 2021;8(5). doi:10.1212/NXI.0000000000001037

230. Cree BAC, Gourraud PA, Oksenberg JR, et al. Long-term evolution of multiple sclerosis disability in the treatment era. *Ann Neurol*. 2016;80(4):499-510. doi:10.1002/ANA.24747

231. He A, Merkel B, Brown JWL, et al. Timing of high-efficacy therapy for multiple sclerosis: a retrospective observational cohort study. *Lancet Neurol*. 2020;19(4):307-316. doi:10.1016/S1474-4422(20)30067-3

232. Howell OW, Reeves CA, Nicholas R, et al. Meningeal inflammation is widespread and linked to cortical pathology in multiple sclerosis. *Brain*. 2011;134(9):2755-2771. doi:10.1093/brain/awr182

233. Calabrese M, Poretto V, Favaretto A, et al. Cortical lesion load associates with progression of disability in multiple sclerosis. *Brain*. 2012;135(10):2952-2961. doi:10.1093/BRAIN/AWS246,

234. Cagol A, Ocampo-Pineda M, Lu PJ, et al. Advanced Quantitative MRI Unveils Microstructural Thalamic Changes Reflecting Disease Progression in Multiple Sclerosis. *Neurol Neuroimmunol Neuroinflamm*. 2024;11(6). doi:10.1212/NXI.0000000000200299

235. Oh J, Arnold DL, Cree BAC, et al. Tolebrutinib versus Teriflunomide in Relapsing Multiple Sclerosis. *New England Journal of Medicine*. 2025;392(19):1893-1904. doi:10.1056/NEJMOA2415985;JOURNAL:JOURNAL:NEJMS

236. Fox RJ, Bar-Or A, Traboulsee A, et al. Tolebrutinib in Nonrelapsing Secondary Progressive Multiple Sclerosis. *New England Journal of Medicine*. 2025;392(19):1883-1892. doi:10.1056/NEJMOA2415988;SUBPAGE:STRING:FULL

237. Sormani MP, Rovaris M, Valsasina P, Wolinsky JS, Comi G, Filippi M. Measurement error of two different techniques for brain atrophy assessment in multiple sclerosis. *Neurology*. 2004;62(8):1432-1434. doi:10.1212/01.WNL.0000120663.85143.B3

238. Pardini M, Brown JWL, Magliozzi R, Reynolds R, Chard DT. Surface-in pathology in multiple sclerosis: a new view on pathogenesis? *Brain*. 2021;144(6):1646-1654. doi:10.1093/brain/awab025